NASA CONTRACTOR REPORT 166310

UH-60A Black Hawk Engineering Simulation Program: Volume II-Background Report

J.J. Howlett
United Technologies
Sikorsky Aircraft
Stratford, Connecticut 06602

Prepared for
Ames Research Center
under Contract NAS2-10626

National Aeronautics and
Space Administration

Ames Research Center
Moffett Field California 94035

FOREWORD

This report is Volume II of two volumes prepared by the Sikorsky Division of United Technologies Corporation for the National Aeronautics and Space Administration, Ames Research Center, Moffet Field, California under Contract NAS2-10626.

This contract, which was to define and validate a mathematical model of the UH-60A BLACK HAWK helicopter at the Ames Research Center, was funded by the U.S. Army Research and Technology Laboratories (AVRADCOM), Ames Research Center and administered by the National Aeronautics and Space Administration. Ms. Carolyn S. LaFollette was the Contract Administrator and Mr. Thomas S. Alderete, Simulation Investigations Branch, was the Technical Monitor. The Sikorsky Division Project Engineer for this contract was Mr. J. Howlett. Engineering assistance was provided by Mr. W. Gerdes, Mr. D. Ruttledge and Mr. P. Gold. Simulation software support was provided by Mr. D. Simpson.

TABLE OF CONTENTS

LIST OF FIGURES

LIST OF FIGURES (Continued)

1.0 SUMMARY

A non-linear mathematical model of the UH-60A BLACK HAWK helicopter has been developed under Contract NAS2-10626. This mathematical model, which is based on the Sikorsky General Helicopter (Gen Hel) Flight Dynamics Simulation, provides the Army with an engineering simulation for Performance and Handling Qualities evaluations. Initially it will be applied in an analysis mode with eventual application to real time pilot-in-the-loop simulation.

This mathematical model is a total systems definition of the BLACK HAWK helicopter represented at a uniform level of sophistication considered necessary for Handling Qualities evaluations. The model is a total force, large angle representation in six rigid body degrees of freedom. Rotor blade flapping, lagging and hub rotational degrees of freedom are also represented. In addition to the basic helicopter modules, supportive modules have been defined for the landing interface, power unit, ground effects and gust penetration. Information defining the cockpit environment relevant to pilot-in-the-loop simulation is presented. This same model was activated on Sikorsky's DEC PDP KL10 computer to generate check cases for use during the validation of the simulation at NASA.

Volume I of this report defines the mathematical model using a modular format. The documentation of each module is self-contained and includes a description, mathematical definition and input for the BLACK HAWK. Volume II provides background and descriptive information supportive to an understanding of the mathematical model.

2.0 INTRODUCTION

This report is Volume II of two volumes, which document the mathematical model of the UH-60A BLACK HAWK helicopter. This work was funded under Contract NAS2-10626 by the U.S. Army Research and Technology Laboratories (AVRADCOM), Ames Research Center.

The objective of this contract was to provide the Army and NASA with a well documented, operational and verified engineering simulation of the BLACK HAWK helicopter. This work, undertaken by Sikorsky, provides the Army with a Flying Qualities analysis methodology for the BLACK HAWK helicopter which could eventually be extended to a real time pilot-in-the-loop simulation. The mathematical model provided under this contract is a total system, free flight representation based on the Sikorsky General Helicopter (Gen Hel) Flight Dynamics Simulation, illustrated on Figure 2.1. It is defined at a uniform level of sophistication currently considered appropriate for Handling Qualities evaluations. This model is also considered to give representative performance trends, but it should not be used to define critical performance characteristics. The modular format presented facilitates the introduction of additional or more sophisticated modules.

Presented in this Volume is background information which is not directly required for the mathematical definition of the BLACK HAWK simulation model, but is supportive to an understanding of the model. Each of the modules presented in Volume I will be discussed. Where mathematical manipulation has been used which has obscured the origin of equations, derivation and explanation will be provided. Origin of experimental data used as input will be identified and a discussion of inherent assumptions in the model will be presented. This volume contains information proprietry to Sikorsky Aircraft Division UTC.

It is not the intention in this report to duplicate information provided in Volume I. However, in some areas for continuity and completeness, repetition is unavoidable. This document should be treated as supportive to Volume I.

The following sections discuss each of the simulation modules presented in Volume I. Extensive reference is made to Volume I, but rather than indicate this in the text, the respective page numbers in Volume I, correponding to the discussion being undertaken, are identified in a right hand margin.

FIGURE 2.1. GEN. HEL. FLIGHT DYNAMIC'S SIMULATION MODEL

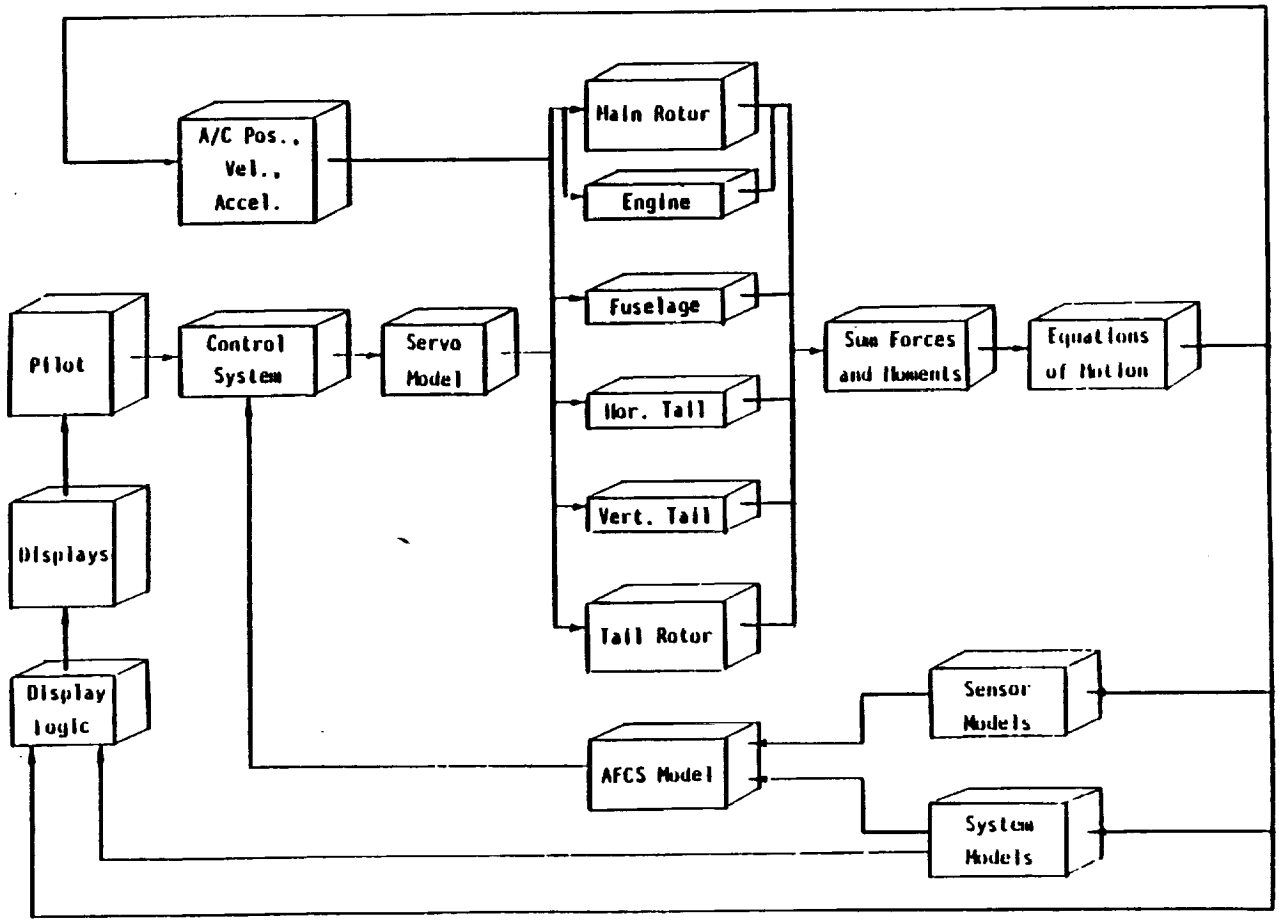

3.0 SIMULATION MODULES DESCRIPTION

3.1 MAIN ROTOR MODULE

3.1.1 Overview of the Main Rotor Module

The main rotor mathematical representation is complex and lengthy. Therefore, an overview is presented to aid in the understanding of the overall model prior to discussing the details.

The main rotor model is based on a blade element analysis in which total rotor forces and moments are developed from a combination of aerodynamic, mass, and inertia loads, acting on each simulated blade. The calculation elements are presented in block diagram form on Figure 3.1.1.

Forces on the blades are derived as a result of total acceleration and velocity components at the blades together with blade pitch control inputs. Accelerations are developed from body motion, blade motion, rotor shaft speed changes and gravity. Velocity components are made up of body velocities, blade motion, rotor speed, self induced downwash and gust velocities.

Before calculations at the rotor blade can proceed it is necessary to implement several axes transformations. Airframe motion developed at the center of gravity must be transferred from the fixed body axes system into a rotating axes frame aligned along the blade span. Total accelerations and velocities at the blade, must be determined in order to develop the inertia and aerodynamic loads on the blade.

The treatment of the blade segment aerodynamic force calculation is completely non-linear. Lift and drag characteristics are provided for in the range $-180 \leq \alpha \leq 180$. Simple sweep theory is used to modify the unyawed blade element lift coefficient. The application of sweep theory to the determination of drag is not well established. For this model, drag is determined by entering the drag map data with the actual yawed angle of attack.

The aerodynamic segmented loads, determined above, are resolved from the local wind axes into blade span axes and summed along each blade to obtain root shears at the hinge. Subsequently these forces are transformed into the rotating shaft axes frame through the flapping and lagging angles. These same loads are used to determine the aerodynamic hinge moments for use in the flapping and lagging motion equations.

FIGURE 3.1-1 MAIN ROTOR FLOW DIAGRAM

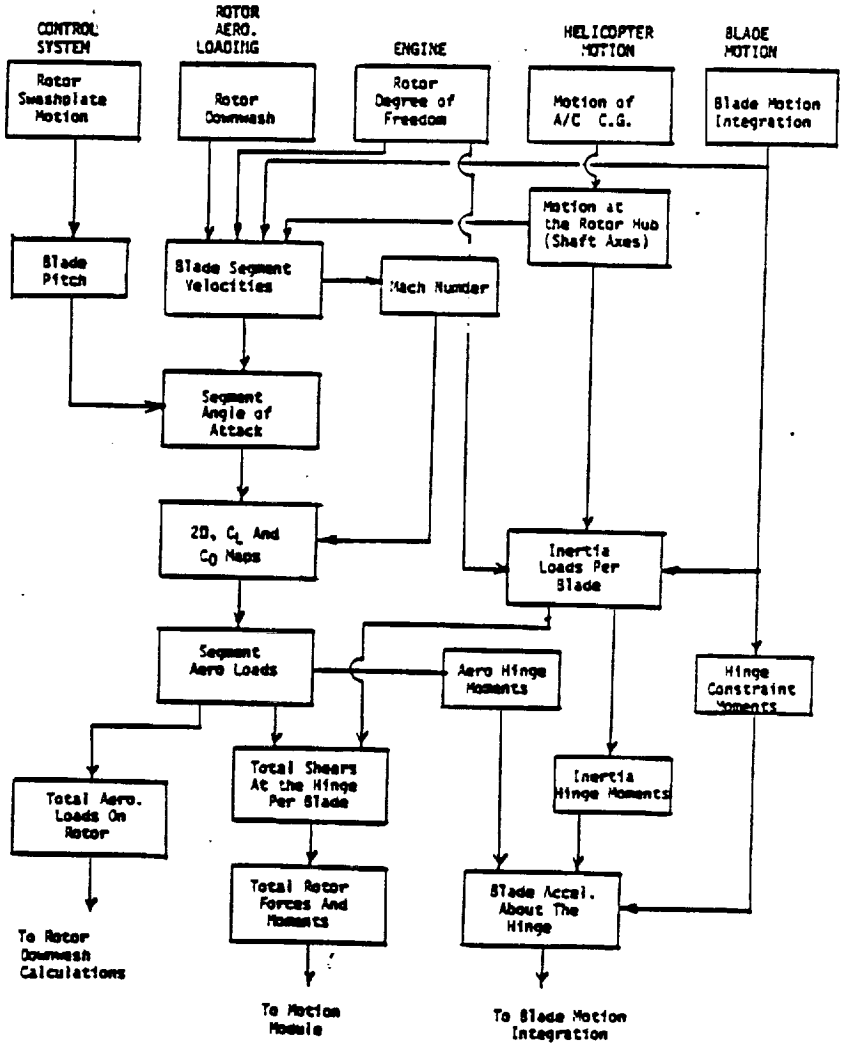

The blade inplane or lagging motion is restrained by a damper system. In the case of BLACK HAWK the damper is non-linear and the kinematics of this system are complicated by geometry. The restraining moment provided by the lag damper is obtained by tracking the damper axial velocity. This is then used to determine axial force from a load-velocity characteristics map.

The motions in the flapping and lagging degrees of freedom are determined from the moment balance about the blade hinges. This balance involves aerodynamic moments, hinge restraint moments, weight moments and inertia moments. The latter are explicitly introduced into the equations of motion.

The three component total shear forces acting at the hinge of each blade in the rotating shaft axes are determined by summing aerodynamic and inertia forces. Rotor hub moments are determined from a combination of the shear forces at the hinges and moments from the blade hinge restraint. Total rotor loads are then obtained by summing all blades and resolving them into fixed shaft axes. An arithmetic manipulation of these equations is introduced on these final equations which allows the simulation number of blades to be different from the actual number. This artifice is intended for use in piloted simulation, where reducing the number of simulated blades can be used to decrease computer execution time requirements.

The oscillating nature of the rotor forces and moments make it expedient to filter their outputs under some circumstances. A simple first order filter is used. The final rotor forces and moments are obtained by transforming the filtered shaft axes forces and moments into body axes with the origin at the center of gravity. These are eventually summed with other component outputs to give the total external forces and moments at the center of gravity.

It is necessary to make provision in these final rotor outputs for the option of selecting to run with the engine module in or out. If the engine is selected out, perfect rotor speed governing is assumed and the shaft torque reaction on the airframe is assumed equal to rotor required torque. If the engine module is activated then it's output torque is introduced into the airframe.

Finally, the rotor wake skew angle is determined. It is the dependent parameter used to establish the variation of rotor wash on the fuselage and tail.

A detailed description of each element of the main rotor model follows. It should be noted that the sequencing of the program flow in the main rotor is critical and should follow the equation flow presented in Volume I.

3.1.2 Detailed Description of the Main Rotor Module

Blade Geometry #5.1-12

The geometric definition for the rotor blade is shown in Figure 3.1.2. Many different methods can be chosen for selecting the segment area distribution. In this BLACK HAWK simulation, an equal annulii area approach was chosen for a programmed, automated set-up. This allows the number of segments to be minimized and distributes them towards the higher dynamic pressure regions outboard on the blade. The programmed set-up can of course be inhibited, and any desired distribution input. The distribution chosen may not be the best at high advance ratios (outside the currently defined BLACK HAWK flight envelope) where significant retreating blade stall is encountered.

The equations presented can be derived from observing that the normalized rotor disk area is equal to π and that the normalized blade length is equal to $(1-\xi-\xi^1)$. Thus the normalized equal annulus area is equal to, $\frac{(\pi - \pi(\xi+\xi')^2)}{\text{Number of Segments}}$ 5.1-13

It should be noted that the equations defined weight the center of action of segment forces by the annulus area. Actual segment area is determined geometrically from the segment mean chord and segment span. The latter being determined by establishing the distance from the hinge (assumed to have the same center for flapping and lagging) to the inboard and outboard edges of the annulii.

Effect of Rotor Blade Weight on CG Position 5.1-13

The Gen Hel blade element rotor; treats each blade as having its own flapping and lagging degree of freedom. Each blade is a separate body which imparts loads on the airframe via the hinge pins and lag dampers. The model is arranged such that the helicopter gross weight and center of gravity (CG) are entered as input for convience. Therefore it is necessary to calaulate actual airframe weight and C.G. before proceeding with the

Foot Note: # These are page numbers in Volume I relevent to the discussion.

FIGURE 3.1.2 BLADE GEOMETRY DEFINITION

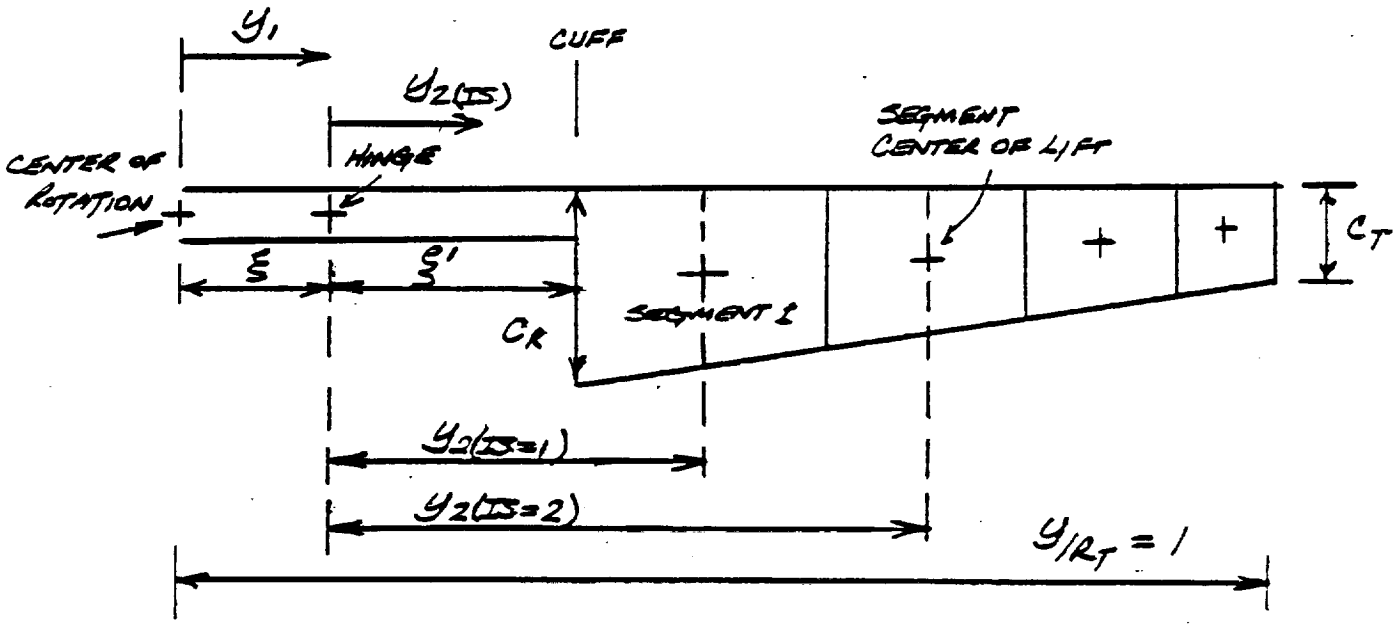

calculation. All forces and moments, and subsequent motion, are referred to the compensated weight and center of gravity. Somewhat inconsistently, but for convenience, the airframe inertia input must be less that component due to the blades.

Accelerations and Velocities at the Rotor Hub in Shaft Axes

Determination of the loading on the rotor blade requires the development of the total acceleration and velocity components at the blade resulting from both airframe and blade motion. These equations are the first part of a systematic transfer of airframe motion in the body axes at the center of gravity, to the rotor blade. The translational accelerations at the rotor hub can be derived using Appendix A of Reference 1. The translational velocities are normalized (using traditional helicopter analysis practice) by rotor tip speed. Gust component terms are introduced into these equations. (These terms are a means of providing gross gust inputs to the rotor when the more complex gust penetration algorithm is not required). The Gust Module Section details the relationship between the various gust inputs. The motion determined at the hub in body axes is formed into a fixed set of shaft axes through the shaft inclination angles i_θ and i_ϕ. The angular accelerations and rates are similarly transformed. These axes systems are illustrated on Figure 3.1.3.

5.1-14

5.1.16

Rotor Shaft Speed Degree of Freedom

5.1-17

Historically, Helicopter Flight Dynamic Simulation Models have assumed that rotor shaft speed was constant. This assumption was made for computing expediency and to a large extent was justifiable for the older heavy rotor systems. However, with the trend towards lower weight fraction for the rotor system, and with the current generation of fuel controls, significant rotor speed excursions are experienced for some maneuvers. More subtle effects are also being experienced with coupling in the basic aircraft modes, as discussed in Reference 2. The BLACK HAWK rotor model presented has been developed to allow rotor shaft motion. Computation with the rotor shaft degree of freedom released necessitates the introduction of a fuel control and engine simulation to close, and stabilize, the rotor shaft speed loop. For this simulation of BLACK HAWK, a linear, time varying coefficient model has been developed. This engine and fuel control model is described in Section 3.6. The actual calculation of the rotor shaft speed degree of freedom is performed in the Engine Module. If the rotor speed degree of freedom is not required it may be selected out. Rotor speed is then fixed at the trim value and engine torque set equal to the rotor torque. This allows a torque reaction to be generated on the airframe.

5.6-17

5.1.-36

FIGURE 3.1.3 BODY AXES TO SHAFT AXES TRANSFORMATION

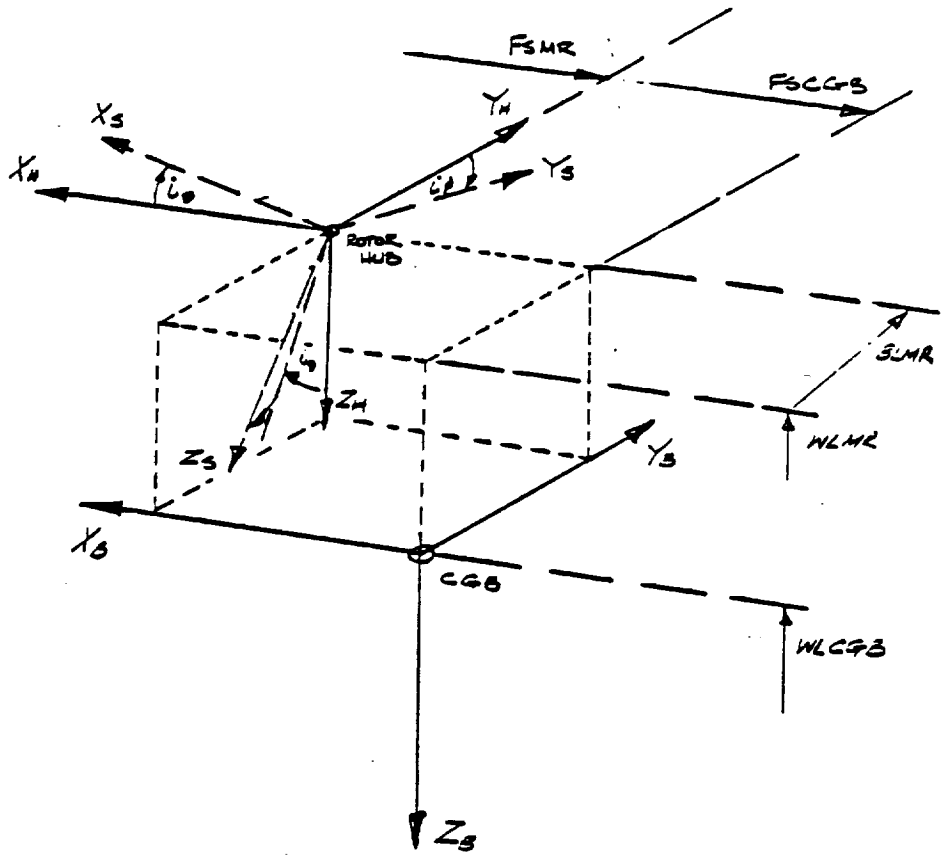

X_B, Y_B, Z_B Body Axes System

X_H, Y_H, Z_H Hub Axes System

X_S, Y_S, Z_S Shaft Axes System

Rotor Azimuth Update 5.1-17

Under normal circumstances, the rotor azimuth update is a direct function of the actual rotor speed and the integration time interval, or duty cycle (TIME), chosen for computing the simulation model. "TIME" should therefore be chosen to meet the frequency response criteria of the simulation investigation or as a minimum, $PSIMR(\psi_{MR}) = 40°$. The latter requirement is to preserve numerical stability. Unfortunately, under real time operating conditions where "TIME" must equal the total execution time of the simulation, (or computer cycle time in the case of a time-shared system) some compromise of the frequency response requirement is necessary. An appropriate discussion of real time operation is given in Reference 3. A software switch is provided for selecting DELPSR independent of TIME. If the simulation is being run with this logic set, and TIME (DELPS/Ω57.3) the implication is that the azimuth update is being scaled, and rotor frequency response will be attenuated. However it may be necessary to run in this mode to achieve real-time operation.

It should be noted in the equations that PSIMR (ψ_{MR}) is specified in the range $-180 \leq$ PSIMR ≤ 180 with zero azimuth being aligned over the helicopter's tail.

Blade Flapping and Lagging Rate and Displacement 5.1-18

The integration algorithm used for developing blade motion is based on a predictive technique which assumes that blade motion is periodic. This assumption is exact at steady state. However, for Handling Qualities investigations, and even higher frequency applications the algorithm is acceptable. It's use in the latter case should be validated for the specific application. Extensive investigation of this algorithm was undertaken by NASA Langley. (Roland Bowles). Unfortunately, this work has not been published. The major attribute of this method is its stability, and the necessity to carry only the last pass flapping rate and displacement along during the calculation. In addition this method is able to cope with large rotor azimuth (ψ_{MR}) changes between program iterations, a situation encountered in real time pilot-in-the-loop applications.

The derivation of this algorithm is given below.

ASSUME THAT $(\beta, \dot{\beta}, \ddot{\beta})_{t-1}$ ARE KNOWN AT SOME BLADE AZIMUTH $(\psi_{MR})_{(t-1)}$ ON THE PREVIOUS PROGRAM PASS AND NOTE THAT $\psi_{MR} = \Omega_{MR}\, t$. ALSO ASSUME MOTION IS PERIODIC

$$\beta_{(t-1)} = a_0 - a_1 \cos(\psi_{MR})_{t-1} - b_1 \sin(\psi_{MR})_{t-1}$$

$$\dot{\beta}_{(t-1)} = \frac{a_1}{\Omega_{MR}} \sin(\psi_{MR})_{t-1} - \frac{b_1}{\Omega_{MR}} \cos(\psi_{MR})_{t-1}$$

$$\ddot{\beta}_{(t-1)} = \frac{a_1}{\Omega_{MR}^2} \cos(\psi_{MR})_{t-1} + \frac{b_1}{\Omega_{MR}^2} \sin(\psi_{MR})_{t-1}$$

WRITE $(\psi_{MR})_t = (\psi_{MR})_{t-1} + \Delta\psi_{MR}$, WHERE $\Delta\psi_{MR} = \Omega_{MR}\, \Delta t$

REWRITE FLAPPING EQUATIONS FOR CURRENT PASS

$$\beta_t = a_0 - \cos\Delta\psi_{MR}\left[a_1 \cos(\psi_{MR})_{t-1} + b_1 \sin(\psi_{MR})_{t-1}\right] + \sin\Delta\psi_{MR}\left[a_1 \sin(\psi_{MR})_{t-1} - b_1 \cos(\psi_{MR})_{t-1}\right]$$

$$\dot{\beta}_t = \frac{\cos\Delta\psi_{MR}}{\Omega_{MR}}\left[a_1 \sin(\psi_{MR})_{t-1} - b_1 \cos(\psi_{MR})_{t-1}\right] + \frac{\sin\Delta\psi_{MR}}{\Omega_{MR}}\left[a_1 \cos(\psi_{MR})_{t-1} + b_1 \sin(\psi_{MR})_{t-1}\right]$$

SOLVE FOR a_0, a_1, b_1 IN TERMS OF $[\beta, \dot{\beta}, \ddot{\beta}]_{t-1}$

AND INSERT IN THE EQUATIONS ABOVE

$$\therefore \beta_t = \beta_{(t-1)} + \dot{\beta}_{(t-1)} \frac{\sin \Delta\psi_{MR}}{\Omega_{MR}} + \left(\frac{1 - \cos \Delta\psi_{MR}}{\Omega^2_{MR}}\right) \ddot{\beta}_{(t-1)}$$

$$\therefore \dot{\beta}_t = \dot{\beta}_{(t-1)} \cos \Delta\psi_{MR} + \ddot{\beta}_{(t-1)} \frac{\sin \Delta\psi_{MR}}{\Omega_{MR}}$$

The resulting per blade flapping and lagging angles are summarized for output purposes into First Harmonic Fourier coefficients of flapping and lagging. The flapping coefficients define the unwarped rotor tip path plane and correlate with the resultant thrust and hub moments on the rotor. 5.1-18 5.1-19

Main Rotor Airmass Degree of Freedom 5.1-20

Rotor Airmass degree of freedom modeling, at a level of sophistication appropriate to Flight Dynamics Simulations, is not well defined and suffers from a lack of test data with which it can be validated. The inflow model presented for the BLACK HAWK simulation is formulated from a combination of established theory and weak empirical extrapolation. This model is primarily based on a prescribed downwash distribution developed as a function of rotor loading. Total downwash at any given blade segment is made up of three elements.

1. A basic momentum component which results from generating aerodynamic rotor thrust. 5.1-21

2. A harmonic momentum component which derives from cyclic aerodynamic hub moment on the rotor disk. 5.1-21

3. A harmonic component due to rotor wake blow-back with increasing forward speed. 5.1-20

The basic component, which can be derived by application of simple momentum theory to the rotor disk, (See Reference 4) results in a uniform distribution as a function of the total rotor aerodynamic thrust loading. 5.1-21 The concept of cyclic components of inflow stems from the fact that any rotor which produces aerodynamic hub moments, should produce harmonic inflow components, as a result of the reaction of the airflow to these aerodynamic moments. 5.1-21 These components would not exist for a centrally hinged rotor in a steady state condition, but, would exist in the steady state for hingeless rotors or rotors with hinge offset (which can produce aerodynamic hub moments). References 5 and 6 provide varying levels of analytical treatment and experimental data supporting the introduction of harmonic terms. Unfortunately, the experimental data deals entirely with hingeless rotors. The transient characteristics of both the thrust and moment components are represented by a first order lag having a time constant of approximately .1 sec at hover and decreasing with increases in total velocity vector. The provision, within the BLACK HAWK model, for aerodynamic hub moment components for downwash, was considered important. However, at this time it is not possible to justify input data. Therefore, the input to these terms has been specified to zero.

In addition to the "self induced" effects discussed above, the 5.1-20 other element of harmonic inflow is a cosine component due to wake blow-back (Glauert downwash factors). The importance of this term, to the realistic prediction of lateral flapping at low speed, was shown in Reference 7. As forward speed increases, the wake of the rotor blows back, and in so during, causes a redistribution of the induced downwash longitudinally across the rotor disk. Because of the rotor phasing, this effect is manifest in changes to lateral flapping and lateral control to trim, especially at low speed. The approach presented for the BLACK HAWK model is to redistribute the thrust induced uniform downwash, as a function of the cosine of blade azimuth position. Many methods are available for determining the harmonic coefficient. They all retain a uniform distribution at hover and phase to a trapizoidal distribution, (aligned with the velocity vector) with increasing forward speed. Differences between approaches relate to the magnitude of the effect. The algorithm used in Gen. Hel. tends to result, at high forward speed, in a distribution of zero downwash at the front of the rotor disk and double the uniform value at the rear. Indications are that this effect should be stronger in the Gen. Hel. model.

The downwash components discussed above are distributed around the azimuth to obtain the total segmental downwash velocities ($UPDMR_I$, $URDMR_I$) in rotating blade span axes. Tangential components of downwash are ignored. 5.1-21

A final comment is necessary concerning the total uniform (average) inflow equation (λ) relative to the total blade segment interference velocities. The latter includes components of gust velocity derived from the rotor penetrating a gust front. When the gust velocity is distributed to each segment during this process a component of velocity is introduced which must be compensated for in the average inflow equation. An artifice has been created whereby an average gust velocity (over all segments), UGAVMR, is added to the inflow equation to maintain momentum balance in the airmass degree of freedom. Further explanation can be found in the Gust Module Section 3.9. 5.1-21

Blade Segment Velocities 5.1-22

All contributions to the total blade segment velocities - airframe translational and rotational velocities, rotor shaft speed, rotor blade motion and rotor interference velocities - have been previously defined. The blade segment total velocity components are developed in three parts. Those independent of blade segment position, those dependent on segment position and interference effects made up of downwash and gust effects. The velocities at the blade segments are obtained by transforming the fixed shaft vectors into the rotating hub axes system, then transferring them to the blade hinge position, transforming them into blade span axes through the Euler angles β_{MR} (flapping) and δ_{MR} (lagging) and finally transferring them to the segment position on the blade. These axes transformations are illustrated on figure 3.1.4. The three orthogonal total velocity vectors ($UPMR_I$, $UTMR_I$, $URMR_I$) are used to calculate the resultant velocity ($UYAWMR_I$), local Mach No. ($MACHMR_I$), yawed angle of attack ($AFYWMR_I$) and the flow yaw angle at the blade segment. The latter variables are illustrated on figure 3.1.5. It should be noted that the radial component of velocity is omitted in calculating the Mach Number which is used in the aerodynamic map look-up. Reference 8 which describes the use of simple sweep theory, indicates that Mach Number should be based on the unyawed component of flow. 5.1-23

FIGURE 3.1.4 SHAFT AXES TO ROTATING BLADE SPAN AXES TRANSFORMATION

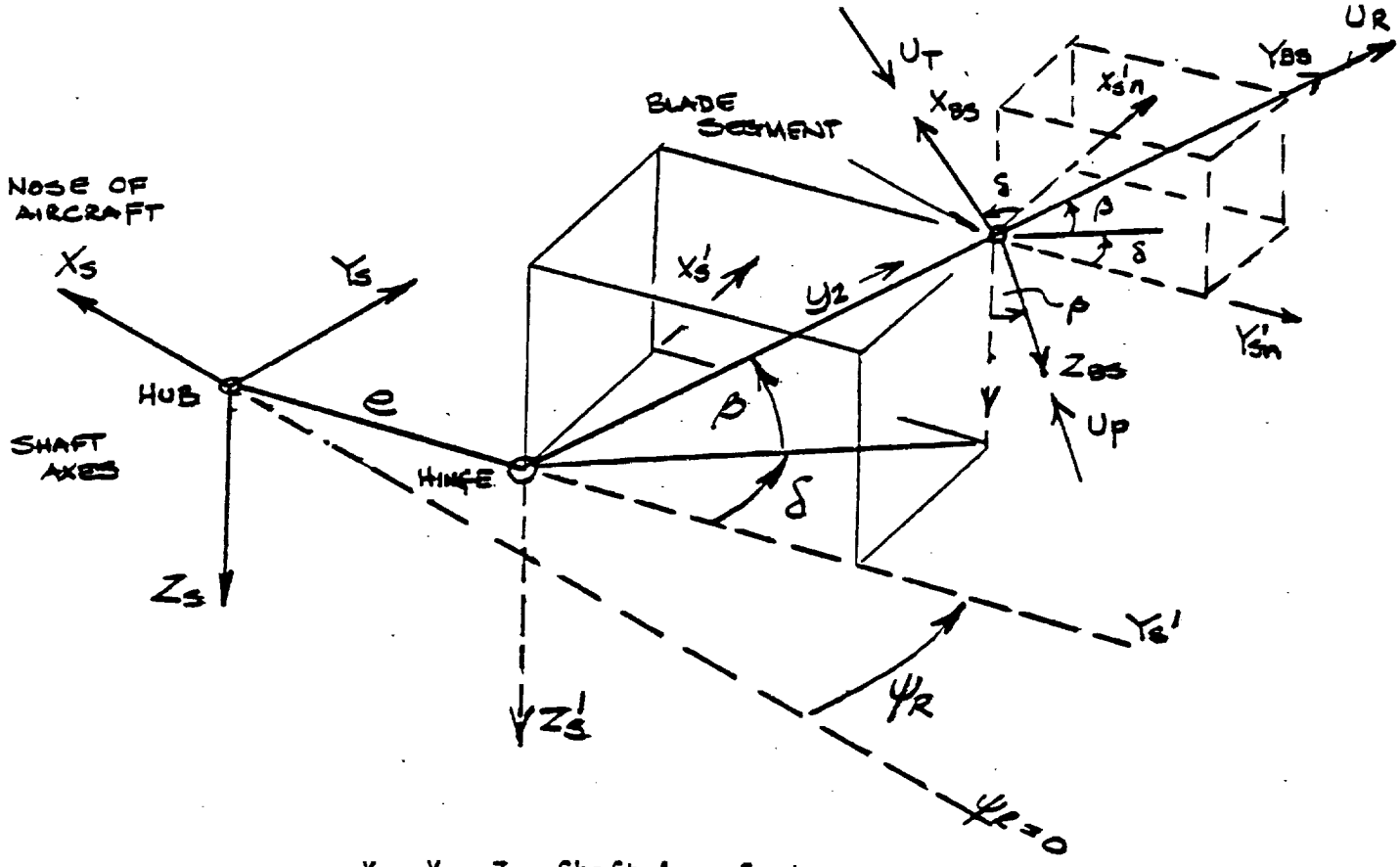

X_S, Y_S, Z_S Shaft Axes System

X'_S, Y'_S, Z'_S Rotating Shaft Axes System

X_{BS}, Y_{BS}, Z_{BS} Blade Span Axes System

U_T, U_R, U_P Blade Element Velocities Along X_{BS}, Y_{BS}, Z_{BS} Respectively

δ and β are Euler Angles with δ Rotation about Z'_S then β Rotation About X_{BS}.

FIGURE 3.1.5 DEFINITION OF YAWED ANGLE OF ATTACK

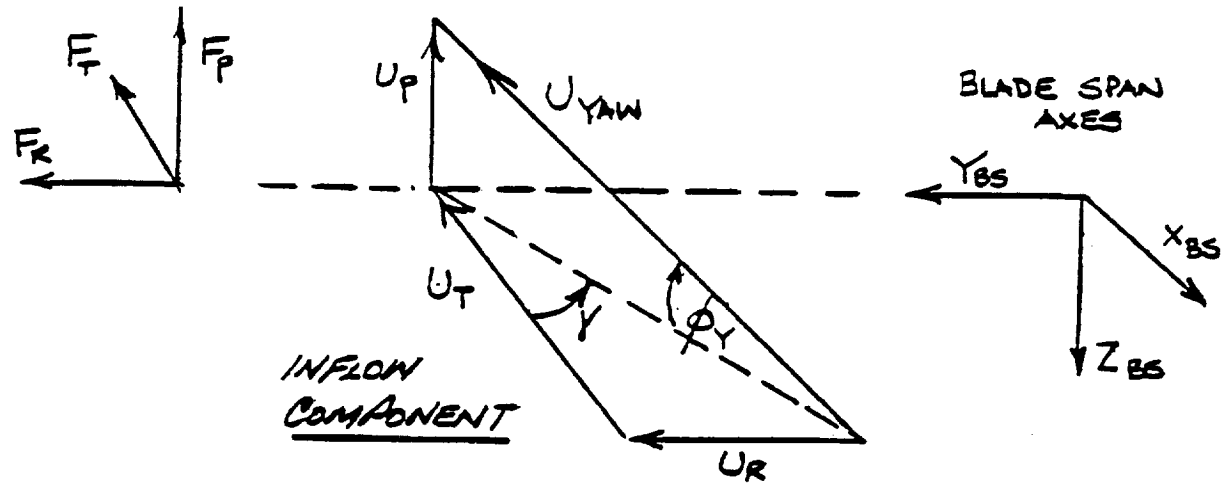

TOTAL YAWED ANGLE OF ATTACK $\alpha_Y = \phi_Y + \theta_Y$

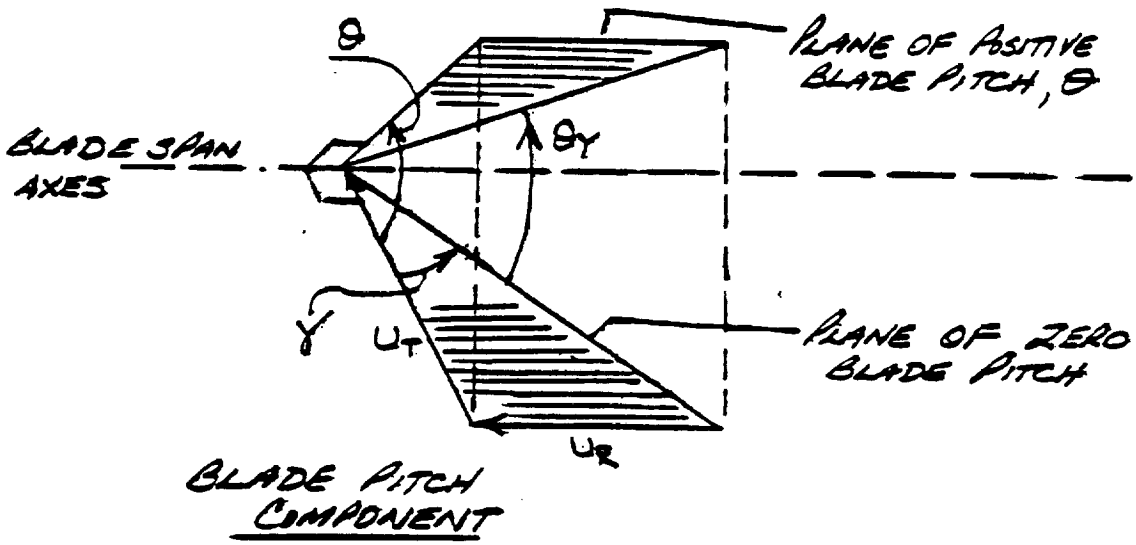

Blade Segment Angle of Attack 5.1-25

The blade segment angle of attack is defined along the yawed direction of the local segment velocity vector as shown on figure 3.1.5. It is made up of geometric blade pitch angle and local wind angle of attack. In turn, geometric blade pitch angle comprises components due to control input, control geometric configuration, preformed blade twist and elastic deformation resulting from rotor loading.

The swash plate impressed blade pitch angle depends on the control input to collective, θcuff, lateral cyclic, A_{IS}, and longitudinal cyclic, B_{IS}. These harmonic components are referenced to rotor azimuth ($\psi_{MR} = 0$) over the tail and displaced by a swashplate rotation angle. The swashplate angle is defined as positive in the normal body axes system sense (ie for BLACK HAWK that is opposing the direction of rotor motion, but has a negative input). Swashplate angle is a means of correcting the phase response of the articulated rotor with offset hinges such that body axes orthogonality is retained by the pilot's controls. 5.1-24

Blade pitch/flap coupling, δ_3, and pitch/lag coupling, α_1, can result from blade hinge axis angular offset or from the geometric orientation of the control push rods. Although these terms are retained in the model presented (for completeness sake), they are both nominally equal to zero for the BLACK HAWK helicopter.

The blade segment dynamic twist model is a prescribed, empirical, representation. This simplified approach has been introduced as an alternative to a more sophisticated elastic representation, to account for the significant torsional deformation of the BLACK HAWK rotor blade. Without these terms, collective blade pitch and blade loading will not correlate with test data. Basically, the technique assumes that blade tip dynamic twist is a function of total blade loading (independent of blade pitching moment), and that this tip twist can be distributed along the blade span as a function of the first torsional mode deflection. The blade loading is harmonically smoothed by using a first harmonic fourier filter. The gain coefficients of the fourier equation are empirically derived. The BLACK HAWK input data only specifies a value for the steady term, as a function of forward speed. As with all empirically derived models they may not be universally applicable. 5.1-24

The final contribution to blade segment pitch angle is that due to preformed twist. This is prescribed in terms of a map as a function of blade segment position. Some caution is necessary because of the non-linear tip section, where an unrealistic 5.1-25 5.1-50

value of twist could be selected based on the automatic segment set up algorithm. This will lead to a bias on collective pitch and distorted blade loading.

The blade angle of attack equation is complicated by the requirement to resolve blade pitch angle into the segment local flow direction as shown in figure 3.1.5. Computationally, information must be retained in the equation to define angle of attack completely. ($-180° \leq \alpha_\gamma \leq 180$). The derivation is presented below.

FROM FIGURE 3.1.5 $\alpha_\gamma = \phi_\gamma + \theta_\gamma$

$$\tan\alpha_\gamma = \frac{\tan\phi_\gamma + \tan\theta_\gamma}{(1 - \tan\phi_\gamma \tan\theta_\gamma)} \quad \text{EXPANDING AS TANGENT}$$

$$\tan\phi_\gamma = \frac{u_p}{(u_T^2 + u_T^2)^{1/2}} = \frac{u_p}{u_T}\left[\frac{u_T^2}{u_T^2 + u_T^2}\right]^{1/2}$$

$$\tan\theta_\gamma = \tan\theta\cos\gamma$$

$$= \tan\theta \frac{u_T}{(u_T^2 + u_T^2)^{1/2}} = \tan\theta \frac{u_T}{u_T}\left[\frac{u_T^2}{u_T^2 + u_T^2}\right]^{1/2}$$

$$\therefore \tan\alpha_\gamma = \frac{\left(\frac{u_p}{u_T} \cdot |u_T| + \frac{u_T}{u_T} \cdot |u_T| \tan\theta\right) \frac{1}{(u_T^2 + u_T^2)^{1/2}}}{\left(1 - \frac{u_p}{u_T} \cdot \frac{|u_T \cdot u_T|}{(u_T^2 + u_T^2)}\right)}$$

By manipulation of this equation and noting that the sign of cos γ in tan θ_Y cos γ is always +VE for ±90° then

$$\tan\alpha_Y = \frac{\left(u_p + u_T \tan\theta\right) \frac{|u_T|}{(u_T^2+u_T^2)^{1/2}}}{\left(u_T - \frac{u_p\, u_T^2 \tan\theta}{(u_T^2+u_T^2)}\right)}$$

$$\text{or} \quad \tan\alpha_Y = \frac{\left(u_p + u_T \tan\theta\right)|\cos\gamma|}{\left(u_T - u_p \tan\theta \cos^2\gamma\right)}$$

Blade Segment Lift and Drag Coefficients

5.1-26 -27

The treatment of the blade segment aerodynamic force calculation is completely non-linear. Lift and drag characteristics are provided for the range $-180 \leq \alpha_Y \leq 180$. Bivariate maps, as a function of angle of attack and Mach Number are defined in the range $-30 \leq \alpha_Y \leq 30$ allowing good definition of blade stall. The complete coverage of angle of attack allows good definition of aerodynamic characteristics on the retreating blade side of the rotor disc. This is important at high advance ratios. The aerodynamic data input to the lift and drag coefficient map is for the SC 1095 airfoil and was derived from two-dimensional wind tunnel tests. (Reference 9). The two-dimensional nature of this data requires the development of an artifice to allow it to be used in a three dimensional environment. It is generally accepted that blade segment lift coefficient can be determined by applying simple sweep theory to the unyawed blade aerodynamic data.

5.1-51 through 5.1-56

This theory is rigorously applied in the linear lift range where the entry to the unyawed lift coefficient is transformed by the cosine of the yaw angle (i.e. $\alpha_{TRANS} = \alpha \cos\gamma$) and the entry Mach Number is a function of the unyawed component of flow. At higher angles of attack some liberties are taken where sweep theory is not valid. These steps are taken to avoid discontinuities in blade lift data as the blade proceeds around the azimuth. Discontinuities can result in an unstable flapping and lagging solution. The application of sweep theory to the

determination of drag is not well established. For this model, drag is determined by entering the drag map data with the actual yawed angle of attack. As previously noted a development of sweep theory can be found in Reference 8. Sikorsky evaluations of this theory, as applied to rotors, are documented in Reference 10.

The logic which controls the transformation of the calculated value of yawed angle of attack, for entry into the aerodynamic map, is developed in the equations. Three ranges are defined for angles of attack greater and less than zero. Essentially, these ranges represent the low angle of attack linear range, a high angle of attack linear range and a center range determined by stall angle of attack. 5.1-26

The loss of lift at the tip of the blade is accounted for by factoring the lift coefficient obtained from the maps. For BLACK HAWK, it is assumed that the blade span out to 97% radius is effective lifting surface. Segments straddling this point or beyond are appropriately factored. Drag coefficient passes unmodified for all segments except for the addition of a delta profile drag component. 5.1-27

It has been assumed in defining the blade aerodynamics that Reynolds Number effects and unsteady flow are of secondary importance and can be ignored. This may not be justifiable under all operating conditions.

Blade Aerodynamic Shears 5.1-28

The aerodynamic force coefficients previously determined in the wind axes system are transformed to blade span axes and dimensionalized to force units. These forces are then summed across blade segment to obtain aerodynamic shear forces at the blade hinge. Subsequently, these forces are resolved into rotating shaft axes. It should be noted that flapping and lagging blade angles are Euler angles and order of treatment must be observed.

Blade Aerodynamic Moments About the Hinge 5.1-28 -29

Blade Aerodynamic hinge moments are developed for each segment from the segment forces and corresponding lift centers and then summed across the blade segments. (It is important to note that flapping motion because of angle definition is taking place in the $Y_{BS} \sim Z_{BS}$ plane.) The flapping moment is then resolved into fixed shaft axes for use in the determination of the aerodynamic harmonic moment components, of the inflow model.

Blade Lag Damper Kinematics 5.1-30

The blade inplane or lagging motion is restrained by a damper system. In the case of BLACK HAWK the attachment points are such that the damper straddles the hinge, and is mounted out of the plane of zero flapping. It is also offset from the blade pitch axes. The kinematics of the damper are therefore complicated by this geometry, and the damper experiences motion due to blade pitch and flap, in addition to lag. A generalized representation of this geometry is given on figure 3.1.6. The axial velocity of the damper is determined by tracking the position of the blade attachment relative to the fixed point on the rotor hub. From this information, an instantaneous axial displacement of the damper strut is obtained. The axial velocity of the damper is then determined based on the change in displacement since the last pass. It should be noted that the blade pitch contribution to the motion is referenced to the cuff. (i.e. blade pitch less twist). The resulting axial velocity of the damper is used to enter the damper map from which axial damper force is obtained.

The force-velocity characteristics of the damper are complex and highly non-linear. For these reasons the damper is represented empirically. The damper characteristics presented, were determined from BLACK HAWK test data, Reference 11. These data were obtained by stroking a damper at various frequencies and displacements typically encountered during flight. The results showed the force-velocity characteristics to be somewhat a function of frequency as might be expected. It was assumed for this BLACK HAWK model that the damper could be represented by the first harmonic frequency. The implication being, that any energy generated at other frequencies will be ignored. Support for this assumption is derived from the fact that the BLACK HAWK ground resonance mode and rotor torsional mode (both dependent on the lag damper characteristics) are representative for this model. 5.1-54 -55

A simple flapping restraint equation is introduced into the model for completeness sake. However, for BLACK HAWK the flapping restraint from the elastomeric bearing is negligible and the input coefficients for this equation are set to zero. It should be noted that because of the damper geometry a component of damper force will be experienced about the flapping hinge.

FIGURE 3.1.6 LAG DAMPER KINEMATIC GEOMETRY

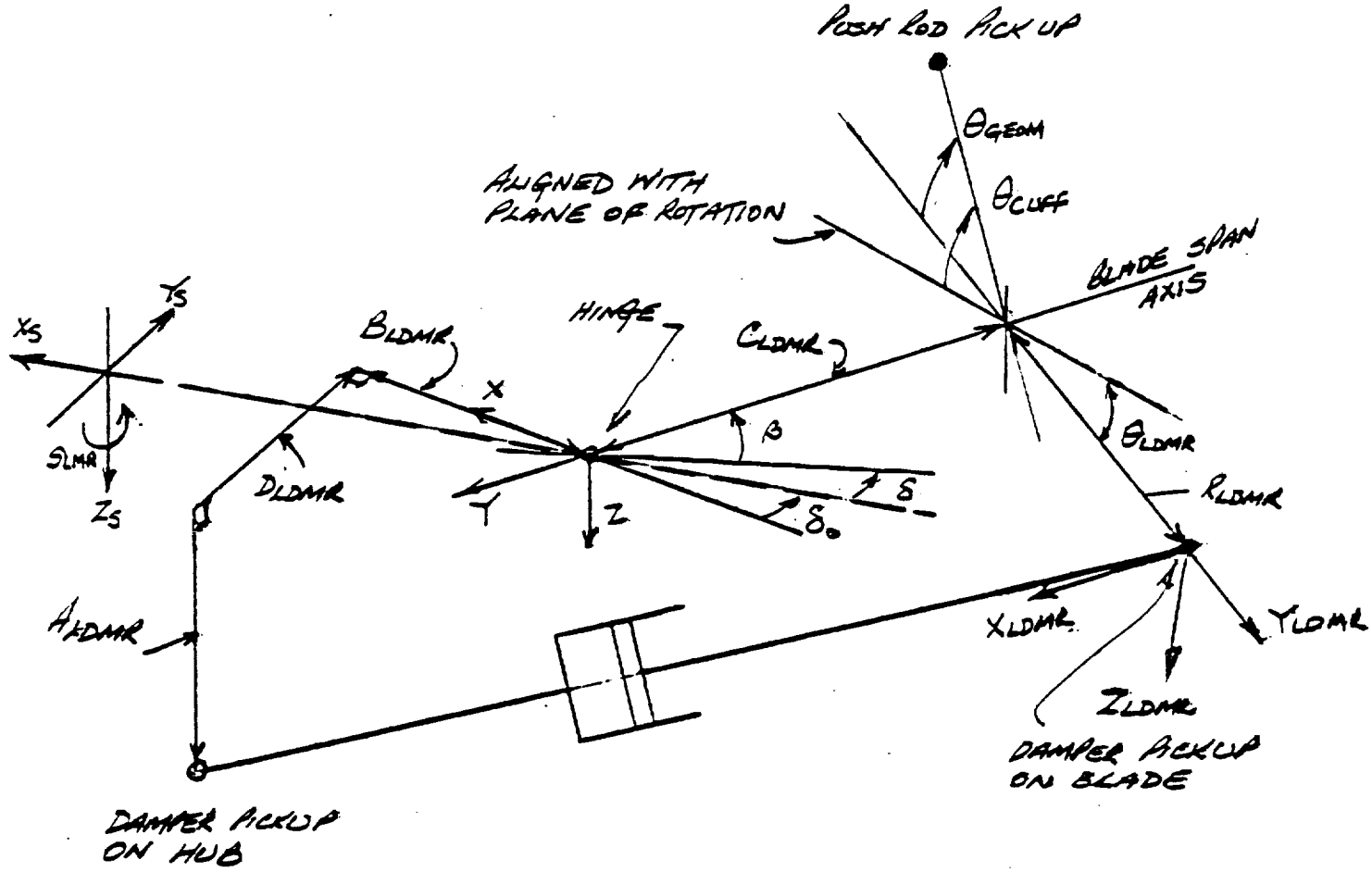

$(XYZ)_{LDMR}$ Lag Damper Axes

X_{LDMR} Aligned with the blade span

and $(Y,Z)_{LDMR}$ rotated through θ_{LDMR}

Blade Flapping and Lagging Degrees of Freedom. 5.1-31 -32

The individual rotor blades in the Gen Hel simulation are treated as separate bodies which are attached to the hub with hinge pins in the flapping and lagging motion planes. Each blade, therefore has its own degrees of freedom, which are coupled to the airframe. That is, airframe motion is impressed on the root end of the blades and in turn blade forces and moments are transmitted into the airframe.

The rigid blade flapping and lagging motion equations provided in this model are defined to take place about hinges which are co-located at a point offset from the center of rotation of the rotor. The contributions to the flapping and lagging motion are the external aerodynamic and hinge restraint moments and the mass and inertia moments. The inertia and mass moments arise as a result of airframe motion, blade motion and shaft rotational motion. It is important to note that because flapping and lagging angles are Euler angles, the motion in these two degrees of freedom is not orthogonal. Therefore, in the lagging equation the external forces derived in blade span axes must be resolved into the intermediate plane of lag motion. This is not true of the flapping degree of freedom. I.E. for the lag equation.

The derivations of the flapping and lagging equations are lengthy and are not presented in this report. The final equations presented (inertia terms) are essentially the same as those given in Reference 12 and validated in Reference 13. It should be noted that some small terms have been eliminated. A software provision to inhibit the lagging degree of freedom has been incorporated. If the lag motion is inhibited then rotor torque must be transferred across the hinge as indicated on page 5.1-35 of Volume I.

Shears at the Hinge

The same inertia forces which create moments about the hinges in the equations discussed above also result in inertia shear forces acting on the hinge pins. The derivation of the shear forces is essentially the same as for the moments. The total shear force at the hinge of each blade is obtained by summing the inertia forces with the aerodynamic forces. 5.1-33 5.1-34

Total Rotor Forces and Moments 5.1-34

The total rotor forces in the fixed shaft axes system are obtained by first resolving the three orthogonal components of blade root shears into these axes and then summing over

all the blades. Total rotor hub moments are obtained in a similar manner. The pitch and roll hub moments are made up (mostly) of shears acting on the hinge pins offset from the center of rotation. The yawing moment, (the torque connotation is retained in the equations) is made up mainly of the lag damper contribution. 5.1-35

An arithmetic manipulation is introduced on the final equations which allows the simulated number of blades to be different from the actual number. This artifice is intended for use in piloted simulation where computer execution time must be minimized. In applying this artifice, the assumption is that three blades are sufficient to define the (first harmonic) tip path plane and that based on disk theory the number of blades can be factored to obtain the total rotor loads.

With the lagging degree of freedom operating, the major portion of rotor torque is developed through the lag dampers. Therefore, if the lagging degree of freedom is inhibited, an alternative equation containing the aerodynamic moment must be introduced as specified in the equations. 5.1-35

Main Rotor Force and Moment Output Filter

The oscillating nature of the rotor forces and moments make it expedient to smooth, or average, these outputs under some circumstances. These normal harmonic variations are antagonistic to the helicopter simulation trimming process, both in terms of seeking a solution, and in terms of the tolerance check for the trimmed solution. This is especially true when the simulated helicopter approaches the boundaries of operation, where the amplitudes of the oscillations become large. Also, in many situations, computing efficiency can be improved by increasing "TIME". This will allow a faster valid trim, but some means of eliminating the consequence "noise" must be introduced. Finally, for the purpose of categorizing and comparing trimmed helicopter conditions (print-out) consistently, it is necessary to suppress the oscillations. The method used in Gen. Hel. is to pass the rotor forces and moments through a first order lag 5.1-36
Other more complex techniques can be applied. The first order lag is used because of it's simplicity and direct application. This lag must be removed when the simulation is being executed in the dynamic (compute) mode. The exception to this rule is in the unique circumstance of a marginal real time simulation, where the number of blades have been artificially reduced to minimze computer execution time. Here it may be necessary to suppress erroneous 'N' per rev. oscillations.

A more detailed discussion of helicopter simulation trimming is presented in Section 4. of this report.

Final Rotor Force and Moment Outputs.

The final rotor forces and moments are obtained by transforming the filtered shaft axes forces and moments into body axes with the origin at the center of gravity. These final main rotor module outputs are eventually summed with other module component outputs to give the total external forces and moments at the center of gravity. 5.1-36

It is necessary to make provision in these final rotor equations for the option of selecting to run with the engine module in or out. If the engine is suppressed, perfect rotor speed governing is assummed and the shaft torque reaction on the airframe is assummed equal to rotor required torque. If the engine module is activated then its output torque is introduced into the airframe. 5.1-36

The motivation for inhibiting the engine module is to decrease the bandwidth of the simulation and corresponding computer requirements. With the rotor degree of freedom being computed there is an impact on simulation numerical stability and rotor azimuth update increment $\Delta\psi_{MR}$. (or "TIME") Therefore, caution should be exercised in selecting to run with or without the rotor speed degree of freedom. Careful consideration should be given to the analysis task being undertaken. A different helicopter simulation response will be experienced, especially in yaw, with engine in or out, depending on the maneuver. (Reference 2) However, this may not be important to the task at hand and the tradeoff of larger rotor azimuth update magnitudes (increased "TIME") may be acceptable. Evidently any maneuver which tends to drive main rotor torque to a negative value will be erroneous without the engine module, since under these circumstances, the rotor clutch would have disengaged.

Rotor Wake Skew Angle.

In this simulation the rotor wake skew angle is defined as the angle that the centerline of the rotor wake makes relative to the normal to the tip path plane (longitudinally). This parameter is used to establish the variation of rotor wash on the fuselage and empennage as a function of rotor thrust and forward speed. Basically, rotor wake angle is used to relate the magnitude of the rotor wash and the geometric proximity of an aircraft component to the centerline of the wake (See Figure 3.1.7) as implemented in this simulation the rotor wash is normalized by the downwash at the rotor disk. It is derived from a Sikorsky off-line computer program (DWSHT) based on Reference 14. 5.1-37

FIGURE 3.1.7 DEFINITION OF ROTOR WAKE SKEW ANGLE

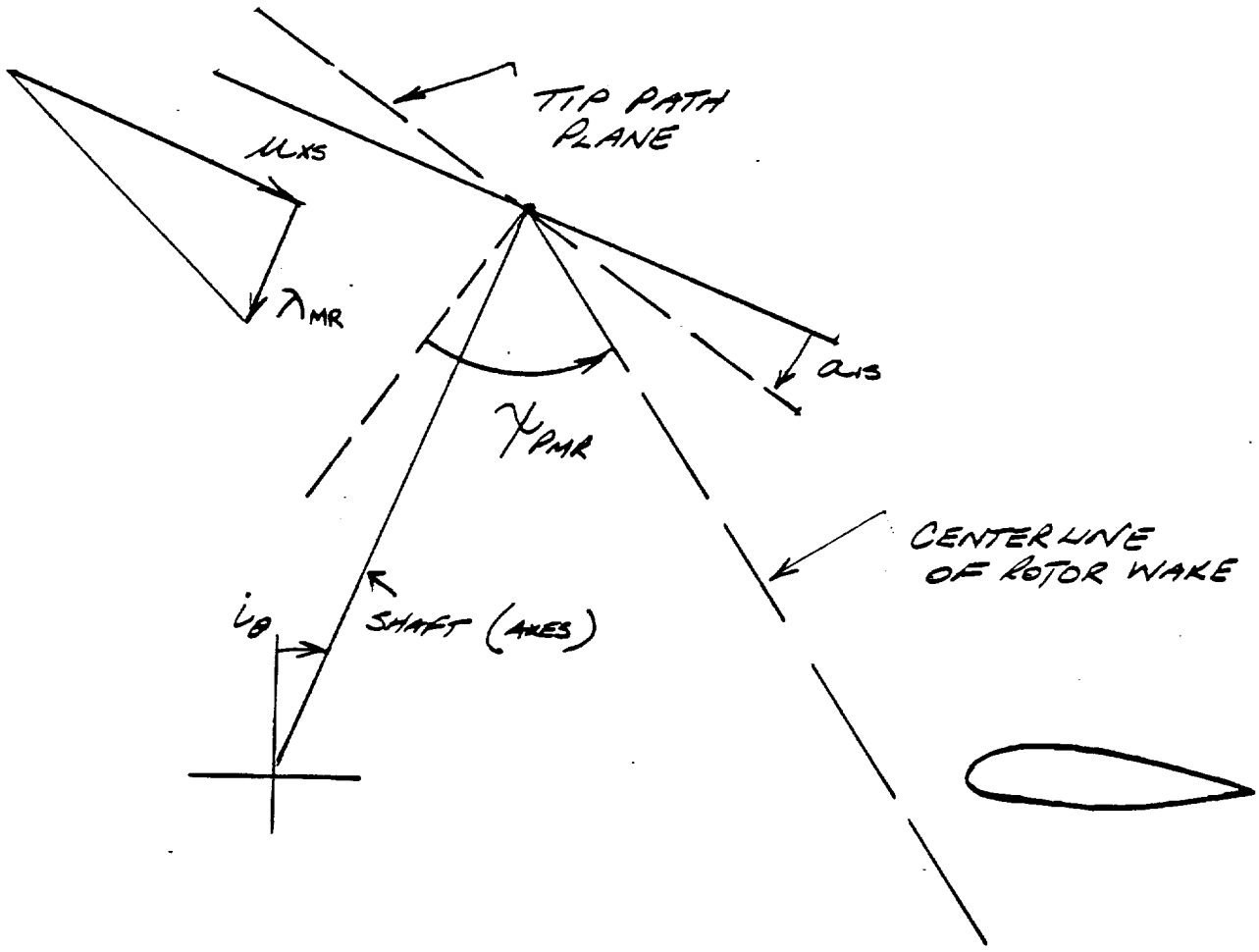

3.2 FUSELAGE MODULE

3.2.1 Overview of the Fuselage Module

The fuselage is defined by six component non-linear aerodynamic characteristics which have been derived from BLACK HAWK Quarter Scale Wind Tunnel Tests. These data have been extended to high angles analytically to cover flight at low speed and hover. The angles of attack and sideslip, used to enter the aerodynamic maps, are developed from the free stream plus wash effects from the main rotor. These rotor interference velocity effects are a function of rotor thrust and forward speed. Care has been taken to make the longitudinal degrees of freedom representative throughout the forward flight envelope. The lateral/directional characteristics are representative for all speeds except side flight close to zero forward speed. It is not considered within the scope of this model to define the complex aerodynamic characteristics at high angle of attack in combination with large sideslip angles. In any event, in this regime dynamic pressure is low and flight is dominated by the rotors. Caution is therefore advised, if this model is used for side flight at high sideward speed.

3.2.2 Detailed Description of the Fuselage Model

The major elements of the fuselage simulation module are presented in block diagram form on figure 3.2.1. This module calculates the aerodynamic forces on the fuselage resulting from the total velocity vectors at the center of gravity. The model is essentially the same as would be used for a fixed-wing aircraft with the notable exception of the rotor wash. The formulation of the model assumes that the aerodynamic forces and moments act at a single point, and are functions of angle of attack and sideslip angle developed at that point, from the total body axes components of velocity. It is also assumed for computing expediency that velocities acting at the center of gravity can be used directly, thus angular rates are ignored.

Rotor Wash on the Fuselage.

The effects of rotor wash on the fuselage have been treated in average terms. No attempt has been made to determine the local flow under the rotor disk and apply it to an elemental analysis of the fuselage. Thus, variations in local velocity have been ignored and the downwash from the rotor is developed for a single point and summed with the free stream. This approach provides the essential effects of more interference velocity with increased rotor load, and varies as the rotor forward speed changes. Provision has been made in the model for three components of rotor wash on the fuselage. For the BLACK HAWK, input

5.2-5

FIGURE 3.2.1 FUSELAGE EQUATION FLOW DIAGRAM

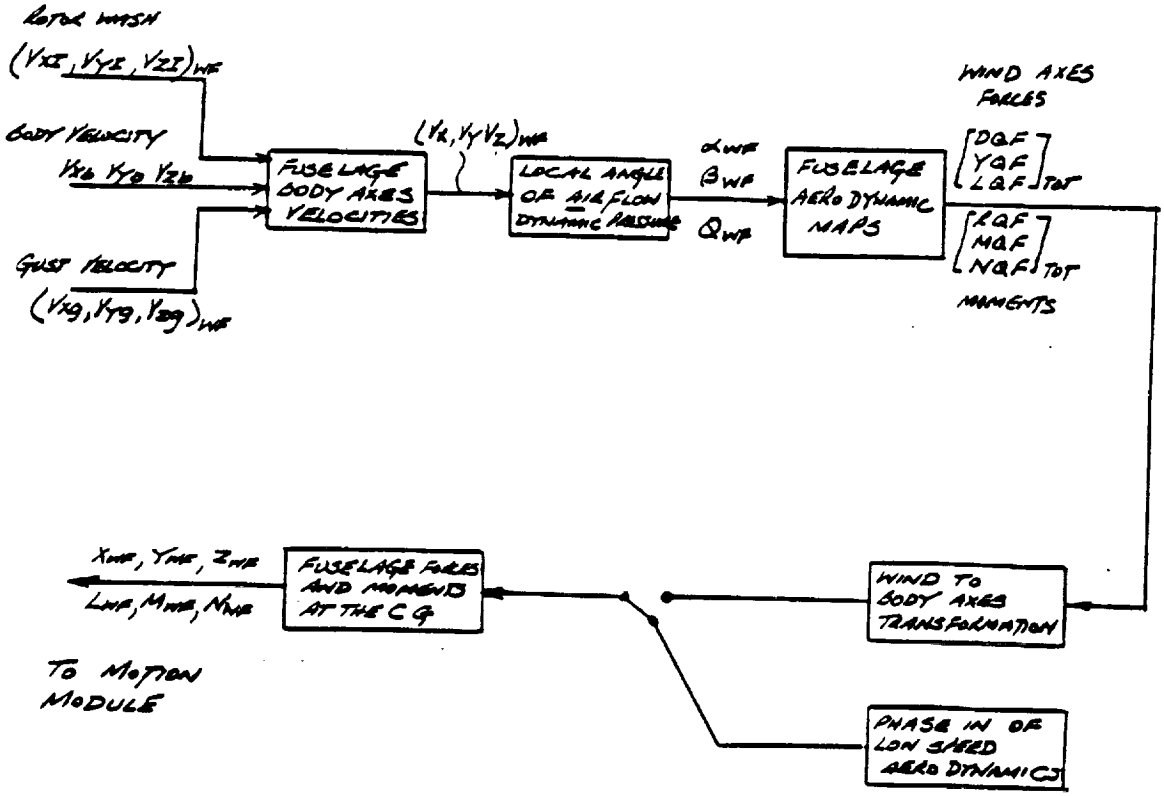

data is only available for the longitudinal and vertical components. As previously discussed in Section 3.1.2 the wash components are normalized by the downwash in the plane of the main rotor and are a function of rotor wake skew angle and longitudinal flapping. The rotor wash data was obtained from the Sikorsky wake analysis program (DWSHT) based on Reference 14. It should be noted that rotor wash data is not provided to cover rearward or sideward flight. In the case of rearward flight the value at $\chi = 0$ is retained. 5.2-20

Angle of Attack and Sideslip

The angle of attack and sideslip are derived from the body axes components of velocity. These comprise the components of flight path velocity, gust components and rotor wash. The definition of the angles are those used in the wind tunnel. That is, angle of attack is the geometric pitch angle subtended by the model relative to tunnel axis at zero yaw angle. It does not change with yaw angle. Angle of sideslip, equal to minus yaw, is defined as yaw table angle in the horizontal plane of the tunnel, irrespective of angle of attack. It should be noted that these angles are not Euler angles. It should also be noted that angle of attack and sideslip are only defined in the range ±90°. Fuselage aerodynamic data is not available for rearward flight. However, to avoid discontinuities near hover the absolute value of Vxb is used. This together with the square root in the sideslip definition implies that during rearward flight the aerodynamics of the fuselage are derived from the corresponding forward flight case. These assumptions are justified, based on the fact that near hover, fuselage dynamic pressures are low and the rotors dominate the flight characteristics. Caution should be exercised if large rearward or sideward airspeeds are comtemplated. 5.2-5 5.2-6

Fuselage Aerodynamic Loads

The fuselage aerodynamic characteristics used in this module are specific to the BLACK HAWK helicopter. The six component force and and moment parameters (ft^2 and ft^3 units respectively) are presented in wind axes as a function of angle of attack and wind tunnel yaw angle (equal to $-\beta_{WB}$). The data has not been generalized in any way and is derived from Quarter Scale Wind Tunnel Tests documented in References 15, 16 and 17. Approximately 2.5 ft^2 of drag was added as a bias to the wind tunnel data to approximate the measured drag on the aircraft, based on performance calculations. The data was also faired to smooth out anomalies, and the side force, rolling moment and yawing moment were made symmetrical as would be expected with rotors and empennage off. The small effects of angle of attack on rolling moment, yawing moment and sideforce have been ignored. Fuselage 5.2-22 through 5.2-37

angular velocity damping components are provided for. The data obtained from these wind tunnel tests up to post stall conditions was extended to ±90° to cover the low speed flight regimes. Near hover, the most important forces (tail off) are the vertical drag and side force which can be estimated fairly accurately. Longitudinal aerodynamic coupling with sideslip is provided for over a limited range, which covers angles likely to be experienced at higher speeds and dynamic pressures.

The wind axes normalized force and moment coefficients are transformed into body axes and transferred from the wind tunnel model mounting point to the fuselage center of gravity position. Forces and moments are obtained by multiplying by dynamic pressure. Because of the definitions of angle of attack and sideslip the transformation equations give invalid body axes forces and moments when these angles both approach 90°. Again as previously discussed caution must be exercised in extracting data for side flight if the lateral speed is high. 5.2-9

To avoid problems during pilot-in-the-loop simulation, filters are presented which fade out the transformation and introduce fixed body axes parameters, estimated specifically for hover and low speed flight. 5.2-10

3.3 EMPENNAGE MODULE

3.3.1 Overview of the Empennage Model

The aerodynamics of the empennage are treated separately from the forward airframe. This separate formulation allows good definition of non-linear tail characteristics that would otherwise be lost in the simplifications of multivariate total aircraft maps. With this approach, changes to the empennage can be made without reloading basic airframe maps. The aerodynamic characteristics are defined by non-linear lift and drag coefficients as a function of local angle of attack. These angles of attack are developed from the free stream velocity, plus rotor wash and fuselage wash. Dynamic pressure effects from the airframe are accounted for by factoring the free stream velocity components. The interference effects are introduced as non-linear maps as a function of fuselage angle of attack and sideslip. All aerodynamic characteristics are analytically extrapolated to 90° angle of attack. The simulation of the empennage is representative in all flight regimes.

3.3.2 Detailed Description of the Empennage Model

The major elements of the empennage simulation module are presented in block diagram form on figure 3.3.1. This module calculates the aerodynamic forces on the horizontal and vertical

FIGURE 3.3.1 EMPENNAGE EQUATION FLOW

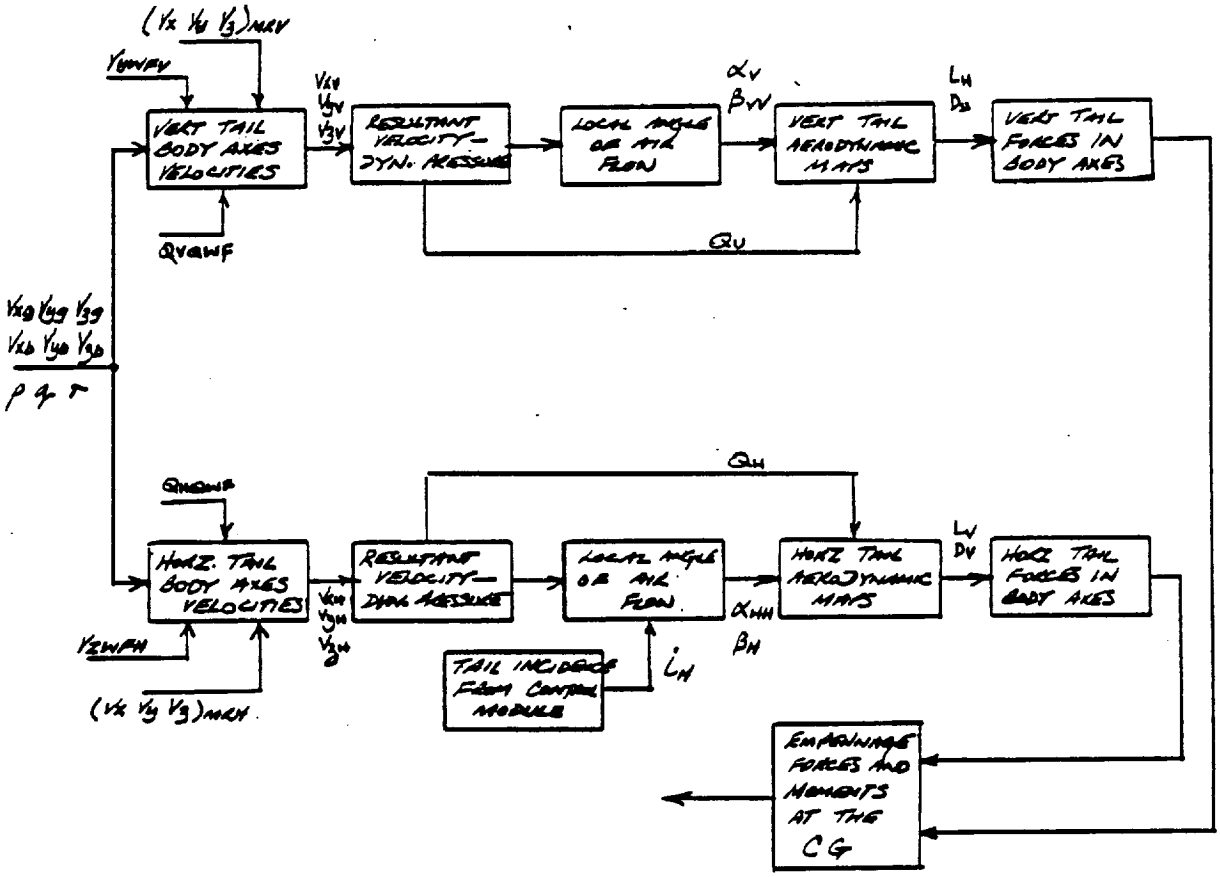

tail surfaces resulting from the local airflow. The component velocities are derived at, and the aerodynamic forces assumed to act at the panel center of pressure. The empennage can experience aerodynamic interference effects from many sources. Components of flow from the main rotor and fuselage are defined for this model. Although the calculation of the horizontal and vertical panel forces are separated in Volume I, the following paragraphs will discuss them in combination.

Local Velocities at the Empennage

Provision has been made in this model for three components of rotor wash at the tail. For BLACK HAWK, data is currently available for only the vertical and longitudinal flow components. In addition, the vertical tail is assummed to experience the same interference valocities as the horizontal tail. As in the case of the fuselage, rotor wash velocity components, normalized by the downwash at the main rotor disk, are developed as a function of rotor wake skew angle and longitudinal rotor flapping. This data was derived from Sikorsky's program DWSHT, based on Reference 14, in a similar manner to that for the fuselage. 5.3-5 5.3-9 5.3-24 -25

The downwash and sidewash from the fuselage are presented as a function of fuselage angle of attack and wind tunnel yaw angle respectively. This data was based on unpowered tail on/tail off wind tunnel test data, documented in References 15, 16 and 17. Interference cross flow components were ignored, as in typical fixed-wing practice. In the calculation of the actual interference velocities, downwash and sidewash angles are assumed to be small. The resulting velocities are delayed to account for the time taken by the airflow to reach the tail. 5.3-27,28 -34,35 5.3-6 5.3-10

The dynamic pressure loss at the tail surfaces, resulting from fuselage/rotor hub blockage, is derived empirically such that, wind tunnel data synthesized from the simulation compares to the original tail on test data. Data is provided as a function of fuselage angle of attack and wind tunnel yaw angle for the horizontal and vertical tail respectively. 5.3-7 5.3-26 5.3-33

It is evident that the wash from the tail rotor will have some interference effect on the empennage. This effect has not been quantified for the BLACK HAWK and has not been introduced into the model. It will be noted, however, that the model has been formulated to allow easy introduction of additional interference components at a later time.

The local velocity components at the tail surfaces are made up of contributions from the basic body axes translational and angular velocities, gust effects, rotor wash and fuselage downwash and sidewash. The loss of dynamic pressure, due to blockage by the fuselage/rotor hub, is introduced by factoring the components of the free stream and fuselage wash terms. Angular velocity components are assumed to be unaffected by blockage. The actual local dynamic pressure is calculated from the resultant local velocity vectors. This approach allows a more representative definition of dynamic pressure at low speeds where downwash from the rotor predominates the flow at the tail. The local angle of attack on the horizontal and vertical tail panels are calculated using the local velocity vectors. The same definition of angles is used as for the fuselage. In the case of the vertical tail, angle of attack has the same connotation as sideslip. The definitions of these angles and tail incidence angles are illustrated on figure 3.3.2.

5.3-7
5.3-11

Empennage Aerodynamic Loads

The lift and drag characteristics for the tail surfaces are based on isolated tail test data , Reference 15, and Reference 18. The latter Reference was used to compensate the wind tunnel isolated tail data for the changes in the size of the horizontal tail following the wind tunnel tests. The trailing edge of the vertical tail was also modified after the tests. Only a small portion of trailing edge was retained and it's camber was reduced to 7 degrees. Reference 19 was used to analytically modify the test data. Tail panel moments about their own axes are not accounted for. The isolated tail aerodynamics are analytically extrapolated to ±90° angle of attack. As for the fuselage, in rearward flight, the tail aerodynamic data look-up will use the corresponding values for forward flight. The lift and drag forces in local wind axes are resolved into body axes at the tail. Finally, the component forces at the empennage, are transferred to the center of gravity together with the corresponding moments.

5.3-29,30
31,32
5.3-36,37
38,39

3.4 TAIL ROTOR MODULE

3.4.1 Overview of the Tail Rotor Module

The BLACK HAWK canted tail rotor is represented in this simulation by the linearized, Bailey theory, closed-form, model. Terms in tip speed greater than squared have been eliminated. The local airflow encountered by the tail rotor is developed in a similar manner to those for the empennage. Corrections for tail rotor pitch/flap coupling and blockage due to the proximity of the vertical tail have been introduced into the basic Baily model. This model does not account for stall effects and there

FIGURE 3.3.2 EMPENNAGE AXES SYSTEM

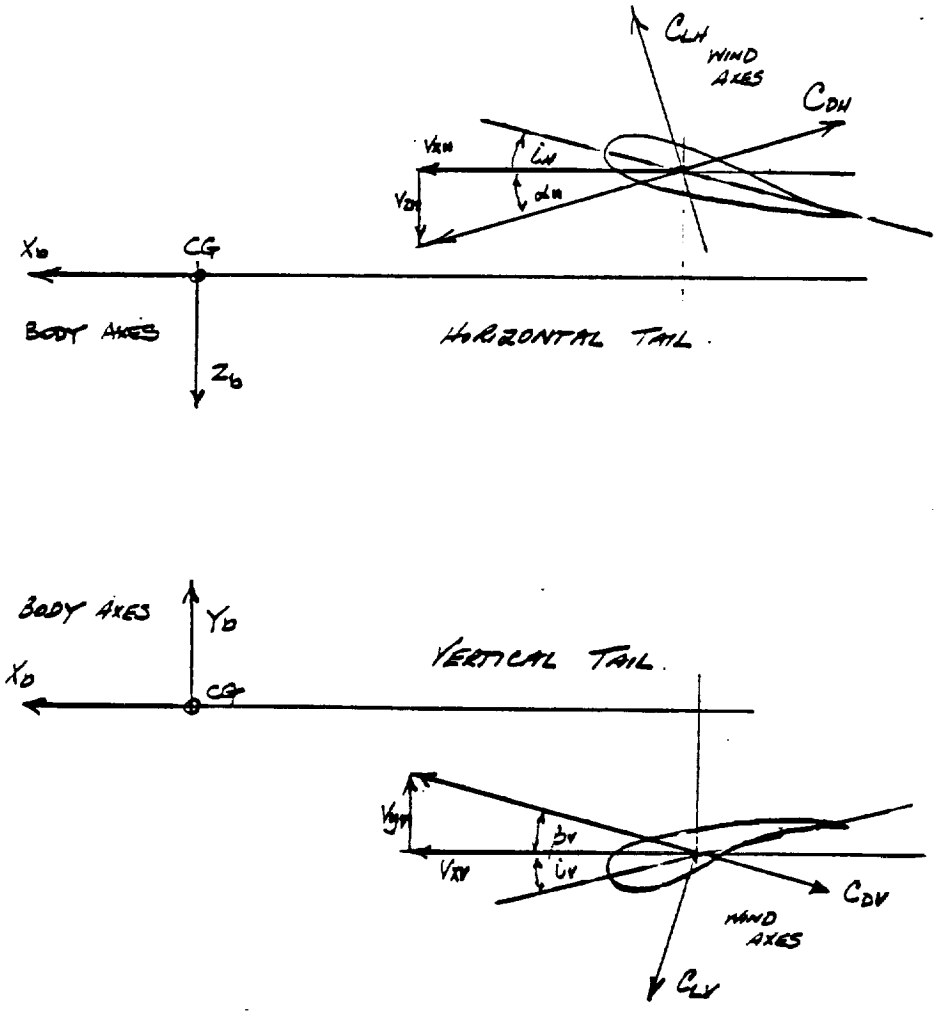

is no treatment of the reverse flow at high speed. Further assumptions can be found in References 4 and 20. The model presented calculates thrust which is considered to be the only significant output from the tail rotor. However, there is an increasing awareness for the need to introduce a torque calculation (for power train) and a longitudinal flapping calculation which would allow tilting of the thrust vector in the drag direction.

3.4.2 Detailed Description of the Tail Rotor Module

This module calculates the thrust force, generated by a canted tail rotor, resulting from blade pitch control input and local airflow. The tail rotor is represented by a simplified, closed form Bailey solution as developed in Reference 20. The major elements of this model are presented in block diagram form on figure 3.4.1. The orientation of the axes system has been defined such that the main rotor blade element analysis may be inserted as an alternative module, if dictated by the level of sophistication of the analysis.

Local Velocities at the Tail Rotor

Interference effects at the tail rotor have been defined in a similar manner to those for the vertical tail. The main rotor wash characteristics are assumed to be equivalent to those for the horizontal tail. Sidewash and downwash components are those defined for the vertical and horizontal tail respectively. The dynamic pressure loss due to the main rotor hub and fuselage are assumed equal to that for the vertical tail. These approximations are considered acceptable and provide some simplification of the simulation. 5.4-4,5

The airflow, in body axes, impinging on the tail rotor is developed from the free stream, body angular rate effects, gust velocities and the previously discussed interference effects. The three component, summed velocities, are then resolved through the cant angle into tail rotor shaft axes as defined on figure 3.4.2. These velocities are normalized by tail rotor tip speed to make them consistent with the normal Bailey equation formulation. The Bailey theory equation is normally presented as the thrust coefficient in terms of the 't' coefficients. It should be noted that the equations have been manipulated to obtain an expression for downwash as shown below. This was found to be necessary to obtain an unconditionally stable solution. It is important that program flow follows the equation flow for a stable tail rotor solution. 5.4-6 5.4-7

FIGURE 3.4.1 TAIL ROTOR EQUATION FLOW DIAGRAM

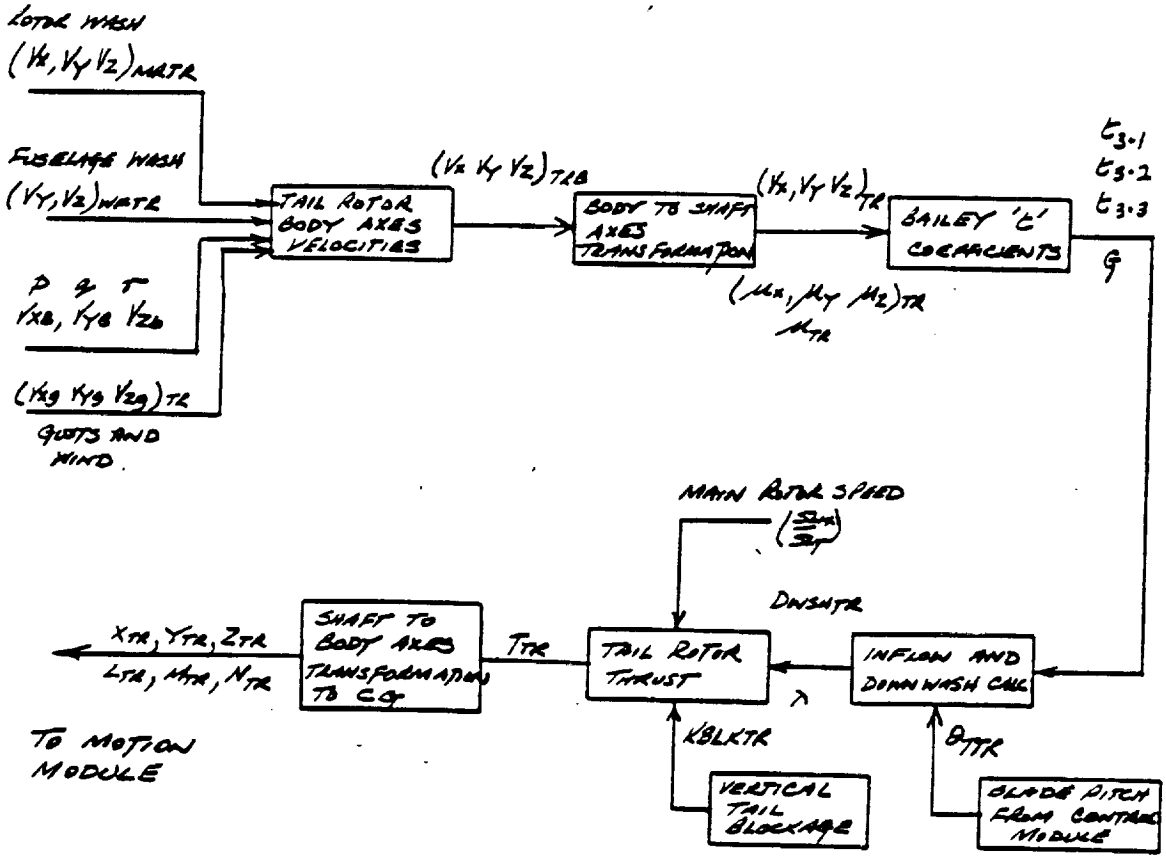

FIGURE 3.4.2 TAIL ROTOR AXES SYSTEM

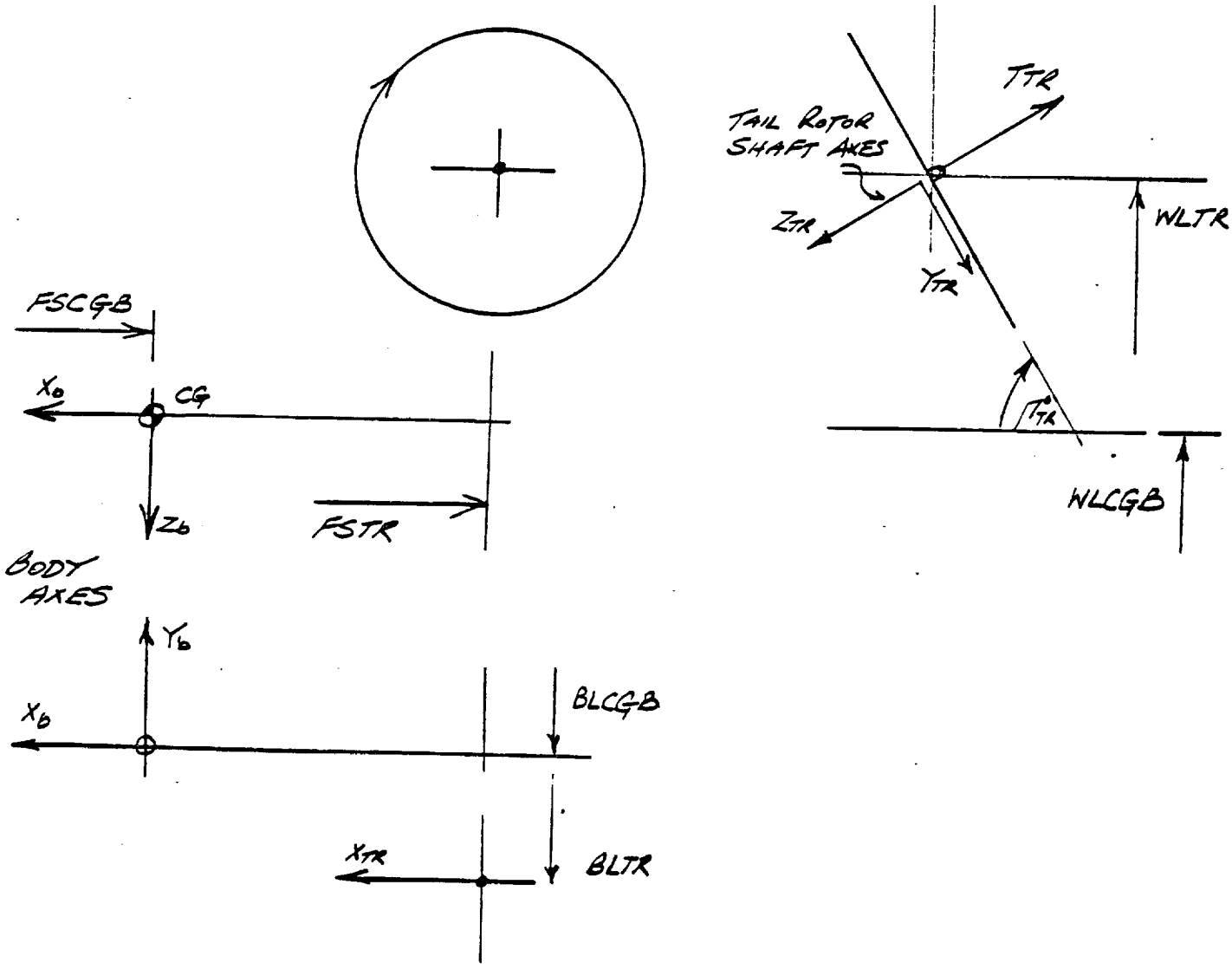

FROM REFERENCE 4 AND 20

$$\frac{2C_T}{\sigma a} = t_{3,1}\lambda + t_{3,2}\theta + t_{3,3}\theta_1 \qquad , \text{LET } G = \frac{\sigma a}{2}$$

$$D_N = \frac{C_T}{a(\mu_x^2+\lambda^2)^{1/2}} \qquad \text{WHERE } \lambda = \mu_z - D_N$$

$$\therefore D_N = \frac{G(t_{3,1}\lambda + t_{3,2}\theta + t_{3,3}\theta_1)}{a^2(\mu_x^2+\lambda^2)^{1/2}}$$

$$D_N = \frac{G(t_{3,1}\mu_z + t_{3,2}\theta + t_{3,3}\theta_1)}{a(\mu_x^2+\lambda^2)^{1/2}} - \frac{G\,t_{3,1}\,D_N}{a(\mu_x^2+\lambda^2)^{1/2}}$$

$$D_N = \frac{G(t_{3,1}\mu_z + t_{3,2}\theta + t_{3,3}\theta_1)}{\left(a(\mu_x^2+\lambda^2)^{1/2} + G\,t_{3,1}\right)}$$

Now Dw can be solved based on a last pass value of λ from which a new value of λ can be obtained. Thus

$$\lambda = \mu_z - D_N \qquad \text{AND}$$

$$C_T = D_N \cdot a(\mu_x^2+\lambda^2)^{1/2}$$

The bailey equations have not been changed but just manipulated in a manner which allows for a stable sequential computation of thrust.

Tail Rotor Blade Pitch

In order to obtain the actual tail rotor collective pitch (θ_{TR}) for the BLACK HAWK, it is necessary to modify the Bailey equations to account for blade pitch/flap coupling (δ_3). This coupling reduces blade pitch impressed by the control system. The Bailey model does not introduce blade flapping and therefore some artifice must be used to obtain the effects of δ_3. The approach taken in this model, is to establish an empirical, linear relationship between tail rotor coning and thrust. This then allows the determination of flapping (and δ_3 effects) from the instantaneous value of thrust developed on the rotor. Linear blade twist effects are accounted for in the basic equation. 5.4-7

Tail Rotor Thrust

The tail rotor thrust equation is developed in a modified form as a function of downwash. This follows from the previous discussion of the downwash equation. The thrust equation incorporates factors for accounting for changes in rotor shaft speed and vertical tail proximity blockage. At low forward speed significant thrust losses due to blockage are experienced, these effects wash out with increasing forward speed. The blockage correction model presented is empirically derived and based on test data. The tail rotor thrust is finally transformed into body axes and the forces and moments transferred to the center of gravity of the airframe. 5.4-8

3.5 FLIGHT CONTROL SYSTEM MODULE

3.5.1 Overview of Flight Control System

The flight control system for BLACK HAWK presented in this module covers the primary Mechanical Control System and the Automatic Flight Control System (AFCS). The AFCS consists of three major subsystems; analog stability augmentation system, digital AFCS, and the stabilator system. These control functions collectively enhance the stability and control characteristics of the BLACK HAWK and maintain desired attitude, speed and heading. A detailed description of the AFCS can be found in Reference 21 and 22.

Flight Control System Description

This description of the BLACK HAWK Flight Control System is presented to provide background information and aid in the understanding of the simulation of the control system. Care has been taken to make the simulation representative, however, some secondary functional differences may exist.

The flight control system defined in this simulation model is comprised of the following elements. They are listed in the order of flow for the simulation.

a) Sensors
b) Stability Augmentation System (SAS)
c) Pitch Bias Actuator (PBA)
d) Flight Path Stabilization (FPS)
e) Mechanical Controls (mixer, actuator, etc.)
f) Stabilator
g) Trim System

The functional relationship of these elements can be identified on the simplified diagrams presented on figures 3.5.1 and 3.5.2.

FIGURE 3.5.1 FLIGHT CONTROLS SIMPLIFIED BLOCK DIAGRAM

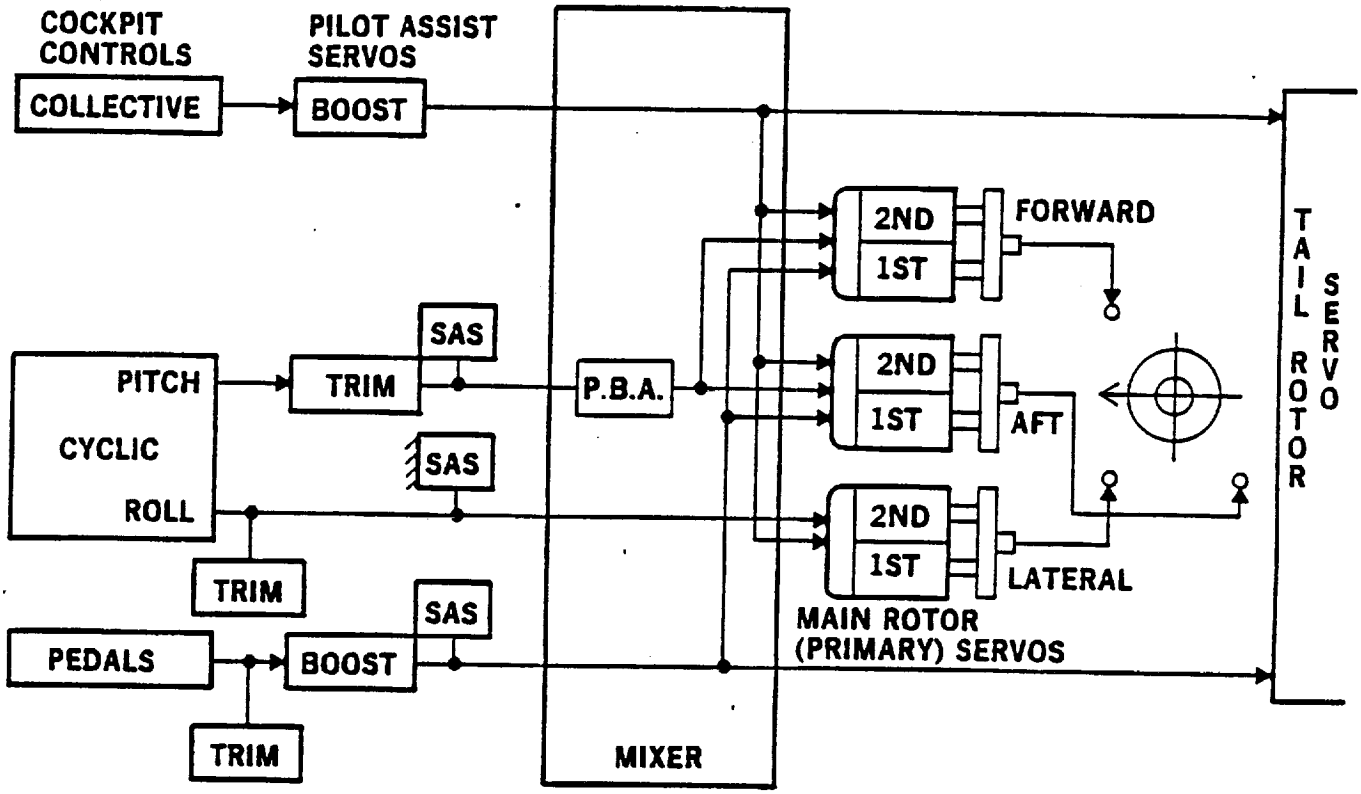

FIGURE 3.5.2 AFCS SIMPLIFIED BLOCK DIAGRAM

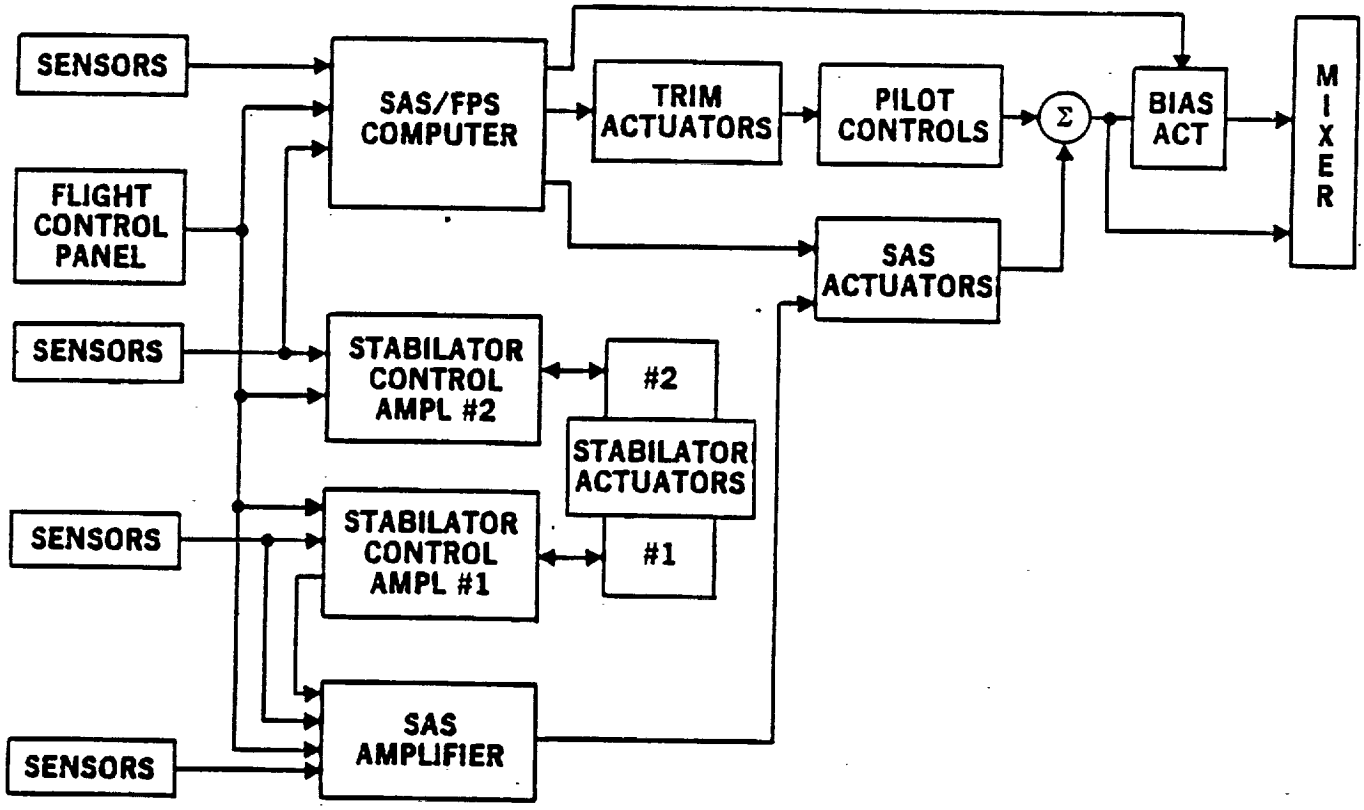

A more detailed understanding of the way in which these elements interact in each individual control channel can be obtained from figures 3.5.3, 3.5.4, 3.5.5 and 3.5.6 taken from Reference 23. These figures present diagramatic representations of the collective, pitch, roll, and yaw control channels respectively.

It is appropriate to note at this time those elements which are not represented in the simulation. The boost servos and primary servos shown on Figure 3.5.1 are not represented. In the latter case this is becuase the swashplate transformations are bypassed for simplification. The servo dynamics are however, included as shaping of the blade pitch inputs. The trim system function is important to pilot-in-the-loop simulation, but has no significance when the the simulation is being used in an open loop (analysis) mode. Therefore, it is not defined within the control system section (5.5) of Volume I, but in the final section (6.0) of Volume I which specifies the cockpit interface with the pilot.

3.5.2 Detailed Description of the Flight Control System Module

A detailed description of the Flight Control System and the corresponding simulation representation is given below.

a) Sensors. These are the helicopter motion transducers which provide feedback input to the AFCS. They are repre-sented in the simulation by high frequency second order transfer functions which match the manufacturers specification for the component. Signal conditioning (6-7 hz First Order Filter) is applied to all sensor outputs. 5.5-6

b) Stability Augmentation System (SAS). This system provides three-axis rate damping and pseudo attitude retention. It enhances the basic helicopter stability about the pitch, roll and yaw axes using rate and lagged rate feedback. A 7sec and 2sec washout of the rate damping signal is incorporated in the pitch and yaw channels respectively to prevent saturation during a steady turn. The yaw lagged rate feedback only functions below 60 knots, so as not to counter the coordinated turn feature which is active at speeds greater than 60 knots. The feedbacks applied to the yaw channel for turn coordination above 60 kts, are roll rate and lagged lateral acceleration. 5.5-7 -8 -9

The SAS is a dual system with one subsystem controlled by the analog SAS amplifier and one subsystem controlled by the digital SAS/FPS computer. (figure 3.5.2) Both SAS subsystem command signals drive a single SAS actuator in each axis. During normal operation with both SAS engaged, each provides one-half of system nominal gain and one-half

FIGURE 3.5.3 UH-60A BLACK HAWK COLLECTIVE FLIGHT CONTROLS BLOCK DIAGRAM

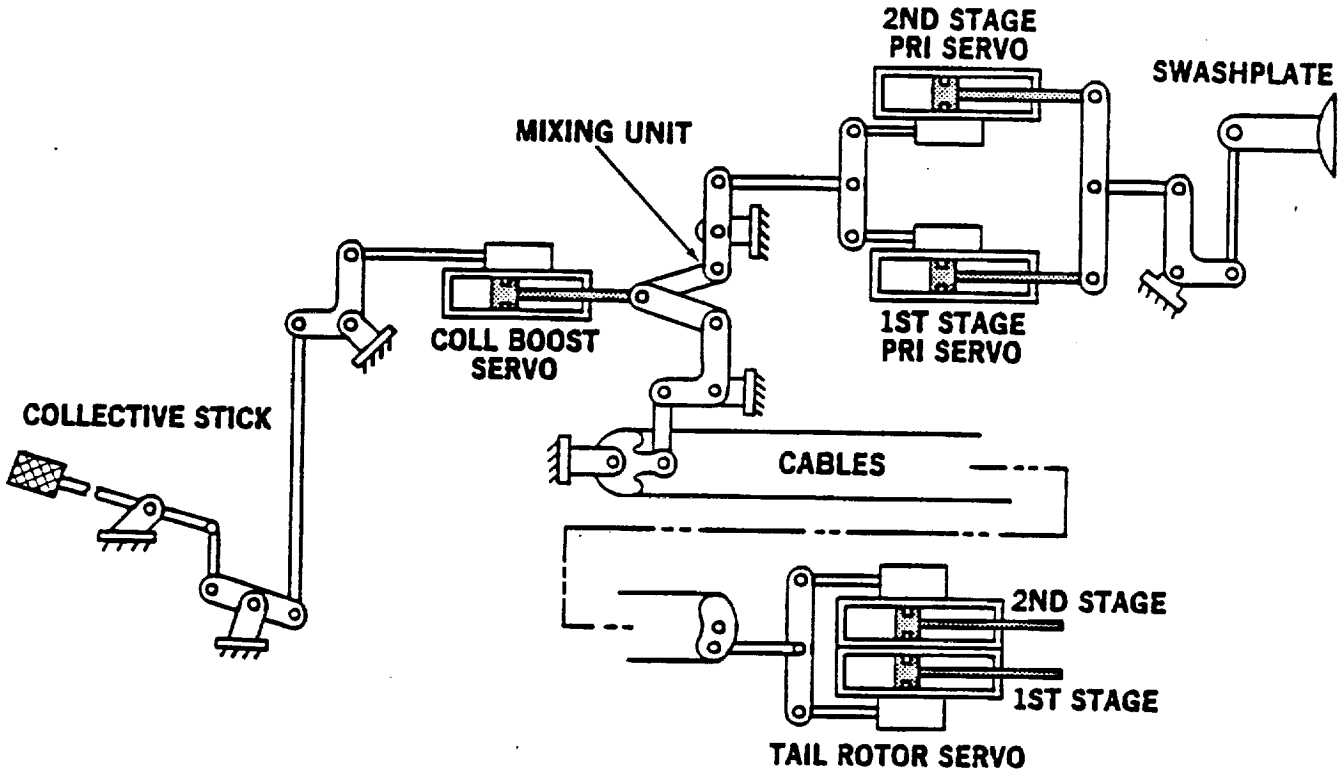

FIGURE 3.5.4 UH-60A BLACK HAWK PITCH FLIGHT CONTROLS BLOCK DIAGRAM

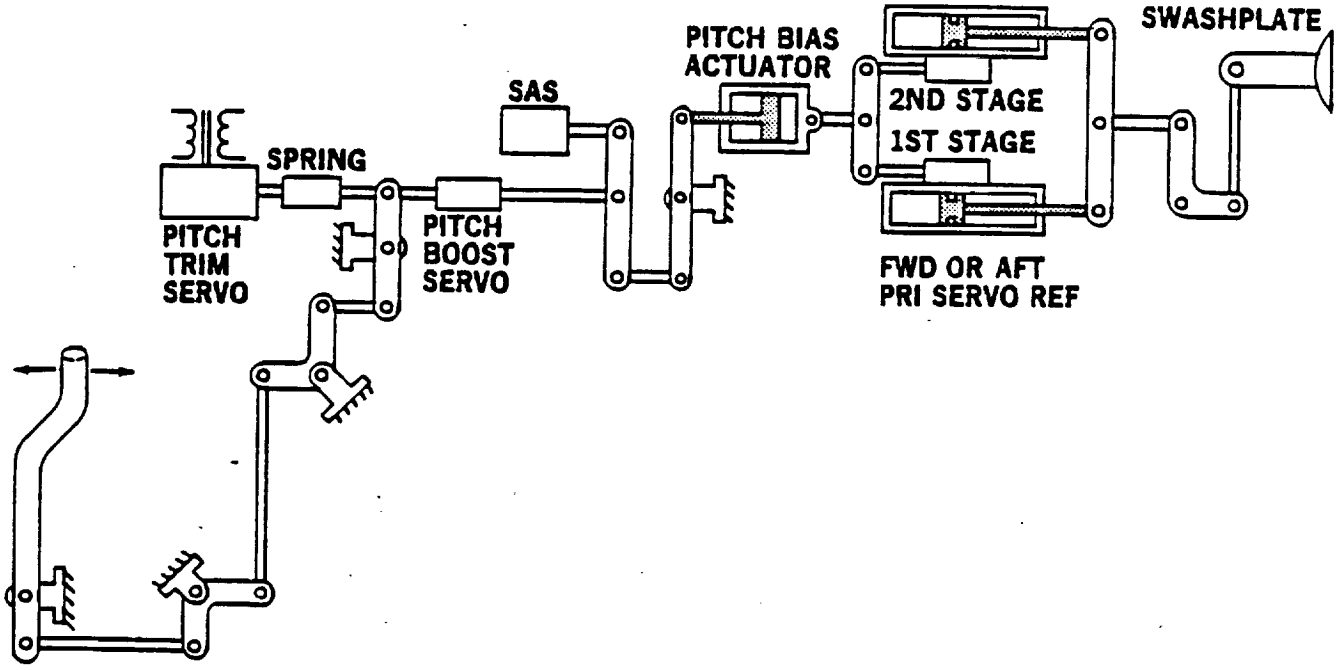

FIGURE 3.5.5 UH-60A BLACK HAWK ROLL FLIGHT CONTROLS BLOCK DIAGRAM

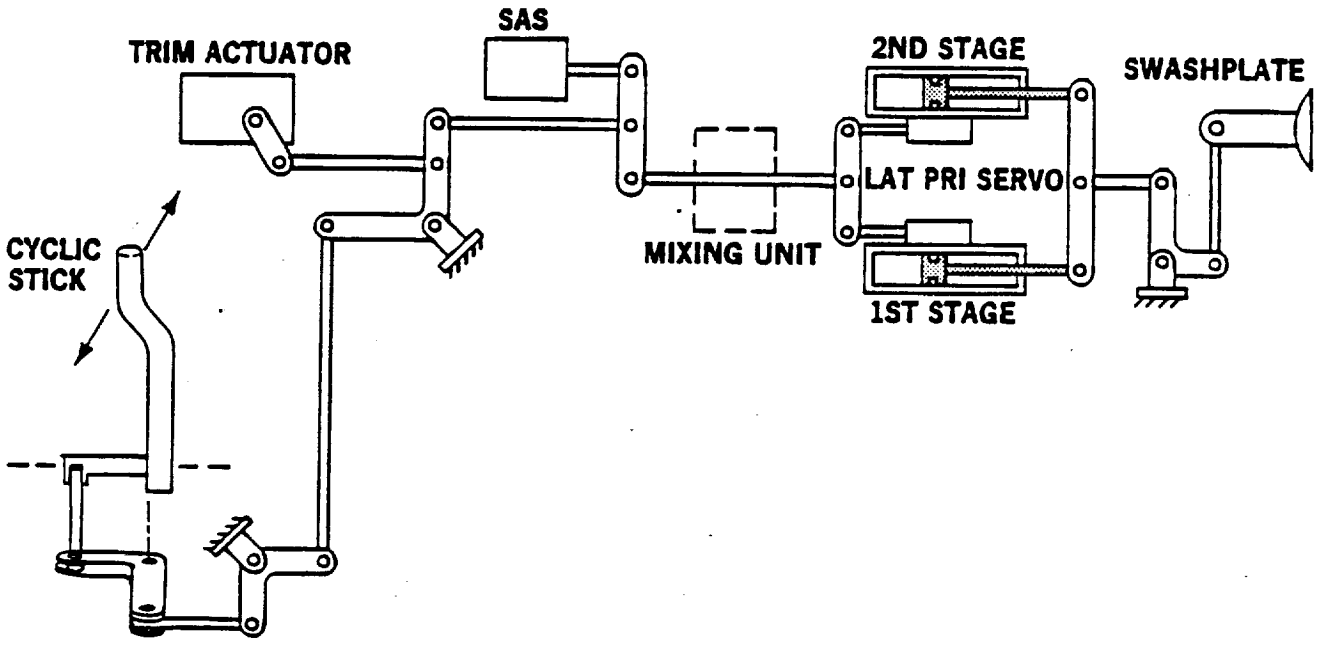

FIGURE 3.5.6 UH-60A BLACK HAWK YAW FLIGHT CONTROLS BLOCK DIAGRAM

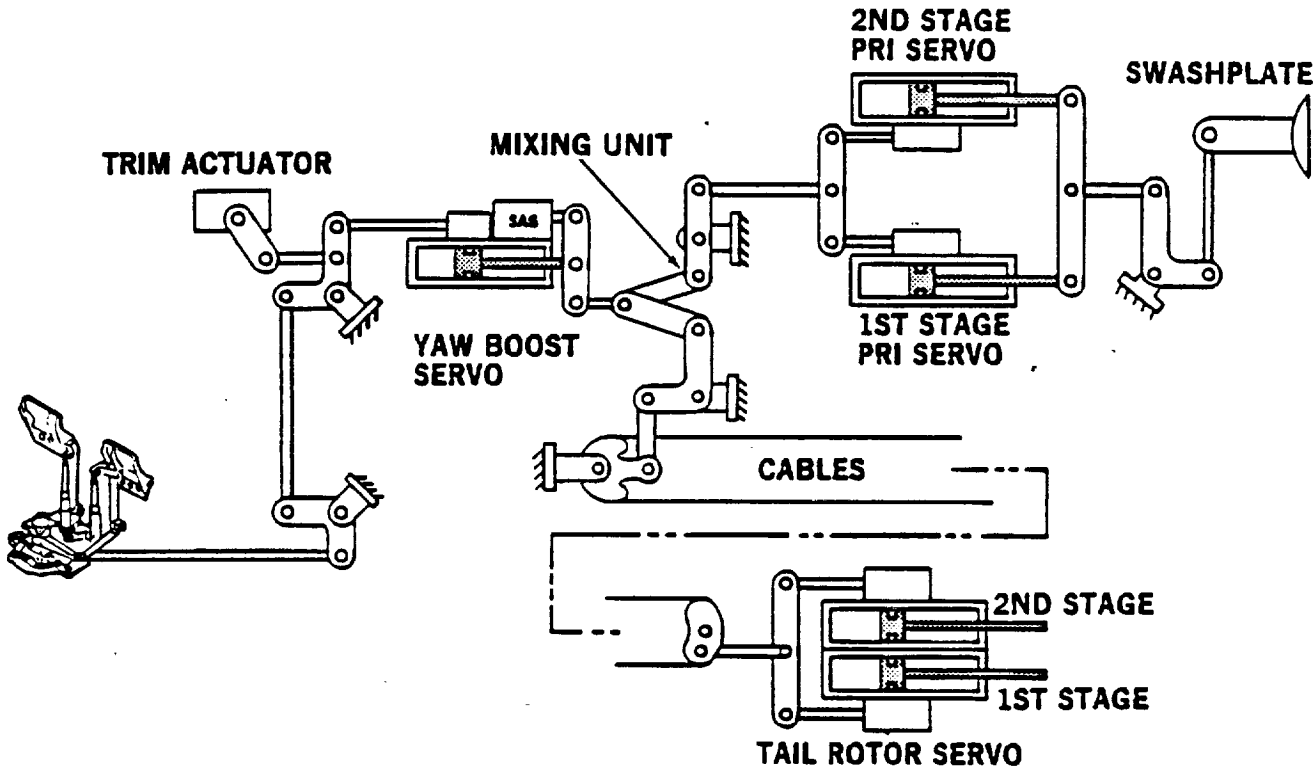

of total system control authority. The control authority of each is electrically limited to ±5 percent of total control travel in pitch, roll, and yaw. SAS inputs to the SAS servo valves are additive to provide a total authority of 10 percent. The sum is limited to ±10 percent authority by mechanical limits of SAS actuator travel. These two channels can be selected separately on the Automatic Flight Control Panel, Figure 3.5.7. If one channel is selected off because of a failure, gain in the 'ON' channel is doubled but the authority remains at ±5%.

c) Pitch Bias Actuator (PBA). The PBA is an integral part of the BLACK HAWK control system. The pilot has no control switch for this system in the cockpit. The purpose of the PBA is to improve the apparent static longitudinal stability for the aircraft through attitude and airspeed feedback. The PBA is, in effect, a variable length control rod which changes the relationship between longitudinal cyclic control and swashplate tilt, as a function of flight parameters. The attitude feedback covers the entire speed envelope. The airspeed feedback is only active between 80 and 180 knots. Below 80 knots, the high gain of the stabilator airspeed feedback, performs the stability function. In addition to the attitude and airspeed feedback, pitch rate feedback is also present. Hence, there is also position feedback to the longitudinal stick proportional to pitch rate. The authority of the PBA is 15 percent of longitudinal cyclic full throw and is limited by the computer to a maximum rate of 3 percent per second. 5.5-10

The functional relationship of the PBA relative to the rest of the control system can be seen on Figures 3.5.1, 3.5.2 and 3.5.4. PBA shaping is derived in the digital computer.

d) Flight path Stabilization (FPS). The FPS system provides the BLACK HAWK with outer loop stabilization through the pedals and the longitudinal and lateral stick trim actuators, as shown on figure 3.5.2. In addition, the FPS contains a coordinated turn feature which complements the SAS at speeds above 60 knots. 5.5-11 -12 -13

The FPS can drive the cockpit control to any position to which the pilot/copilot can trim the controls, resulting in a 100-percent FPS parallel control authority. The AFCS limits the rate of FPS within the maximum override force limits stated in the trim system section. Since FPS inputs drive the cockpit controls through the trim actuators, the TRIM must be ON in order to have FPS. The attitude hold function of the FPS is designed to maintain pitch and roll attitude, plus a desired heading. If TRIM is off the FPS

FIGURE 3.5.7 AUTOMATIC FLIGHT CONTROL PANEL

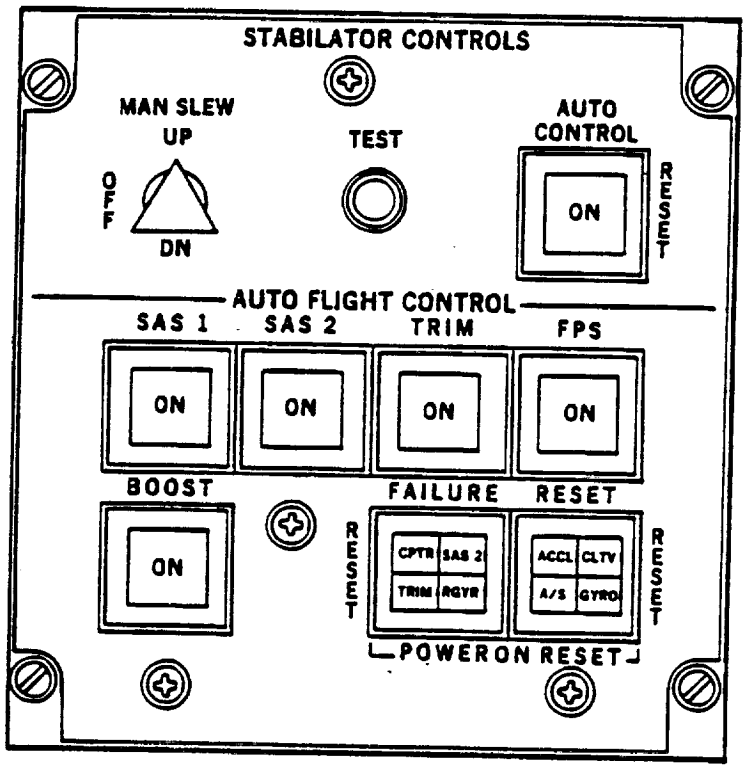

synchronizers are in a track mode and zero error is output. Thus, if the pilot wishes to change trim he can establish a new condition,then disengage TRIM, (which releases the force) then re-engage to have the new trim condition maintained by the FPS. At speeds above 30 knots the pitch axis of the FPS seeks to maintain the airspeed for which the trim attitude has been established. When the reference pitch attitude is changed, a time delay in the airspeed hold function allows time to stabilize at the new trim airspeed, prior to initiating the airspeed hold function. During this time the attitude hold function maintains the pilot-selected pitch attitude.

The FPS presented in the Flight Control module identifies the FPS switch, the 30 kts speed switch and the turn switch. These functions are desirable when using the model in an open loop analysis mode. When the simulation is developed for pilot-in-the-loop investigation the synchronizers must be linked to the trim switch. The FPS is activated by the pilot through a switch on the AFCS panel. (figure 3.5.7)

e) Mechanical Controls. The mechanical control system (essentially control mixing) of BLACK HAWK is shown in diagramatic form on Figure 3.5.8. It is designed to re duce pilot work load by mechanically coupling the controls to account for natural single rotor helicopter coupling responses to given control inputs. The following control couplings are incorporated. 5.5-14 -15 -16 -17

1. Collective stick to tail rotor blade pitch - an increase in collective requires an increase in tail rotor thrust to counter the main rotor torque change.

2. Collective stick to longitudinal cyclic - The center of gravity envelope for the BLACK HAWK lies entirely aft of the main rotor. Therefore, an increase in main rotor thrust from a collective stick increase, causes a nose up pitching moment. In addition, in forward flight, increasing collective causes a higher blade loading on the advancing blade relative to the retreating blade which causes the rotor to flap rearward imparting a nose up pitching moment. To compensate for these nose up pitching moments forward cyclic is coupled to an increase in collective stick.

3. Collective stick to lateral cyclic - The coupling of the collective stick to the tail rotor which is located above the c.g. also causes a right rolling moment. An increase in collective stick increases the main

FIGURE 3.5.8 UH-60A BLACK HAWK FLIGHT CONTROL MIXING UNIT SCHEMATIC

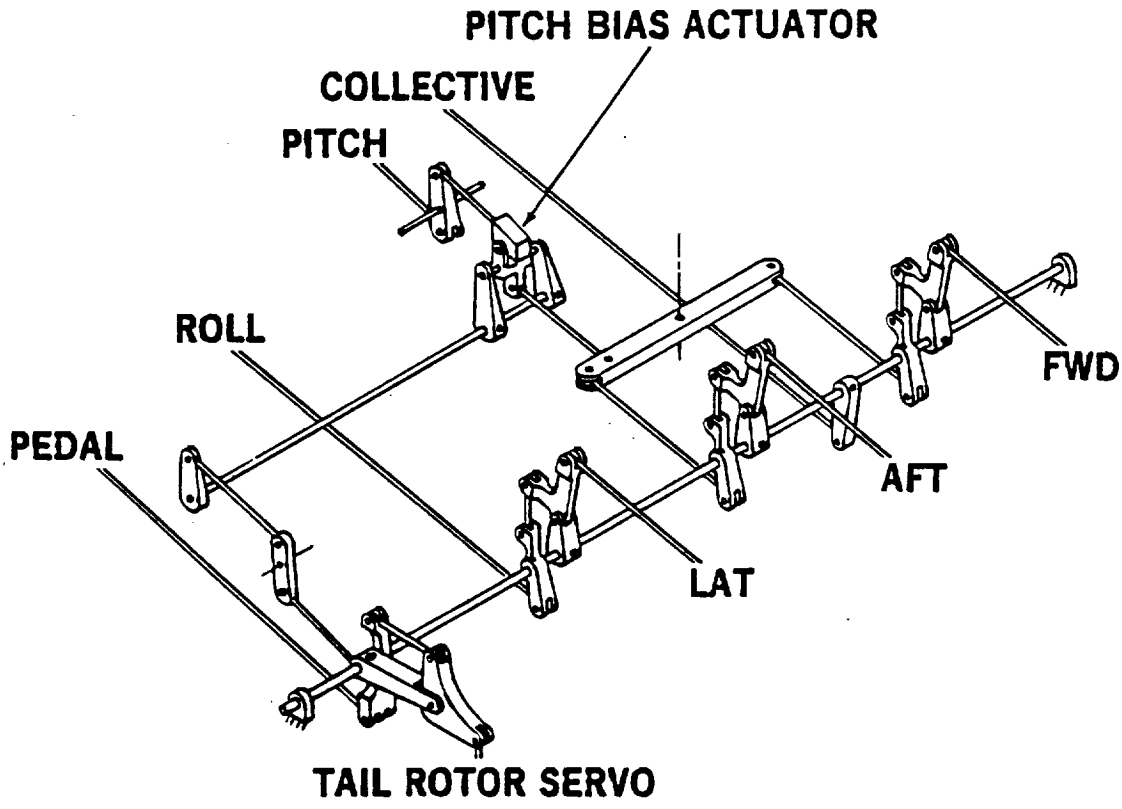

rotor coning which gives an effective increase in the angle-of-attack of the blade over the nose, thus increasing the blade loading. Since the flapping reaction occurs approximately 90 degrees of azimuth later, the rotor flaps to the right causing a right roll. To compensate for these right rolling moments, left lateral cyclic is coupled to an increase in collective stick.

4. Pedal to longitudinal cyclic - Pedals are coupled to the longitudinal cyclic to automatically compensate for the pitching moment caused by the canted tail rotor when pedal position is varied.

The high level of control mixing, together with the various control stops, results in irregular limits on control motion. The control rigging input provided for the control system in Volume I is linear. It does not contain any of these irregular "Cut-offs". Typical BLACK HAWK rigging diagrams are provided on figures 3.5.9, 3.5.10 and 3.5.11 for longitudinal cyclic, lateral cyclic, and tail rotor blade pitch, respectively. It can be seen that corners of the rigging envelope are clipped by various stops in the control system. This loss of travel could be important to pilot-in-the-loop simulation evaluations. It should be emphasized that the rigging diagrams provided are nominal and may not compare exactly to any given BLACK HAWK helicopter. 5.5-20

Two approaches are used in representing the actuators in the Flight Control Module depending on information available. If the actuator is not rate limited and experimental data is available then a second order transfer function is matched to the frequency characteristics. Otherwise, a simplified actuator model is used as shown on the simulation block diagrams in Volume I.

f) Stabilator - The BLACK HAWK helicopter has a moving stabilator, the position of which is dependent on a number of feedbacks. These include airspeed, collective, pitch rate and lateral acceleration. The schedule of these feedbacks was selected to satisfy a number of requirements. In low speed maneuvers a stabilator incidence as high as 40 degrees is required to reduce the impact of rotor downwash on the stabilator with its associated high aircraft nose attitudes. In the normal speed range from 80 knots to V_H effectively a constant stabilator value of zero 5.5-18

FIGURE 3.5.9 LONGITUDINAL CYCLIC RIGGING

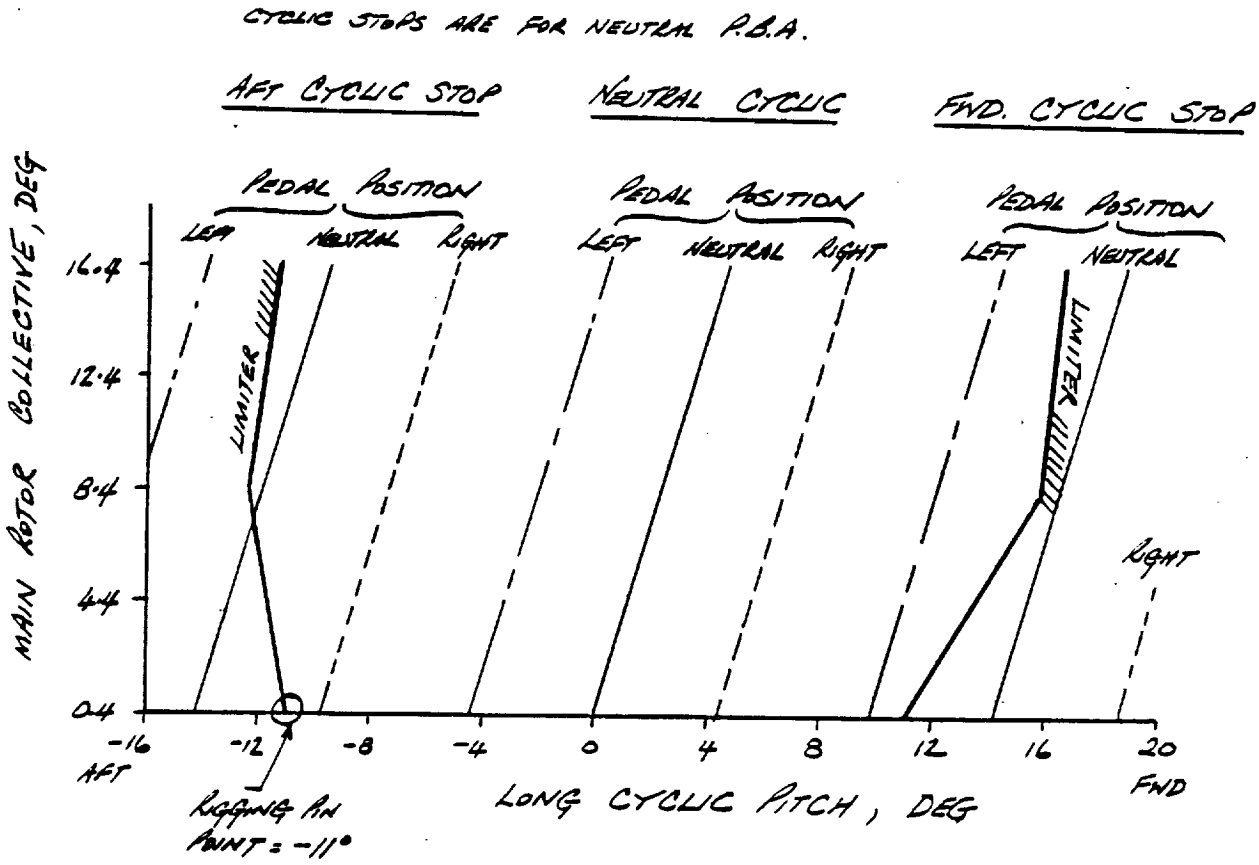

FIGURE 3.5.10 LATERAL CYCLIC RIGGING

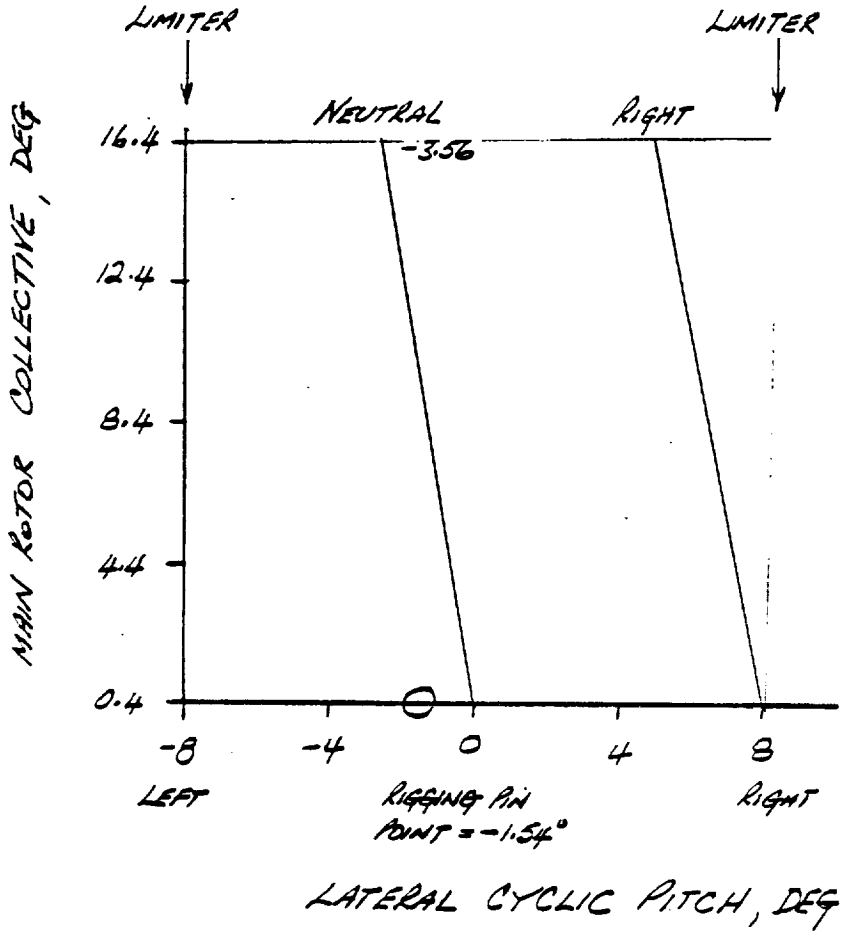

FIGURE 3.5.11 TAIL ROTOR CONTROL RIGGING

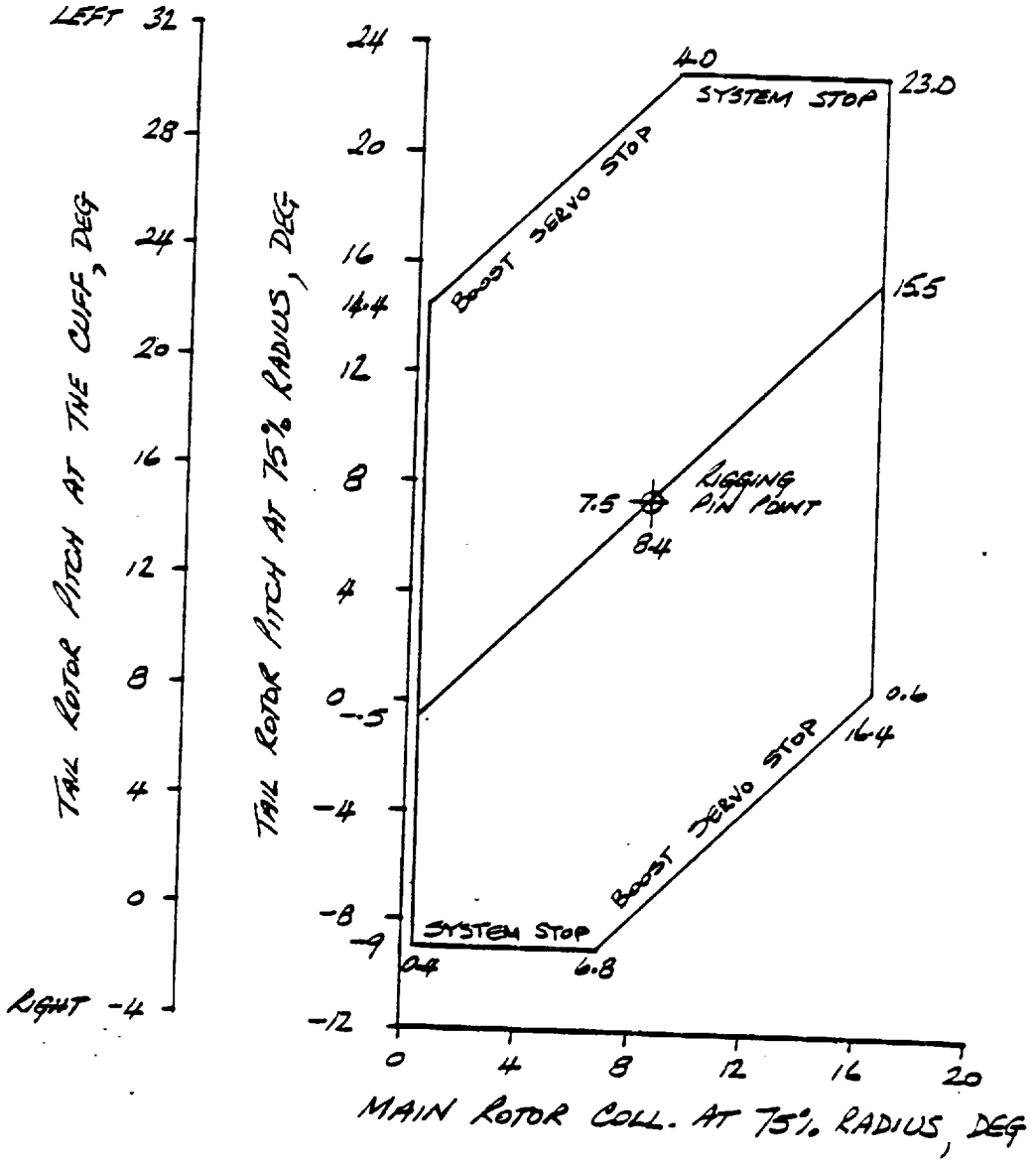

degrees provides satisfactory aircraft pitch attitudes and levels of flapping through the weight - c.g. envelope. The steep gradient of stabilator incidence with airspeed from 40 to 80 knot is a necessary transition slope.

The requirements for the collective feedback are based on the need to reduce the pitch attitude excursion with collective inputs in forward flight over that accomplished by the mechanical coupling previously discussed. The pitch rate feedback is primarily effective in improving the BLACK HAWK maneuver stability (stick force per g) in turns. As the aircraft enters higher load factor turns the pitch rate increases driving the stabilator more leading edge up and therefore the aircraft more nose down. This in turn requires the pilot to displace the longitudinal cyclic stick further aft from trim in order to keep the nose up. Since the force system is effectively a spring force which is proportional to displacement from trim, the higher the g level the higher the stick force. The lateral acceleration feedback is added to the stabilator system to counter coupling of pitch attitude with sideslip.

The stabilator system is composed of two analog amplifiers (see figure 3.5.2) which operate from independent input sources and command the position of two electric jackscrew actuators acting in series. During normal operation these jackscrews operate in unison, with each providing one-half of the stabilator position input. The system is independent of other SAS/FPS subsystems although it shares common inputs. The system is activated from a switch on the AFCS panel (figure 3.5.7). The pilot can activate a manual slew at any time.

g) Trim System - As previously discussed the trim system is not directly applicable to the simulation being used in an open loop, analysis mode. However, it will form an integral part of pilot-in-the-loop system. The validity of the system in the simulation will be critically dependent on the capability of the simulator cockpit stick force system. The background information presented here is applicable to Section 6.0 in Volume I.

The trim system provides control centering about a position selected by the pilot, a spring breakout force plus gradient, and a pedal damper force. The

system is activated by a switch on the AFCS control panel (figure 3.5.7).

With the trim system selected OFF there is no control force gradient or control centering in the cyclic control system or directional control system. Directional control movements will still be resisted by a pedal damper. This damping force is continuously active without regard to TRIM switch position. With the trim system ON, directional and lateral control forces are developed in the electromechanical trim actuators. These actuators incorporate an electrically controlled rotary spring assembly which allows the pilot to select the zero force control trim position. The designed maximum override force for full opposite control position, is 80 pounds in directional and 19 pounds in lateral cyclic control. Longitudinal cyclic control forces are developed in an electrohydromechanical pitch trim actuator with a designed maximum override force of 20 pounds.

With the trim system selected ON and FPS OFF, the pilot/copilot may change the cyclic trim control position through two means: a cyclic trim release switch and cyclic beep trim switch. The beep trim switch is a four-position switch mounted on the cyclic stick grip. Activation of the trim release button switch releases the force gradient on the longitudinal and lateral cyclic. The position of the cyclic control when the trim release switch is opened (released) becomes the new cyclic trim position. At airspeeds below 60 kts, when the pedal switches are closed, the electronic control on the yaw force gradient spring is repositioned by pedal movement and resisted only by the pedal rate damper. When the pilot removes his feet from the pedals which releases the pedal switches, the electronically controlled rotary spring reengages, holding the pedals at the new trim position through the pedal breakout, plus gradient spring. Above 60 kts the pedal switches and the TRIM REL switch together provide yaw trim release.

3.6 ENGINE/FUEL CONTROL MODULE

3.6.1 Engine/Fuel Control System

Prior to presenting a description of the engine/fuel control simulation a short description of the T700 system is presented. It should be noted that features in the actual engine described

below (for completeness sake), may or may not be represented in the simulation. The following information is extracted from Reference 24.

The General Electric T700-GE-700 is a compact, lightweight turboshaft engine rated at 1543 horsepower. It has a combination axial/centrifugal compressor, an annular combustor with central fuel injectors, an air-cooled gas generator turbine, and a free power turbine with a coaxial drive shaft extending forward through the gas generator. The forward end of the drive shaft is connected, via a splined joint, to the engine output shaft assembly. The compressor has variable stator vanes. These components are illustrated schematically on figure 3.6.1. Basic T700 engine data characteristics are given on Table 3.6.1.

The engine control system from the pilots point of view is comprised of four primary elements. Power control system; Load Demand System; Engine Speed Trim Control System and Overspeed protection. The power control levers in the cockpit (figure 3.6.2) are connected to the power available spindles (PAS) on each engine's hydromechanical unit (MHU). Each power control lever has four detent positions; OFF, IDLE, FLY, and LOCKOUT. The power lever is advanced to FLY for flight. The PAS setting represents the highest power that could be supplied if demanded. Power turbine speed is not governed until the power lever is advanced from IDLE. The simulation assumes that the PSA is always in the FLY position. This simplifies the engine simulation module with no loss to fidelity for handling qualities evaluations.

TABLE 3.6.1

Model	General Electrical T700-GE-700
Type of Engine	Turboshaft
Output Power (intermediate rating)	1543 shp at sea level, standard static uninstalled conditions
Type of Compressor	Combined axial/centrifugal
Number of Compressor Stages	6 stages, 5 axial and 1 centrifugal
Variable Geometry	Inlet guide vanes, stage 1 and 2 stator vanes
Type of Combustion Chamber	Single annular chamber with axial flow.

FIGURE 3.6.1 T700 ENGINE SCHEMATIC

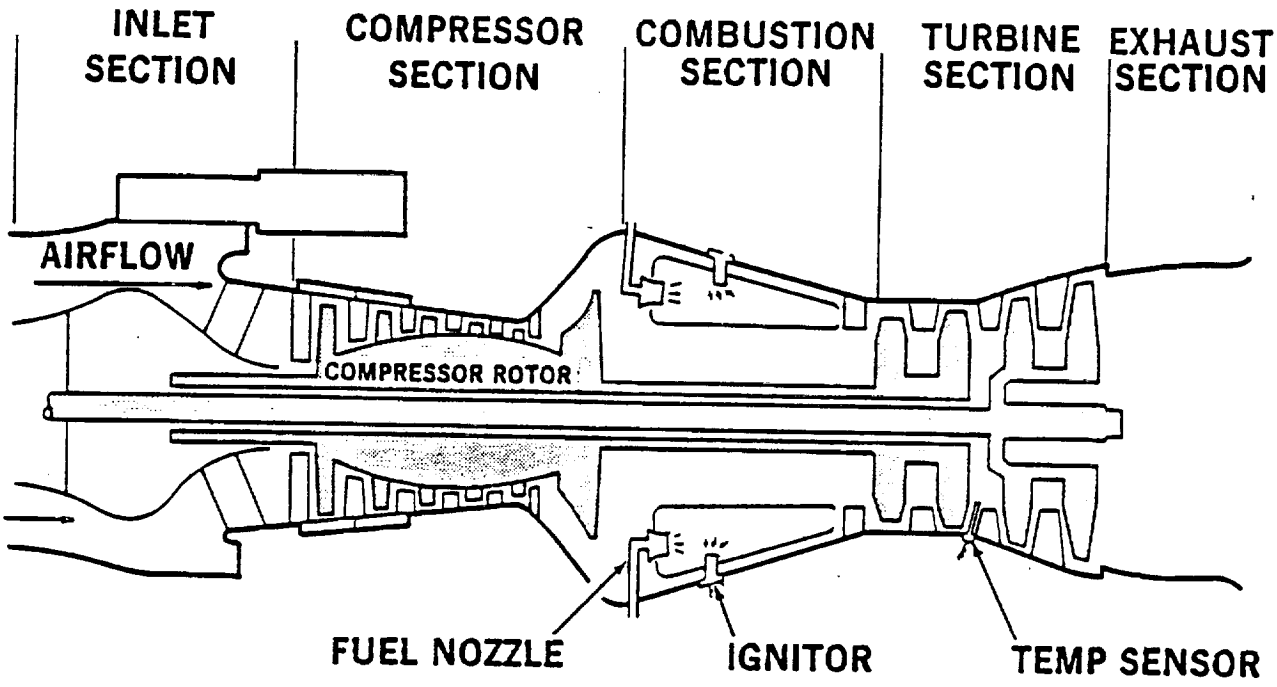

FIGURE 3.6.2 ENGINE CONTROLS

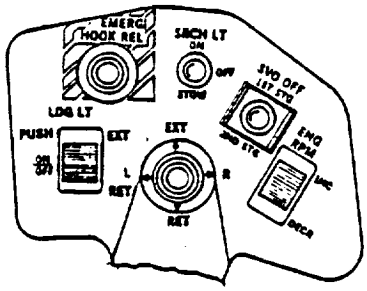

COLLECTIVE STICK

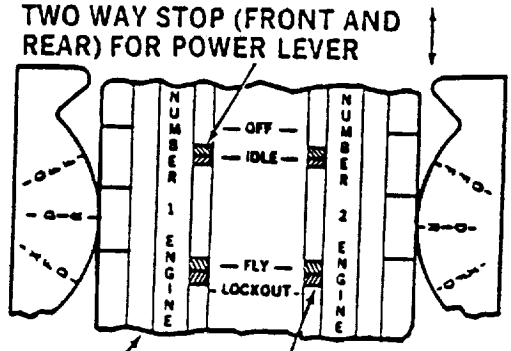

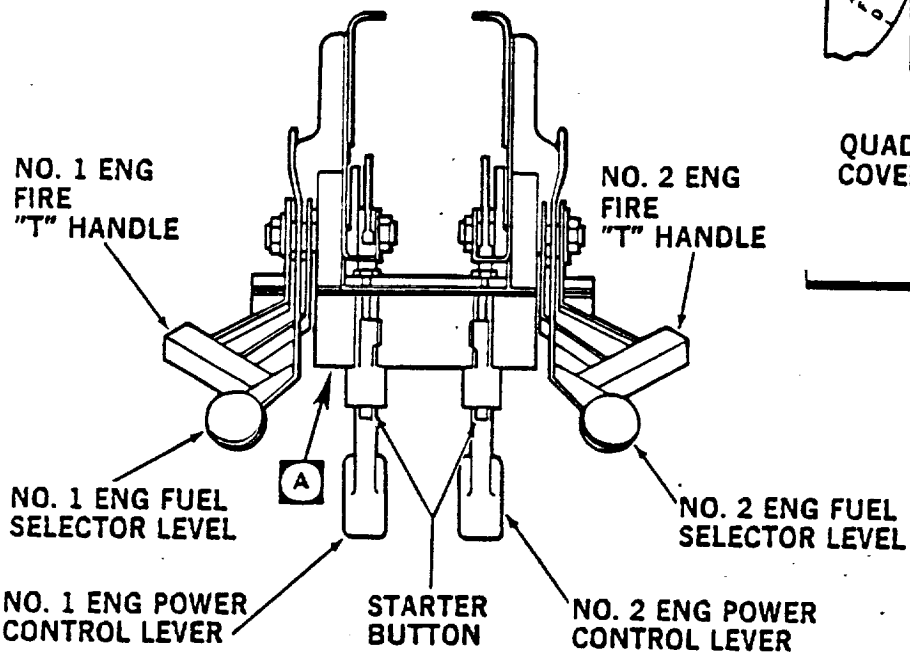

TABLE 3.6.1 (Continued)

Gas Generator Turbine Stages	2
Power Turbine Stages	2
Direction of Engine Rotation (from rear, looking forward)	Clockwise
Engine Weight (dry)	415 lb

The Load Demand Spindle (LDS) input is a function of the collective pitch. It provides compensation to reduce transient droop of N_p. The spindle, inputs load demand signals directly into the hydromechanical unit. A reduction in collective pitch decreases LDS position, reducing fuel flow and giving immediate and accurate gas generator response. The new setting is trimmed by the ECU to satisfy the Np/Nr and load control requirement set by the Electrical Control Unit (ECU). This function is represented in the simulation.

The speed control system allows the pilot to adjust Np/Nr between 96.4% and 100.5% by activation of the beeper trim switches on the pilot's collective grip as shown on Figure 3.6.2. The engine Np/Nr speed reference signal, sets the datum for the Electrical Control Unit (ECU). An overspeed protection system protects the power turbine from destructive overspeeds. If a malfunction should cause Np to reach 106%, the electrical overspeed system will automatically decrease fuel flow to the engine as necessary to prevent Np/Nr from exceeding 106%. This feature is not represented in the simulation. For those area's of simulation operation where overspeed could be experienced (Burst from autorotation for example) caution should be exercised during analysis of the results.

The engine control quadrant, figure 3.6.2, centered on the upper console permits either the pilot or copilot to select engine speed. The ENG POWER CONT lever positions are marked NUMBER 1 ENGINE and NUMBER 2 ENGINE, and identify the OFF, IDLE, FLY and LOCKOUT positions. They are connected mechanically to each engine's HMU and are used to govern engine speeds. The HMU starts to open whenever the power control lever is advanced more than 2° from OFF and increases proportionately with engine speed to FLY.

3.6.2 Detailed Description of the Engine/Fuel Control Module

Historically the rotor shaft speed degree of freedom has been ignored by flight dynamics simulation models. It was expedient to fix rotor speed at a nominal value and avoid the (computing) problems associated with releasing the rotor shaft degree of freedom. Under some circumstances this is still acceptable. However, there is now increased awareness of the consequences, as discussed in Reference 2. These include differences in initial response to control input and interactions with airframe modes. The former results from the energy initially absorbed by the shaft degrees of freedom. The latter is due to phase lags between rotor speed response and torque reaction on the airframe.

The engine/fuel control module developed for this simulation is a linearized representation of the T700 system, with coefficients which vary as a function of engine operating condition. All the usual restrictions and assumptions of linear simulation are applicable and should be observed. Maneuvers which result in large torque changes from trim may result in discrepancies in the simulation. In the future development of the model, for pilot-in-the loop simulation, an artifice must be created for tracking and updating the steady state engine torque levels and fading them with those generated from the linear model. The engine is assumed to be operating in a sea level environment. One engine/fuel control system is represented and the total torque is obtained by doubling that for a single engine. Torque balance control is therefore eliminated. The model ade quately provides for closing the rotor shaft speed loop through out the normal operating envelope of the helicopter. However, it is emphasized that engine/fuel control systems are highly nonlinear. Therefore, maneuvers which result in significant rotor speed excursions may result in discrepancies in the sim ulation. Typically, the simulation does not represent temper ature or engine speed limitations and the acceleration schedule is a fixed value. This module should not be used for engine performance evaluations. More complex engine/fuel control representations are available and the modular formulation of the BLACK HAWK simulation facilitates their introduction, if required, at a later time.

The basic engine control system operation is through the interaction of the Electrical Control Unit (ECU) and Hydromechanical control unit (HMU). In general, the HMU provides for gas generator speed control and rapid response to power demand. The ECU trims the HMU to satisfy the requirements of the load so as to maintain constant rotor speed. The Load Demand Spindle (LDS) is a function of collective pitch setting and provides

compensation to reduce rotor transient droop. Any steady state errors resulting from inconsistent collective positioning are trimmed by the ECU. In general, isochronous governing of the rotor speed is maintained by developing an error relative to the reference speed and commanding more or less power to stabilize at the required speed. Basically, this process involves the speed error demanding a change in gas generator speed via the shaping of the ECU electrical newwork. This signal is summed with the LDS input in the HMU, and compared with the actual gas generator speed. The subsequent error, commands changes in fuel flow leading to a higher or lower gas turbine speed and changes in the gas flow. This in turn provides increased or decreased power at the driveshaft from the power turbine. A detailed background to the complete T700 engine/fuel control system is given in References 25 and 26.

Engine/Fuel Control Simulation Representation

The major elements of the simulation of the engine/fuel control are shown on the simplified block diagram, figure 3.6.3. They comprise the collective control interface with Gen Hel, fuel control, gas turbine, power turbine and rotor shaft speed degree-of-freedom interface with the Gen Hel rotor. In this model, the simplification of linearization has been retained at the same time as providing a reasonable envelope of operation, by allowing the linear coefficients to vary as a function of gas generator speed.

Initialization of the engine/fuel control module is accom-plished by using the steady state engine performance required to trim the helicopter simulation in free flight. Specifically engine output torque can be plotted as a function of gas generator speed. Hence, inverting this relationship, allows the direct determination of gas generator speed to trim the torque required by Gen Hel, to maintain reference rotor shaft speed. (This torque is specified at rotor shaft speed) Now, if the load demand spindle input from collective was ideally matched to the operating condition, it would set the HMU such that the engine would be in trim. However, differences are usually present which must be trimmed by the ECU. The balance conditions for I.C. are forced in the simulation by making the power turbine speed equal to the reference speed and arranging that the incremental demand on the fuel control, $(\Delta NGG)_{REF}$, is equal to zero. The error falls out as a trim bias on the ECU. The IC flow path is shown as dotted on figure 3.6.4. The other prerequisite of trim, is that engine torque supplied must equal that required by the rotor, such that no accelerating torque exists on the shaft in the IC mode. 5.6-9

FIGURE 3.6.3 ENGINE/FUEL CONTROL INTERFACE WITH THE ROTOR

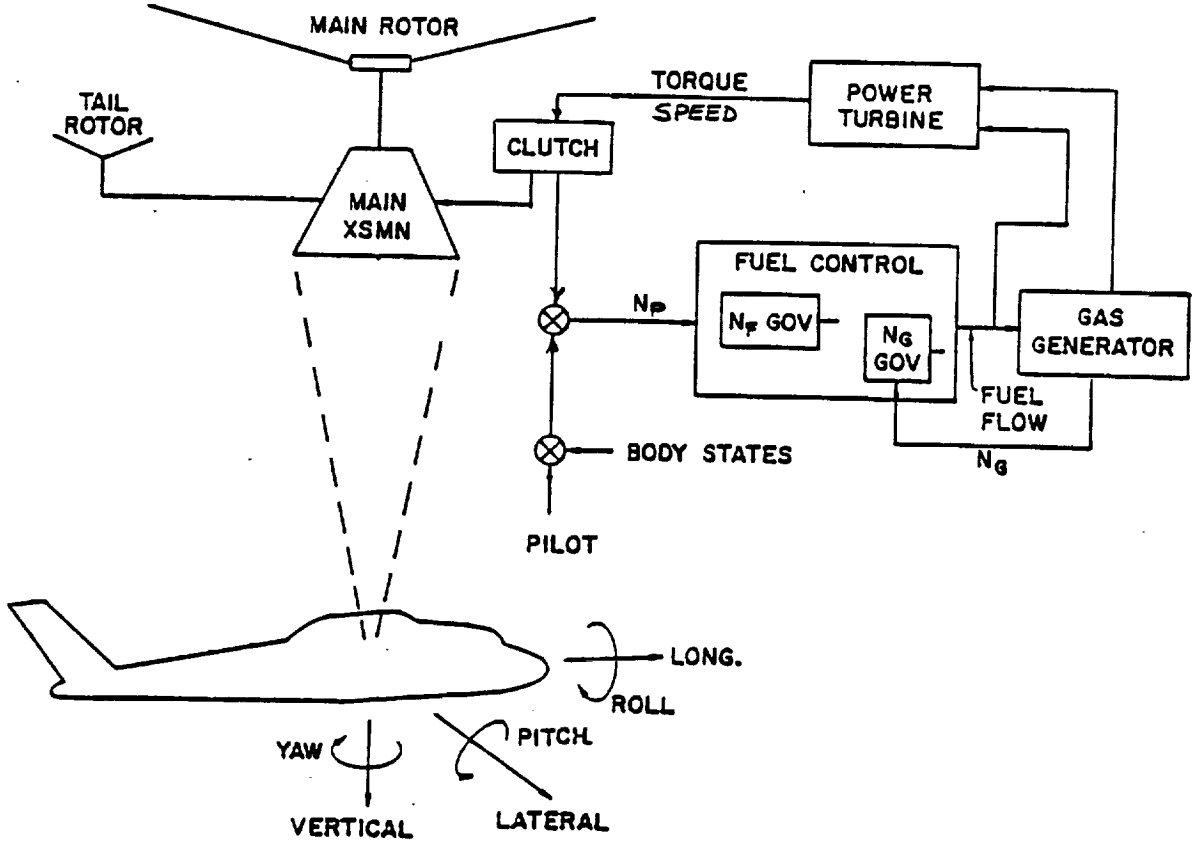

FIGURE 3.6.4 ELECTRIC CONTROL UNIT (ECU)

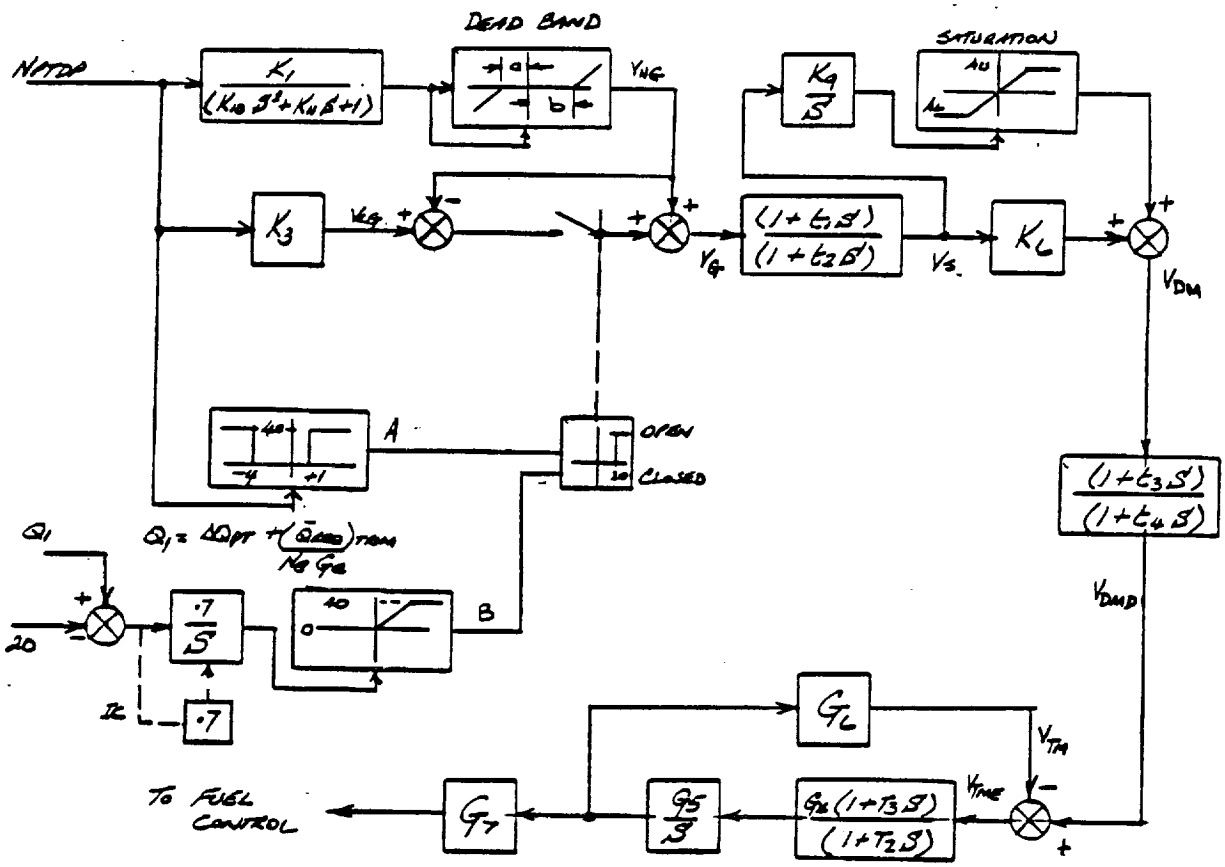

In the compute mode, any excursions in power turbine speed will result in outputs from the ECU, which will modulate fuel flow. If the helicopter is flown from a low power operating condition to a higher level, gross changes in fuel flow are commanded by the collective compensation. The ECU will adjust to compensate any mismatch which would lead to power turbine speed (rotor speed if the clutch is coupled) excursions. The computational flow for the ECU is given in analog form on figure 3.6.5. There is essentially a high, or low, gain loop active, depending on speed error and torque level. 5.6-11 -12 -13

The gas generator speed required to match the torque demand is set in the HMU. In the simulation this set signal is a perturbation from trim which is compared with the actual gas generator change in speed from trim. The error causes an incremental change in fuel flow which accelerates the gas turbine, as shown on figure 3.6.4. 5.6-14 5.6-15

In the model, torque output from one engine (ΔQpt) is derived from three sources. From direct changes in fuel flow, from changes in gas generator speed and as a result of changes in power turbine speed. This latter term is turbine damping. These increments are summed to obtain a total change in engine torque from trim, which is subsequently factored by the number of operating engines and engine/rotor gearing ratio, to obtain engine torque output to the rotor shaft. This increment is also used to provide the torque reaction on the airframe (which is incorporated into the main rotor module for computing convenience). 5.6-16

Rotor Speed Degree of Freedom

The interface of the engine with the main rotor (it should be noted that tail rotor torque is not calculated and is accounted for approximately by factoring main rotor required torque) is via a free running clutch which will disengaged the rotor from the engine at a zero torque level. Under these circumstances, the engine speed feedback to the fuel control will cause the engine to seek an operating condition dictated by the control. The clutch will reengage when the rotor speed drops below power turbine speed as shown on figure 3.6.6. The introduction of a clutch in the drive system allows autorotation entries and recoveries to be executed. 5.6-17 -18

The rotor can be visualized in simple terms as a damper responding to changes in rotor speed. However, the significant effect of the rotor relates to the changes in torque loading as a result of control inputs and changing states. Rotor shaft accelerations result from torque differences in output from the power turbine and torque required by the rotor. The simulation

FIGURE 3.6.5 ENGINE/FUEL CONTROL BLOCK DIAGRAM

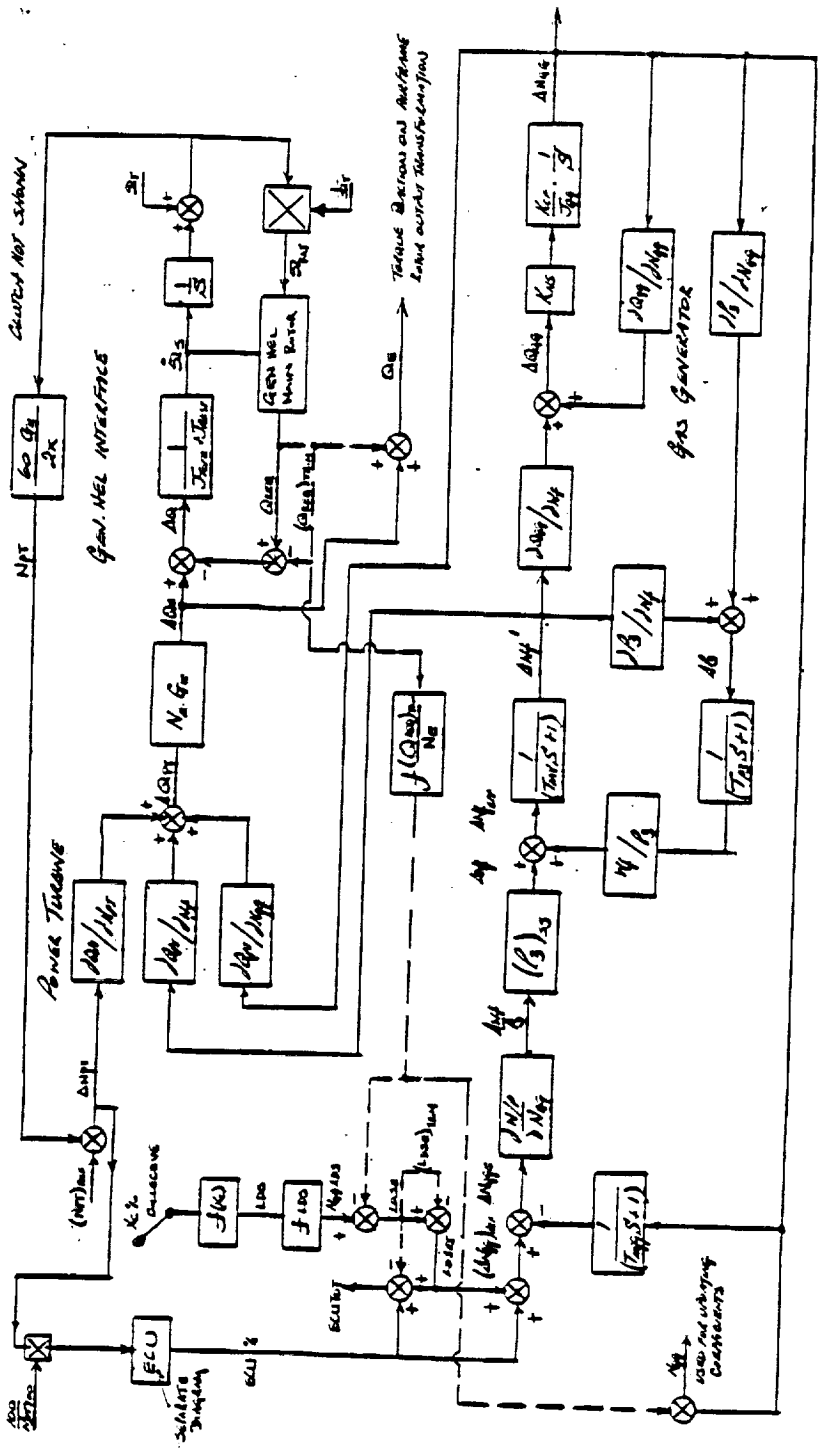

FIGURE 3.6.6 ROTOR DEGREE OF FREEDOM CLUTCH MODEL

ORIGINAL PAGE IS
OF POOR QUALITY

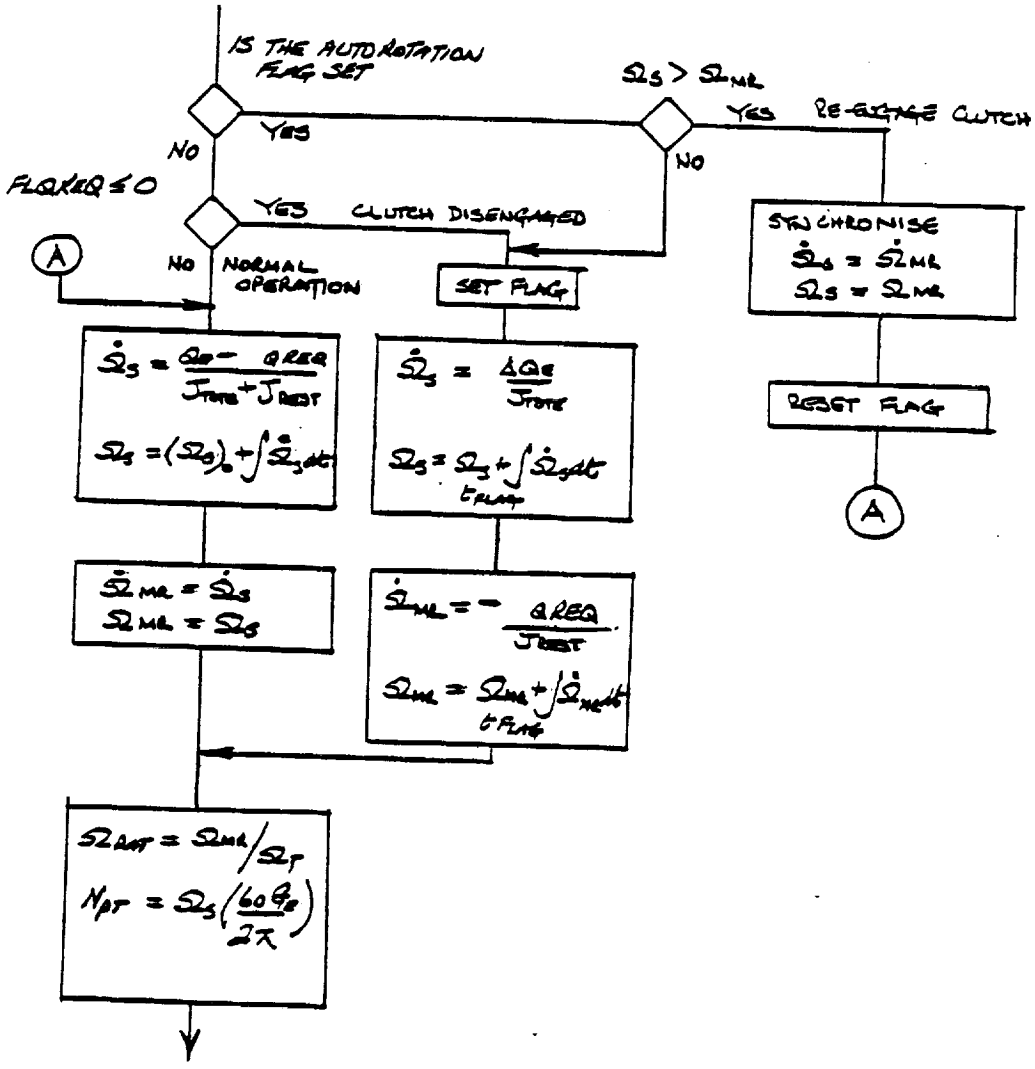

is initialized at trim such that the rotor is at the input speed and torque is in balance. Under normal powered flight conditions the clutch is locked and the difference between engine torque and rotor required torque must accelerate the total transmission inertia. (Note this inertia does not include rotor blades. They are separate bodies, with their own degrees of freedom) Under these circumstances, power turbine speed and rotor shaft speed are equal, as shown on the block diagram, figure 3.6.6. Each program pass, the rotor required torque is checked to see if it drops below zero. If it does, the clutch disengages, and a different flow path is executed, in which the power turbine and rotor shafts accelerate under their own torques and inertias. Because of the harmonic characteristics of rotor torque, it is necessary to perform the logic check for zero torque level on a filtered signal. In coding the clutch model, care must be taken to ensure that, if a trim in autorotation with split needles is requested, the appropriate flow path and initialization of shaft speed and rotor speed are executed. A detailed flow diagram of the clutch model is presented on Figure 3.6.7(a) and (b).

3.7 LANDING INTERFACE MODULE

3.7.1 Overview of Landing Interface Module

This module calculates the forces and moments at the airframe C.G. resulting from landing gear interaction with the ground plane. All necessary space/body axes geometry calculations are incorporated in order to track a free helicopter landing on the ground. The landing gear is represented by separate non-linear tire and strut dynamic characteristics as shown in Figure 3.7.1. Tire in-ground-plane loads are developed as a non-linear function of the tire deflection and normal load. These forces are adjusted depending on the friction criteria which determines tire skid characteristics at the deck surface. Finally, strut loads are summed with other external forcel and moments at the helicopter CG.

3.7.2 Detail Description of the Landing Interface Module

Two axes systems are used in this landing interface module as shown in Figure 3.7.2. All landing gear forces and moments are formulated in axes parallel to the primary body axes system passing through the C.G. The space axes system, of which the ground plane is set at WLFD, is used to determine the landing gear proximity to the ground. Inplane friction forces are checked in the space axes system.

FIGURE 3.6.7(a) ROTOR CLUTCH MODEL - DETAILED PROGRAM FLOW DIAGRAM

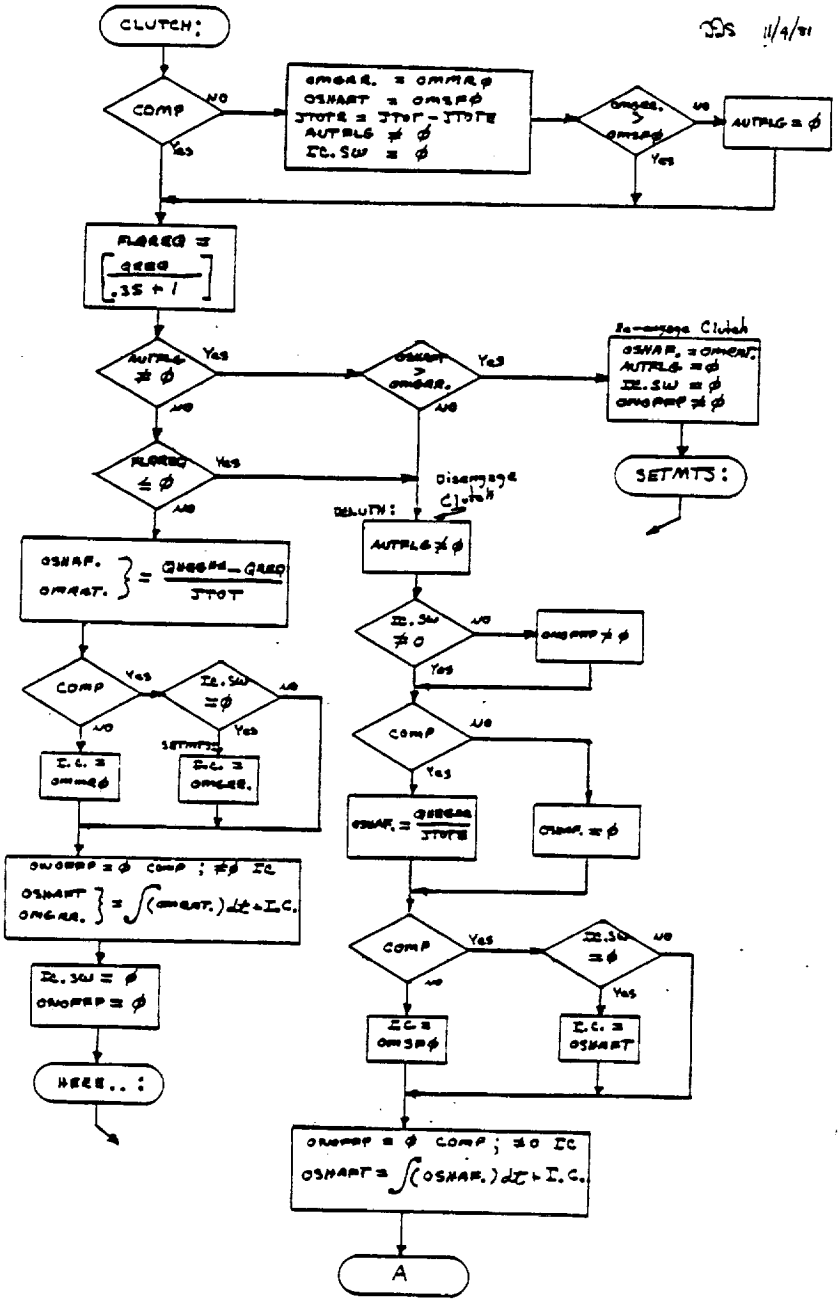

FIGURE 3.6.7(b) ROTOR CLUTCH MODEL - DETAILED PROGRAM FLOW DIAGRAM (Cont'd)

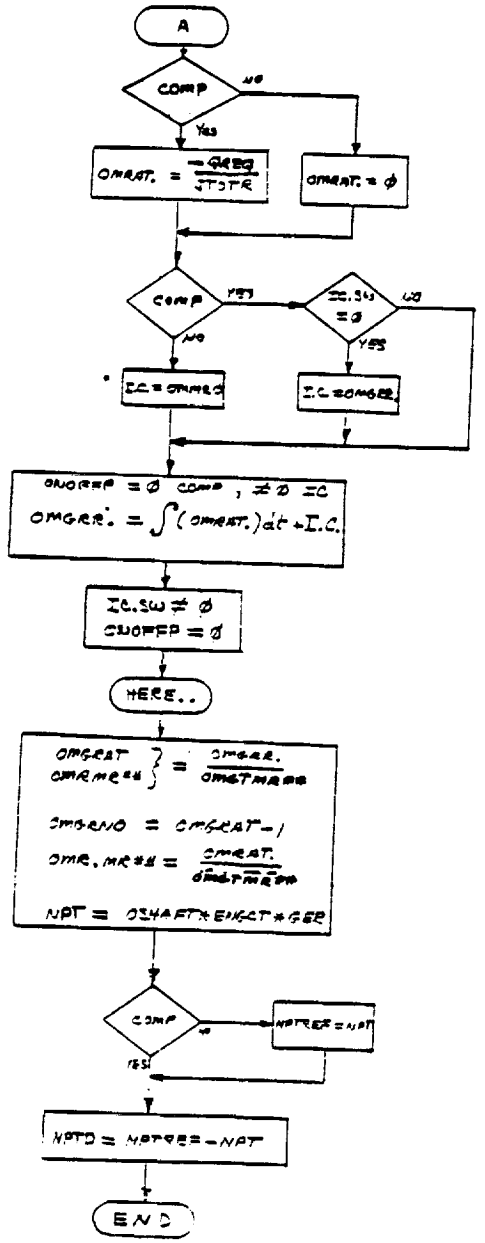

FIGURE 3.7.1 LANDING GEAR TIRE AND STRUT REPRESENTATION

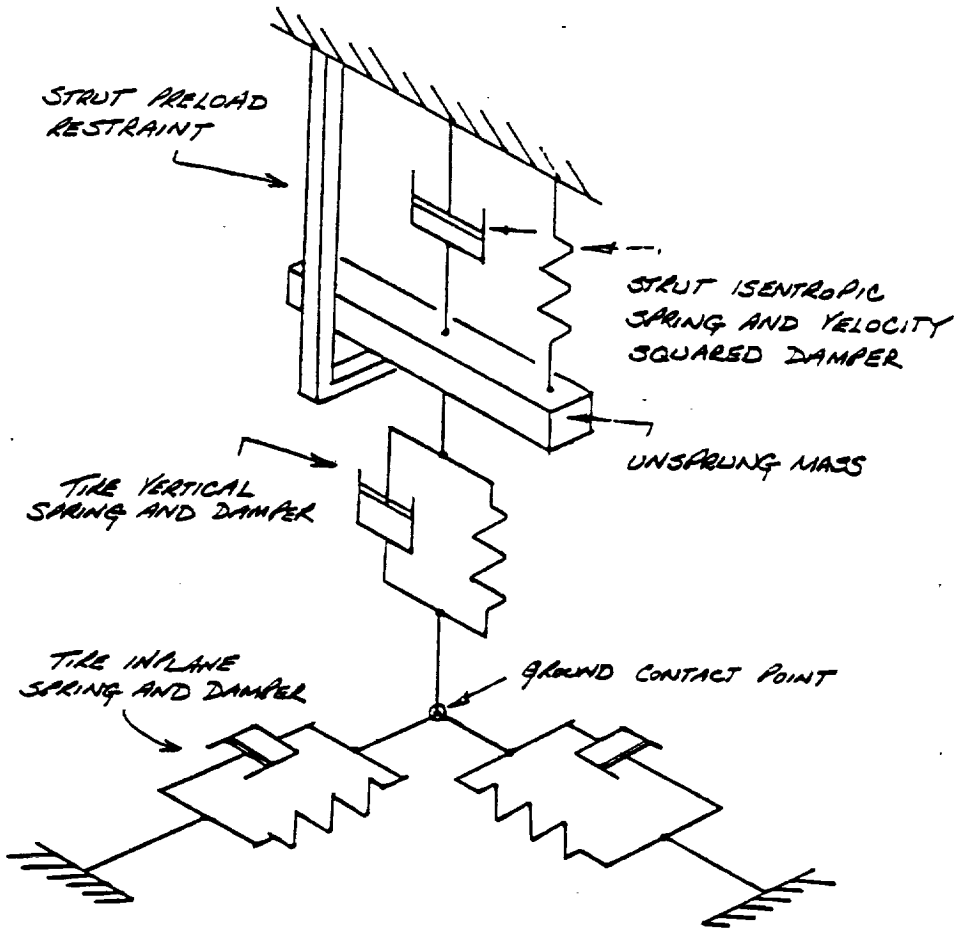

FIGURE 3.7.2 LANDING MODULE AXES SYSTEM

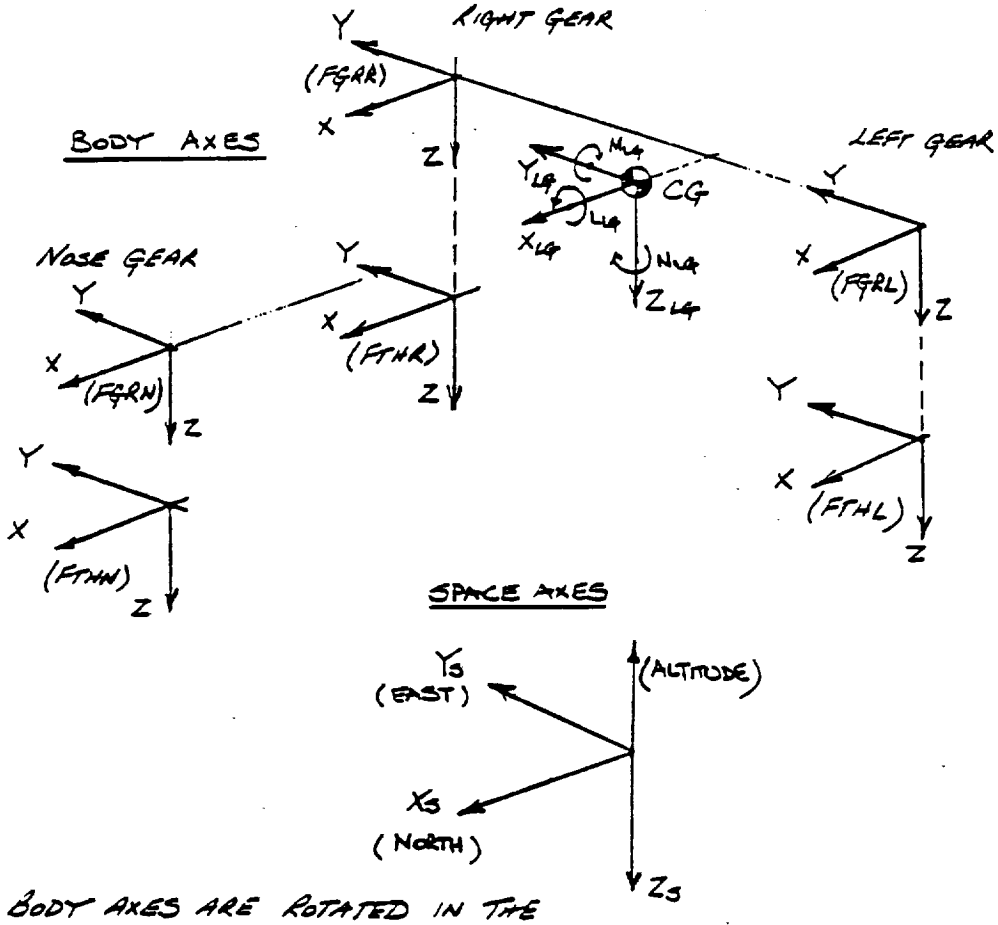

BODY AXES ARE ROTATED IN THE SEQUENCE: ψ_b ABOUT Z_b, θ_b ABOUT Y_b, ϕ_b ABOUT X_b TO REACH THE SPACE AXES SYSTEM

Tire Contact Geometry

In the equations defining the geometry of the landing gear, Figure 3.7.3, it is assumed that the strut moves along the line parallel to the helicopter Z axis. No account is taken of drag linkage constraints which cause the axle to move in an arc in the X-Z plane. This geometry, together with the Gen Hel calculated position of the helicopter C.G. position in space, is used to establish the location of the tire, axle reference and gear reference points for each gear in space axes. These coordinates are used later to determine the proximity of tire contact and subsequent tire and strut deflections. 5.7-9,10, -11,-12

The determination of tire contact, for an arbitrary orientation of the helicopter relies on establishing the length of the normal from the ground plane to the axle reference position and the true angle which this line makes with the gear line. The derivation of these geometric relationships are given in Reference 27. (ie the true angle between two lines is given by Cos θ_{TRUE} = Cosα_1 cosα_2 + Cosβ_1 cosβ_2 + cosγ_1 cosγ_2 where α, β, γ are the direction cosine angles) For this case $\alpha = \beta = 90$ and $\gamma = 0$ for the normal to the ground. Thus, the true angle is equal to the last term in the helicopter to space transformation matrix. When the distance along the gear line becomes less than the tire radius, contact of the tire with the ground has occurred. Subsequently, this difference is defined as radial tire deflection. In practice tire contact can occur at any point on the width of the tire. In the model the contact point is assumed to be at the center of the tire tread, irrespective of the distortion resulting from radial or axial loading. The geometry for tire contact is illustrated on figure 3.7.4. 5.7-13 5.7-13,14

In order to establish the degree of inplane deflection and corresponding loading on the tire, it is necessary to track the intersection of the landing gear line relative to the ground plane. Using the positions of the axle reference and the gear reference in space, two equations of the gear line can be developed, (each projected into a 2D plane) and solved for the X-Y intersection with the ground plane. When contact for an individual tire is established, the point of intersection is retained and on subsequent iterations through the program, tire deflection is determined by comparing the new and old gear line intersections. The coordinates of the initial contact are retained until the tire leaves the deck or are modified by the tire slipping. If contact is lost, for any given tire then the initialization is reset to zero. This is necessary, since the tire/gear can bounce in and out of contact. The re-initialization for the contact point following tire slipping is discussed later. Following the transformation of the deflections into helicopter body axes, the three components of deflection at each 5.7-15 5.7-16

FIGURE 3.7.3 LANDING GEAR GEOMETRY

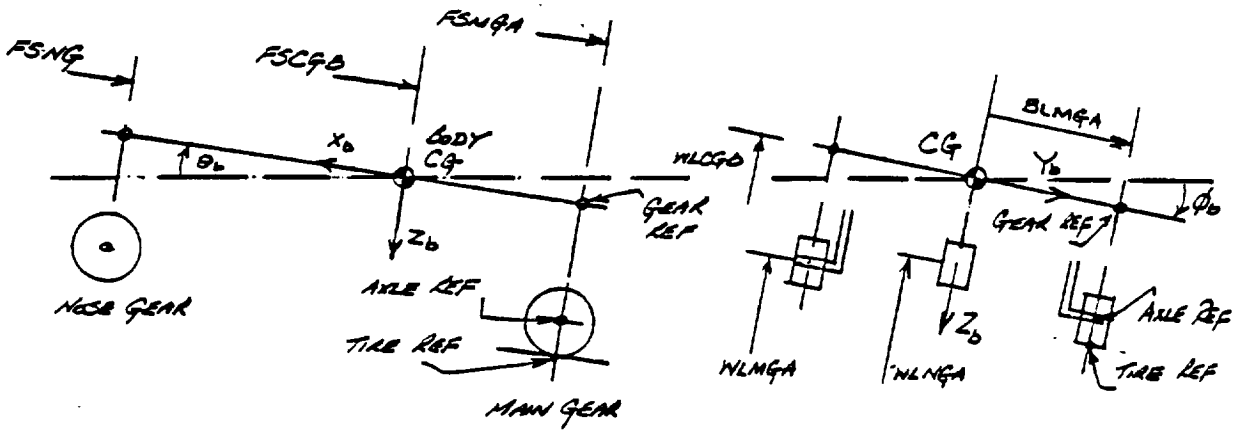

FIGURE 3.7.4 GEAR/GROUND-PLANE INTERFACE GEOMETRY

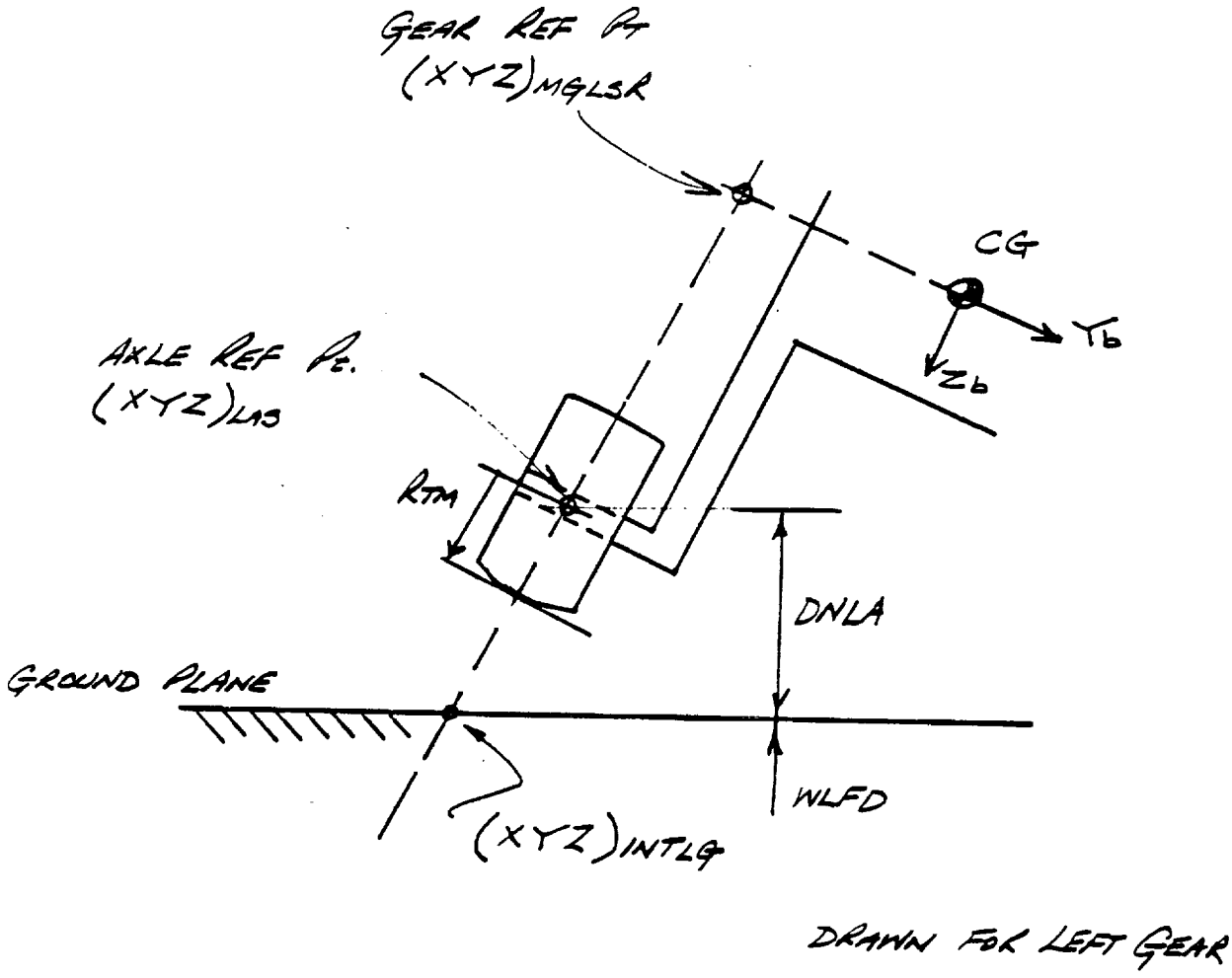

tire can be used to determine, from the tire characteristics data file, the potential three components of tire force. "Potential" qualifies these loads, because until the tire is checked for slipping, the actual inplane loads cannot be defined.

Tire Loads

5.7-17 -20

The tire loads are made up of two components - that due to spring stiffness and that due to damping. The vertical stiffness data is well defined by the manfacturers load deflection tests and is used directly in the simulation. However, the inplane loads are less well defined, and the assumption is made that they can be treated as separate orthogonal components. Laterally a non-linear stiffness is extracted from test data as a function of vertical tire deflection and tire pressure. Longitudinal stiffness is based on Reference 28. The damping terms are tuned to a fixed frequency and while the acceptability of this technique is clear for, say ground resonance analysis, it's suitability for impact landing is not clear. In any event, it is necessary to filter the damping terms to effectively smooth the velocity obtained by numerical differentiation of tire deflection.

Tire Inplane Friction Load Check

5.7-18 -19

Following the determination of tire forces from the helicopter relative motion, a test of the ability of the inplane friction forces to resist the applied forces without slipping, must be established. The tire forces obtained in helicopter axes must be transferred to the ground plane for the friction check. In executing this transformation it should be noted that in order to retain the X-Y alignment of the forces with body axes when transformed to the ground plane, ψ_b must be set to zero in [AHBS]. Here again it should be noted that no attempt has been made to treat the friction criteria based on the resultant inplane force. The method retains orthogonality of the inplane forces. In practice the resultant force does determine slip conditions but the model becomes more complex and the simplified approach facilitates the introduction of brakes. Classical friction considerations provide for a coefficient of static friction and a coefficient for sliding friction. In the former case (when brakes are set), the maximum amount of inplane load which can be resisted without slipping, is proportional to the coefficient of friction and the normal loading. When this level is exceeded, motion will result. Then the force resisting the motion will depend on a reduced (sliding) coefficient of friction. In practice, there is a smooth transistion between the two conditions. However, the model assumes a discrete change. When the brakes are activated, it is assumed that the wheels are

locked. For brakes off, a very low coeffeicient of friction is introduced into the tire X direction. The wheel degree of freedom is not currently represented and therefore spin up inertia loads are not calculated. If slip is not occurring, calculated tire forces are passed unchanged. If slippage is occurring, the inplane forces are set to the value for sliding friction. The final tire loads are transferred to the axial reference point.

For the conditions where the inplane loads exceed the allowable static friction level and the tire slips, a re-initialization of the tire contact point must be undertaken. Under conditions of no-slip the tire inplane deflection is developed from consecutive calculations of the gear line intersection with the ground plane. During slip conditions, the contact point for the tire moves, and the initialization of the gear-line intersection must be revised to reflect the tire movement and establish a new value for the contact point to be used on the next pass through the program, as shown on figure 3.7.5. It is assumed that the actual tire deflection can be determined from the sliding friction force and the tire inplane stiffness. 5.7-21

Landing Gear Strut Loads

Under steady conditions, the loads transferred to the airframe by the strut will be equal to the tire reactions. However, under transient conditions, the acceleration of the unsprung mass can modify the loading. A diagramatic representation of the strut is shown on figure 3.7.1. Three elements of the strut are modelled. The preload restraint, the isentropic air spring and a velocity squared damper. Under light loading condition (where a significant portion of helicopter weight is reacted by the rotor), the strut operates in the preload range. Under these conditions, where tire reaction load is less than the strut preload setting, tire loads are transferred to the airframe with zero strut deflection. Once the preload setting is exceeded, the strut (unsprung mass) is accelerated depending on it's own dynamic characteristics, the tire applied loads, and the unsprung mass. Note that logic precludes the equation flow reverting back to the preload mode until the natural transient provides a zero strut deflection condition. 5.7-23

The model for the strut air spring assumes isentropic expansion of the air as the strut deflects. While this is a reasonable assumption for large deflections experienced during a landing transient an adeabatic expansion assumption may be more appropriate once the strut has deflected and is moving about some average deflection point. Strut damping is achieved by forcing fluid through an orifice and is represented in the model by a fixed coefficient, velocity squared term. The strut system

FIGURE 3.7.5 REINITIALISATION OF GEAR LINE INTERSECTION POINT

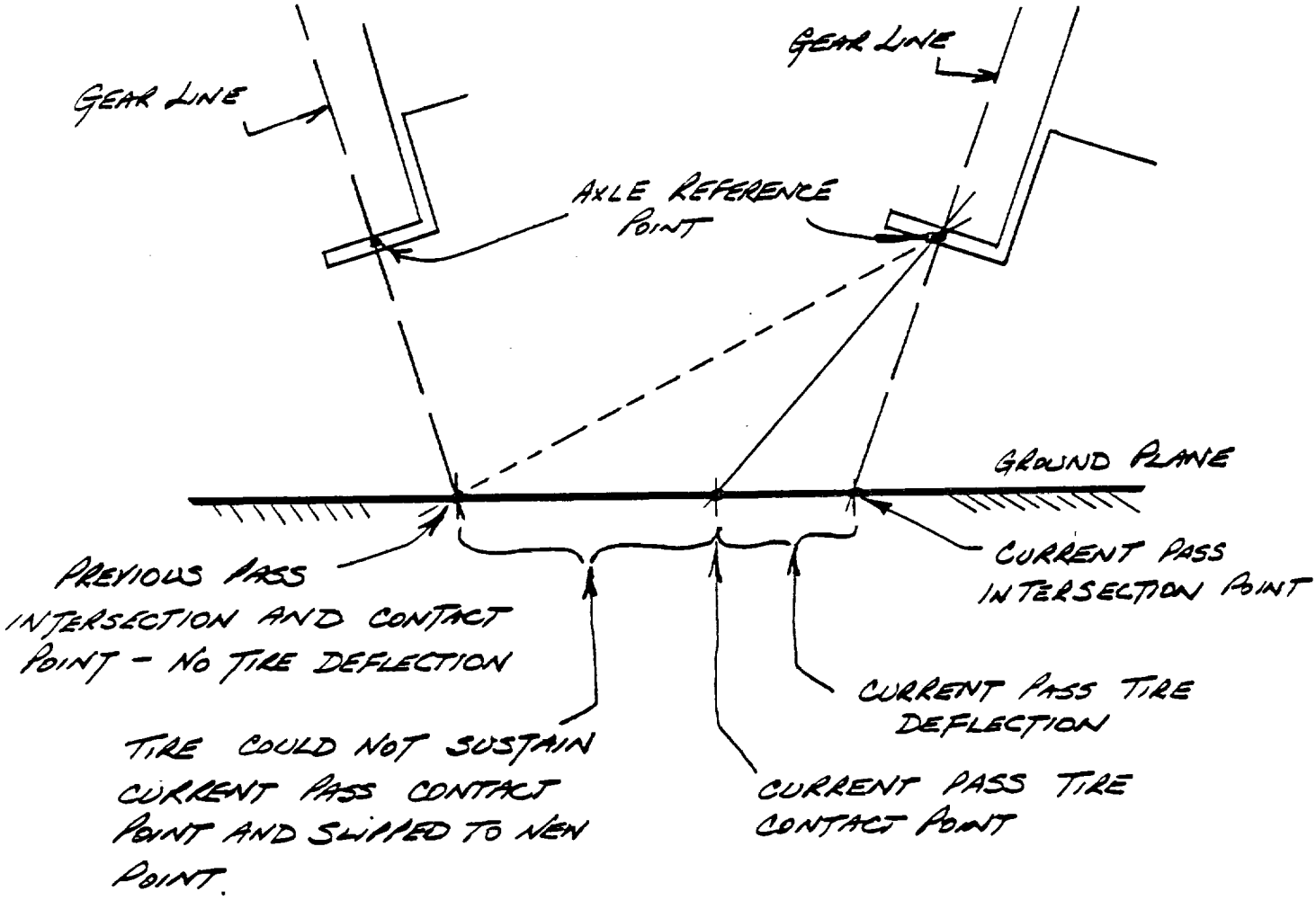

contains high frequency components and care should be taken in selecting the integration time interval, if a straight sequencial algorithm is used. A software switch is provided which allows bypassing the strut calculation, such than tire loads are transferred directly to the airframe. This will give approximate solutions under some circumstances without loading the simulation down with the strut calculations. Finally, the strut loads are transferred to the helicopter C.G. for summation with other external forces. 5.7-25 -26

This landing interface algorithm and the corresponding input data has been used by Sikorsky to analyze hard landings and ground resonance. The results obtained compared acceptably with test data.

3.8 GROUND EFFECT MODULE

This module simulates the effect of ground proximity on a helicopter by modifying the rotor forces and moments through a manipulation of the inflow equation.

The airflow surrounding a helicopter when it is close to the ground is highly complex, especially under transient flight conditions. Most of the experimental data available is for steady conditions where the flow pattern has stabilized. Any transient data is highly configuration oriented. It is likely that recent and on-going research on this subject (Reference 29) will lead eventually to an empirical model describing the local rotor inflow velocity due to the hyperbolically shaped ground vortex and its image that has been shown to exist at low speeds. Unfortunately, sufficient data for correlation of such a model has not yet been published.

With these limitations in mind a model was formulated which accounts for the gross effects of changing inflow through the rotor when it is operating close to the ground. The algorithm incorporates an altitude and forward speed effect. The latter effectively washes out the altitude effect based on the rotor wake skewing rearwards with increased speed. BLACK HAWK hover flight test results, Reference 30, were used to develop an empirical factor with which to force correlation. This ground effect factor modifies the main rotor calculated downwash when altitude is less than five times rotor radius. The downwash change causes a change in rotor loading, especially effecting rotor thrust. 5.8-3

3.9 GUST MODULE

This module produces local air velocities at all rotor-blade segment positions and at the fuselage and empennage component

aerodynamic centers, caused by various types of gusts. The gust input may be discrete or continuous having deterministic and non-deterministic characteristics respectively. The discrete 5.9-10
gust functions which can assume the shape of a step, ramp or pulse, are explicitly defined as a function of penetration distance. The continuous gust is represented by the Dryden model. 5.9-12
Conceptually this model is relatively simple. However, the computer mechanization is somewhat complicated by the need to store and retrieve gust data for any blade segment, at any blade azimuth station, at any state of penetration. The blanket storage of this data is not feasible and a "rotating ring array" was developed to cope with this problem.

In the computer implementation, large "rotating ring arrays" of gust data are generated. Specifically vertical and horizontal gust tables, TABLEV and TABLEH, of size equal to MAXPNT data points are loaded to represent gust velocities at TABINK distance apart. Because the "rotating ring array" is, in fact, a table it should be noted that the first and last table locations are co-incident on the "ring array". In general the helicopter can be visualized as wrapping around the ring array as shown in figure 3.9.1.

Loading the Tables with Gust Velocities

Two gust tables are specified TABLEV vertically and TABLEH horizontally. For the discrete gust function, lateral components of gust result from specifying relative helicopter/wind headings. For the continuous gust the horizontal gust must be aligned approximately along the aircraft x axis to be within the assumptions of the Dryden model. If lateral Dryden gusts are required the model can be expanded to include this component.

During the IC condition it is necessary to enter sufficient data into the tables to allow for deviations in helicopter airspeed after entering the compute mode. At the same time, because the table is effectively a "ring", data cannot be loaded towards the end of the table. If this occurred, erroneous gust input would be experienced on the aft portion rotor disc after entering the compute mode. This concern is evident from the illustration on figure 3.9.2. Using this "rotating ring" concept, the helicopter will cover a distance 2(RMR + ΔFT) on the closed table. As TABINK ($=V_{FLD}$*TIME) decreases in valeu, more of the table will be covered by the aircraft. A logical test must be made to avoid the aircraft doubling over. An appropriate test is if (ICUPD + 12) data points are equal to INPPNT the table margin is insufficient for the operating conditions. This limit is illustrated on figure 3.9.3. TheΔFT defined, (Figure 3.9.1) also serves the purpose of providing a dead space at the beginning of the table, allowing a short period following entry to

FIGURE 3.9.1 DEFINITION OF GUST RING ARRAY

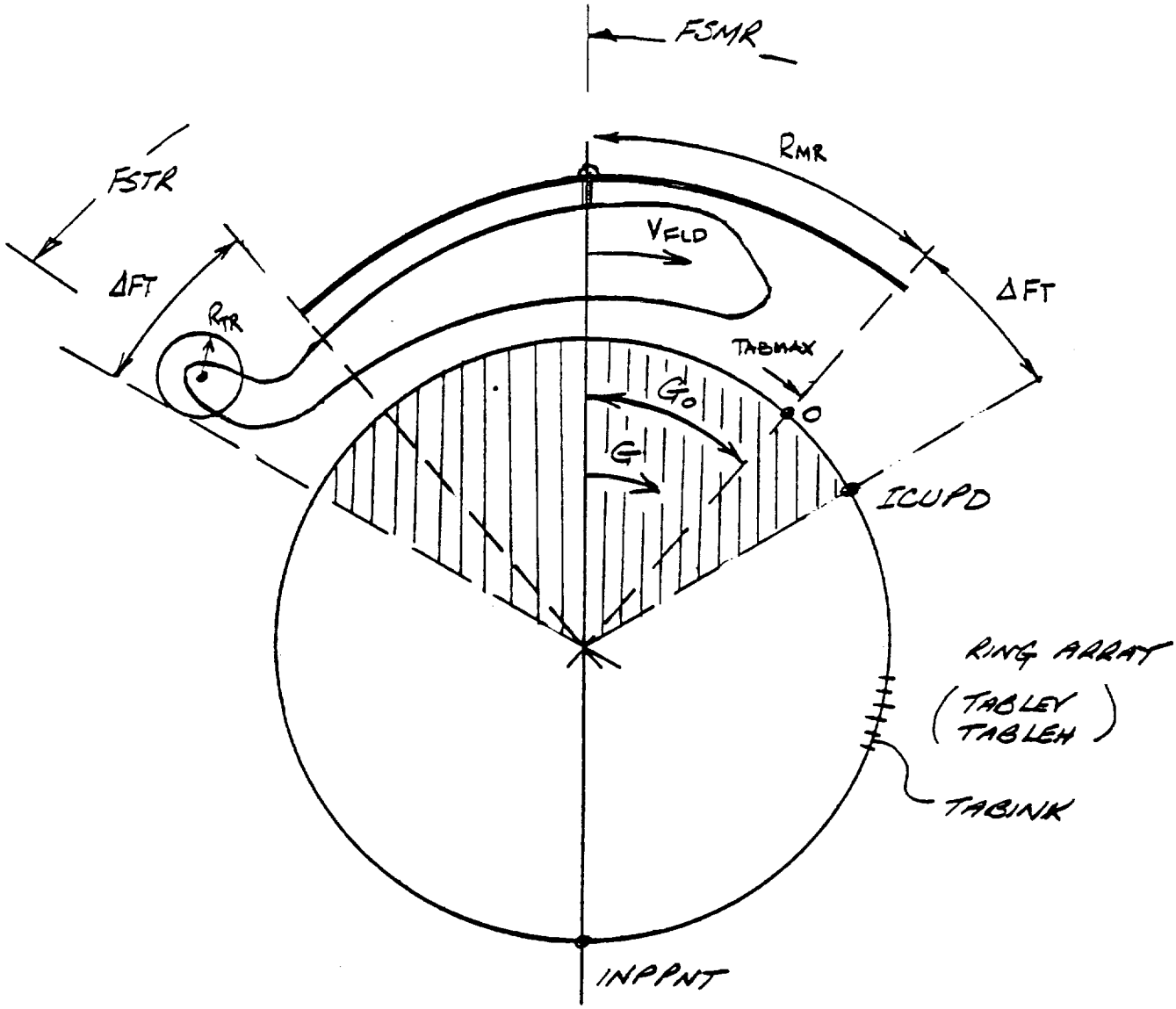

FIGURE 3.9.2 GUST TABLE LOADING RESTRICTIONS

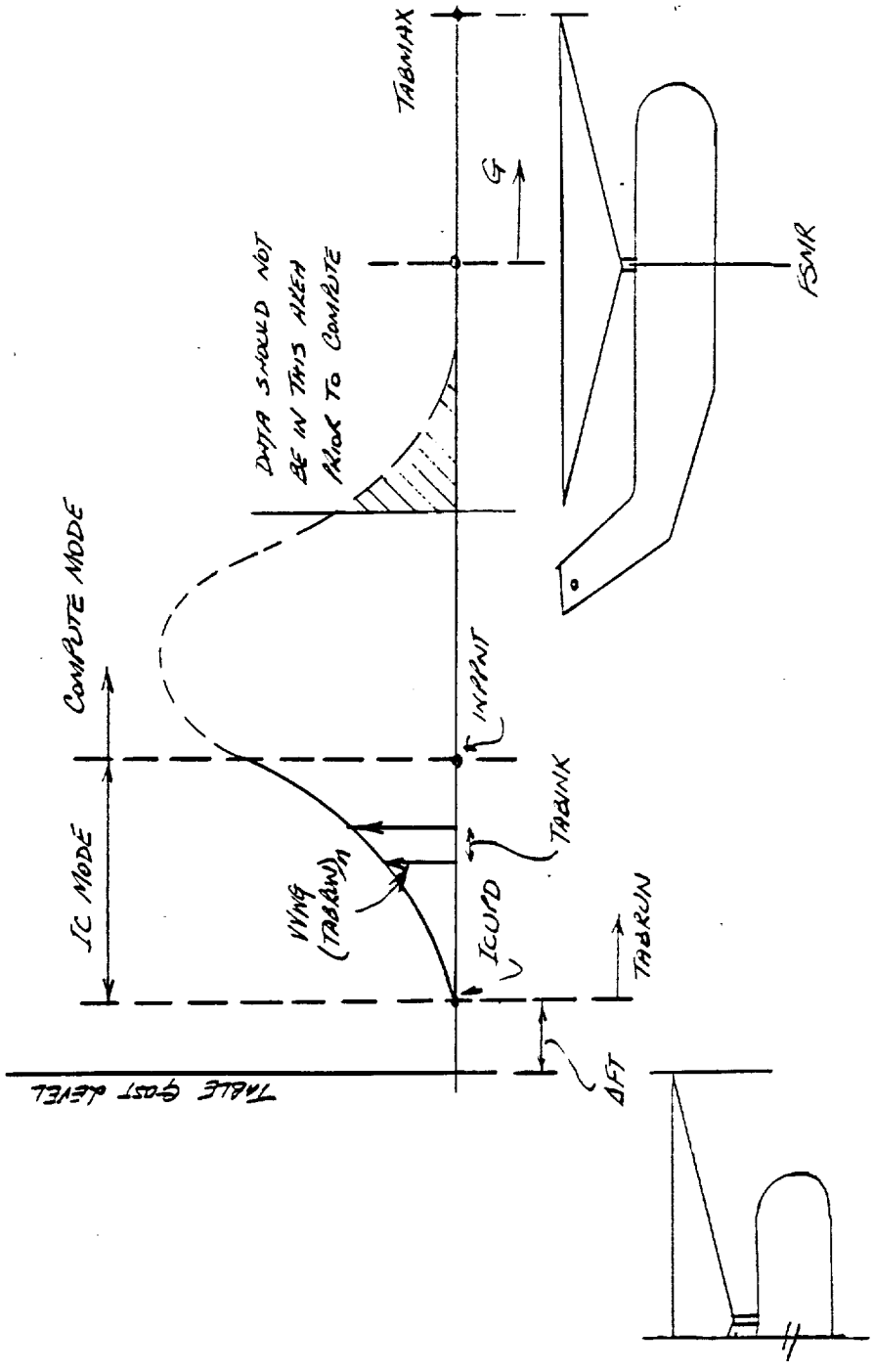

FIGURE 3.9.3 EFFECT OF DECREASING "TABINK" ON TABLE LOADING

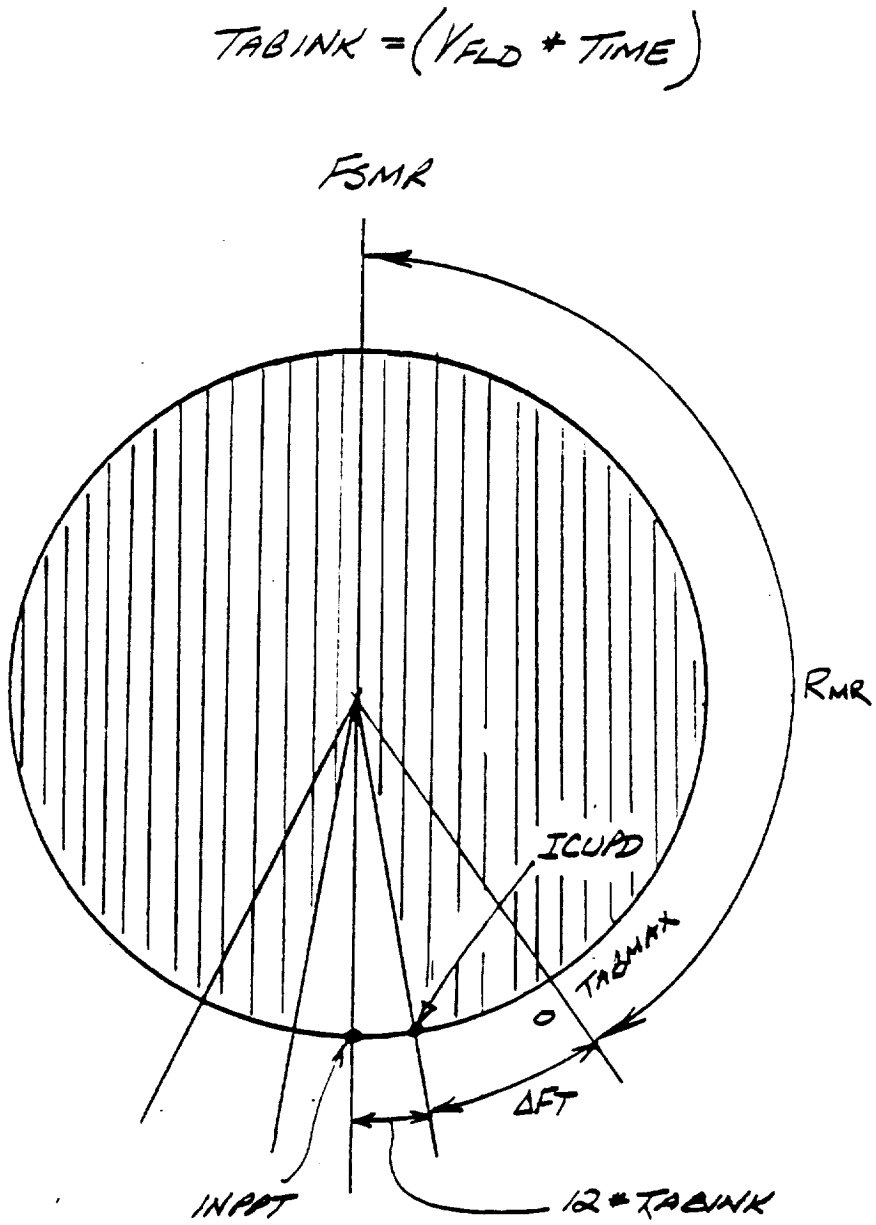

the compute mode before the rotor experiences the gust. Thus, data is loaded between ICUPD and INPPNT in the I.C. mode. In the compute mode a data point is placed in the table for each program pass. It represents the gust velocity at a distance, TABINK, ($=V_{FLD}$*TIME) from the previous entry, where V_{FLD} is the propagation rate of the gust front, (in I.C.). Thus the helicopter tends to remain diametrically opposite the table update point. When TABMAX is reached new data will refresh the data at the beginning of the table, (hence rotating ring).

Gust Penetration Distance and Table Look-Up

A penetration distance G(ft) is defined as a function of the propagation velocity, V_{FLD}, which represents the distance that the aircraft reference hub centroid has penetrated the gust front. This reference is used to calculate the penetration of other points on the rotor, GPRS, (see Figure 3.9.4). These values are used to set the pointer for the table look-ups. 5.9-9

Initially the helicopter is oriented to place the front of the rotor tip path plane at the end of each gust table, (ie Go = -RMR) see figure 3.9.2. Now, if in the compute mode the helicopter maintains its trim speed a fixed point on the helicopter will advance through the table at the same rate as the table is updated. (ie. G increases by TABINK each pass.). However, deviations in helicopter airspeed, will result in the helicopter gaining on or slipping relative to the fixed update rate,(which is determined by the IC value of V_{FLD}).

Penetration of empennage components are determined by delaying the gust value for the rotor centroid by an appropriate amount. 5.9-16

A simplified flow diagram of the computer implementation is shown on figure 3.9.5.

3.10 HELICOPTER MOTION MODULE

This module brings together all the forces and moments acting on the rigid airframe and develops the motion of the helicopter in the body axes system, illustrated in figure 3.10.1. This module also is a catch-all for small elements of the simulation which are not appropriately specified elsewhere.

The external forces and moments in body axes at the airframe center of gravity, calculated in the various modules, are summed to form the total external forces and moments used in the general equations of motion. For convenience the gyro scopic effects of rotating mass (shafts rotor hub etc.) are introduced at this point. These gyroscopics are based on fixed (input) rotational speeds. 5.10-4

FIGURE 3.9.4 HELICOPTER PENETRATION OF GUST FRONT

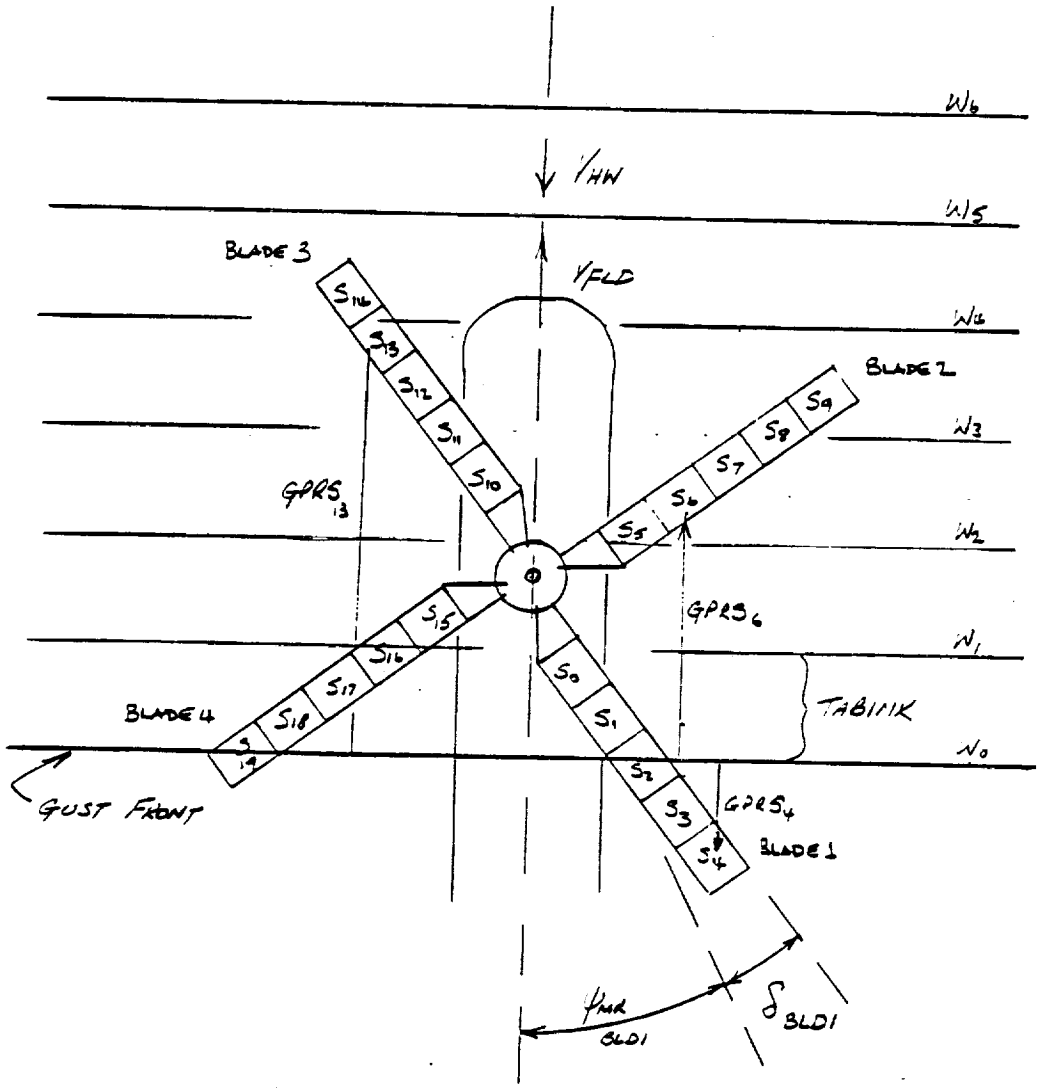

FIGURE 3.9.5 PROGRAM FLOW FOR LOADING GUST TABLES

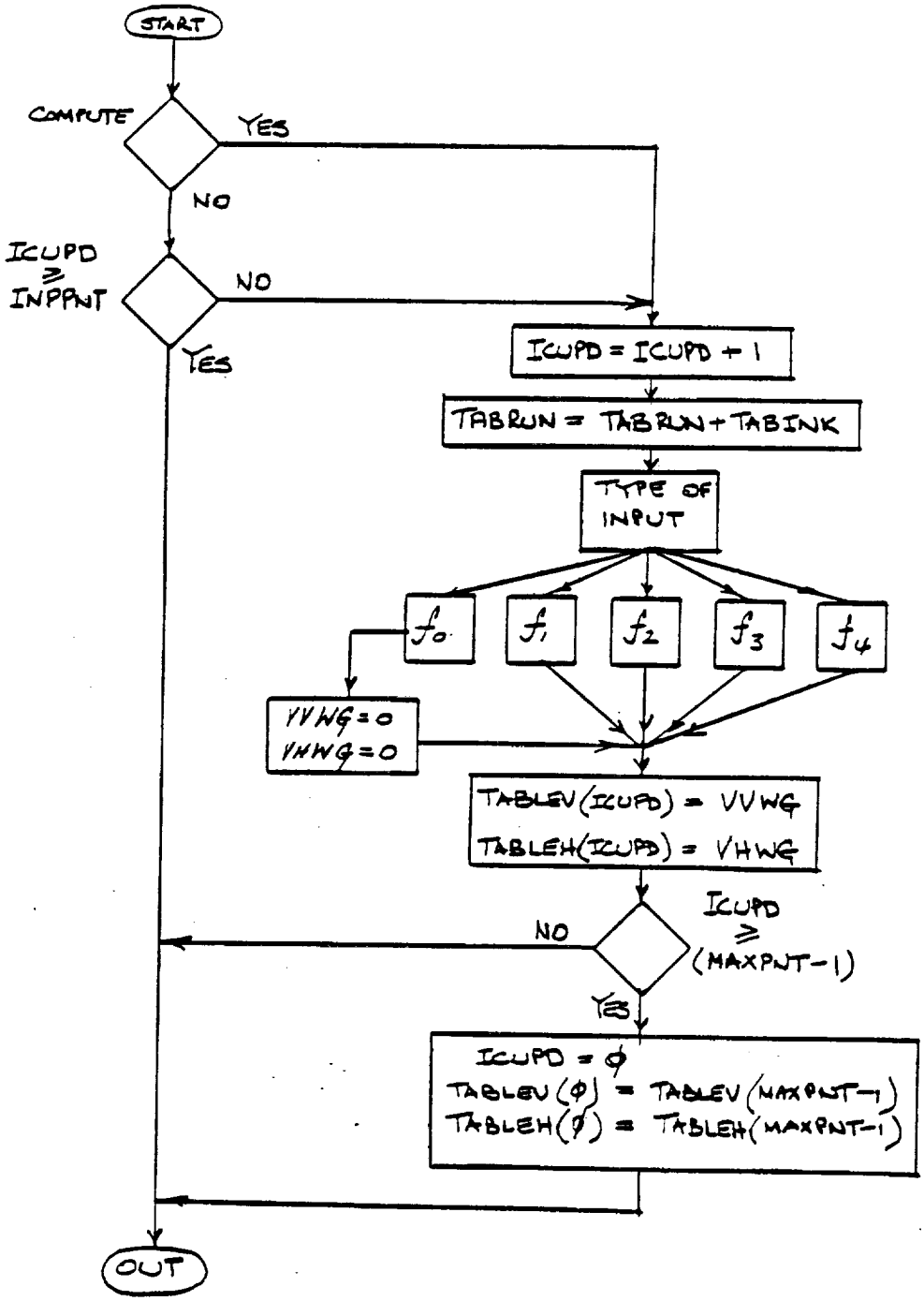

FIGURE 3.10.1 BODY AXES SYSTEM

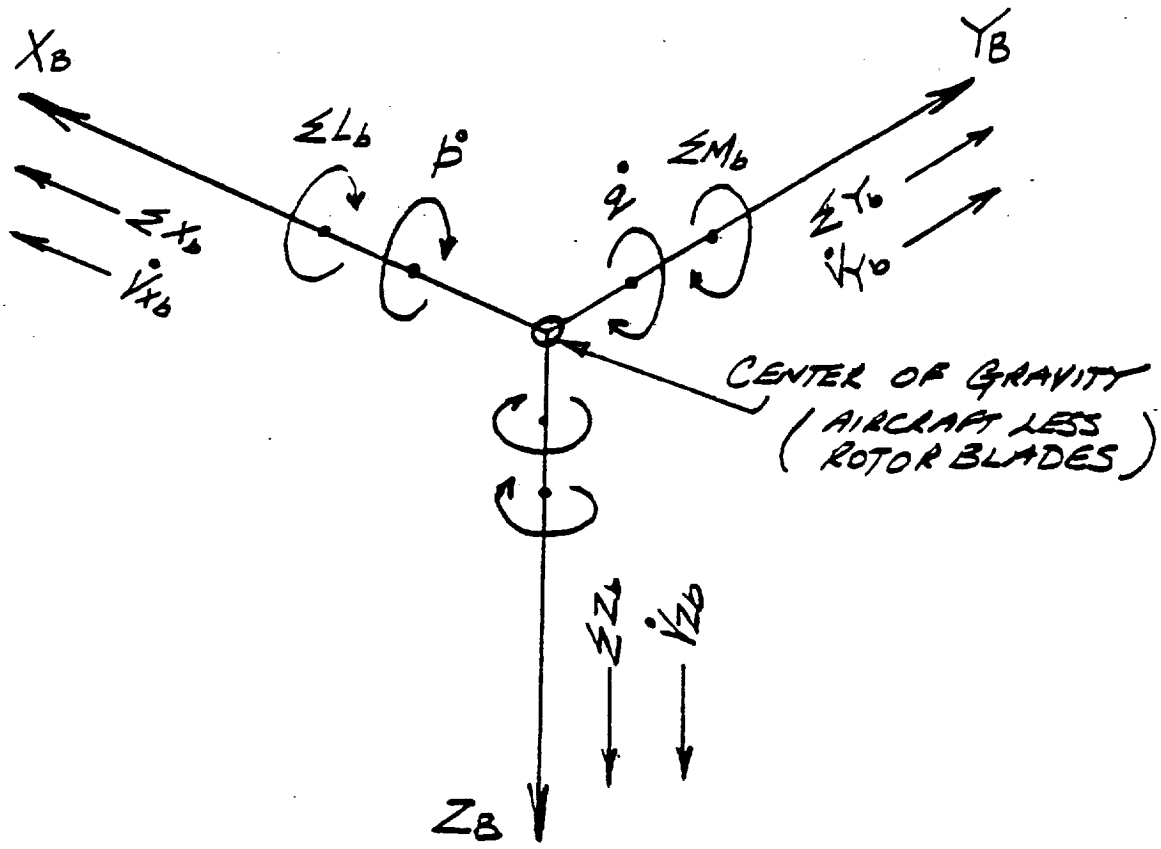

X_b, Y_b, Z_b Body Axes System. Origin at the Center of Gravity. X Axis Parallel to Aircraft Center Line.

The general equations of motion are standard and can be found in Reference 1. A comparison will show that some small terms have been ignored. It should be noted that these equations are written about the airframe center of gravity. (that is less rotor blades which are treated as separate bodies). Gross Weight and C.G. are input to the program and are modified in the rotor module to provide airframe values as discussed in Section 3.1.2. However, airframe inertia must be provided as input. The lateral C.G. offset components have been eliminated from the equations of motion presented, such that the coupling between degrees of freedom can be reduced. Thus, only P_{DOT} and R_{DOT} need be solved simultaneously rather than all three angular degrees of freedom. The impact of the simplification is that the dynamic effects of lateral C.G. offset are not modelled. Statically, no accuracy is lost and the simulation can be used for such analysis. The solution of the acceleration equations depends on last program pass values of all variables except translational velocities. Here a half pass predictor is used to ensure numerical stability. The introduction of these predictors is based solely on passed experienced. The motion in space axes is developed using the standard Euler equations for the angular velocities and a 3 axes transformation in the sequence ϕ_b, θ_b, ψ_b for the translational velocities. 5.10-6 5.10-5 5.10-7,10

The equations for motion at any point on the airframe are written in terms of accelerations that a pendulum, suspended at any point on the airframe, would experienced. They are defined in the opposite sense to normal body axes accelerations. These terms are used for control system feedbacks and for determining the accelerations and velocities at any point on the airframe or pilot's seat for motion system drives. The so called 'g' vectors are derived from these accelerations. 5.10-10,11

The remaining equations in this module are either generated specifically for a control system feedback or for output. They are self explanatory. 5.10-12,13

Reference to the summation of external force and moment equations, indicates components $(XYZLMS)_{ADD}$. These components are provided such that emperical correction terms, which may not have analytical foundation, can be introduced into the simulation. A typical use of these elements is the downwash correction terms. Here an empirical correction is made to the sideforce, rolling moment and pitching moment due to downwash variations under conditions of sideslip flight. Information is not available to develop a more sophisticated model, thus this empirical fit of wind tunnel test and flight test data has been introduced at this point. 5.10-4 5.10-19

4.0 SIMULATION TRIMMING CONCEPTS

Several approaches to trimming the helicopter simulation are available. These vary from simple single channel loop closures, to multi-loop, steepest descent methods employing simplified rotor calculations to initialize the trimming algorithm. The method recommended for the BLACK HAWK simulation, and presented below, is based on the integral of the error between the current state and the commanded state. In most applications the latter is zero. Conceptually this trimming method is simple and with appropriately selected gains, very stable.

The general form of the trimming algorithm is:

$$\text{CONTROLLER} = \text{GAIN} \int (X_{\text{CURRENT}} - X_{\text{COMMANDED}})\,dt$$

where X is most often an acceleration, but can be any other parameter. The controller for the specified degree of freedom is adjusted by the integral of the error until balance is obtained and the integral goes to zero. Using this method all trimming loops can, and should, be closed simultaneously.

For computing efficiency it is desirable to define the flight path in the X-Z plane only. Thus $Vxb = 1.69\ Vcom.\ \cos(\theta b - \gamma c)$

$$Vzb = 1.69\ Vcom.\ \sin(\theta b - \gamma c)$$

where Vxb, Vzb are body axes velocities

Vcom	commanded flight path airspeed (knots)
θb	pitch attitude
γc	climb angle

This approach, which eliminates Vyb, avoids the trimming sequence having to operate through a cumbersome three axes velocity transformation.

Typically in the Sikorsky implementation, the TRIM is based on a rate check of the controller motion. The controller is checked every 20 program passes. If for 5 consecutive checks the controller has not changed by more than the tolerance, that degree of freedom is judged to be trimmed. The helicopter is judged to be trimmed when all of the controllers are within tolerance. If a controller is out of tolerance, the check is reset at the new position. Checks of all channels are continued until the helicopter is trimmed.

C-2

Typical trimming loop closures are given below:

Acceleration	Controller	Gain	Tolerance
For steady level flight			
$V\dot{x}b$	θb	.35	.05
$V\dot{y}b$*	$\emptyset b/Vyb$	-.35/5.0	.05/.05
$V\dot{z}b$	XC	.07	.01
P	XA	-1.0	.01
$\dot{q}$	XB	1.0	.01
$\dot{r}$	XP	-1.0	.01
For climbing flight, change as follows:			
$V\dot{z}b$	γc	-.35	.05
Vc	XC	-.0002	.01
For autorotation, change as follows:			
$V\dot{z}b$	γc	-.35	.05
QHBMR≠	XC	-.00001	.01

*Either $\emptyset b$ or Vyb may be used to trim $V\dot{y}b$. The other must be specified.

≠QHBMR specified equal to zero for autorotation or some desired value for part power operation. Under normal unaccelerated flight trim conditions the body angular rates are set to zero.

5.0 FUTURE SIMULATION MODEL DEVELOPMENT

The BLACK HAWK mathematical model provided to the Army under this contract is considered to be a good engineering representation for Handling Qualities and some Performance analysis. The level of sophistication was selected to permit analysis within the band width of the flight control system. Therefore, in the future development of a real time pilot-in-the-loop model it may be expedient, and from a computing requirement, a necessity, to eliminate certain high frequency elements. An example would be some of the elements in the control system. It should be noted however that phase characteristics are summed and can have an impact at relatively low frequencies.

Based on a variety of correlation investigations,covering several Sikorsky helicopter types, it would be expected that this engineering simulation would provide good trending data and representative absolute comparisons in most flight regimes. However, there are area's in the model that can be improved, but test data is required to establish that more sophistication is meritted, and that the corresponding increase in computation time is justified. The BLACK HAWK flight test program, to be conducted by the Army, will provide valuable information.

The following is a discussion of areas in the model where improvements may be necessary. They have been identified because of reduced confidence in their representation or because for simplification purposes, they have been approximated.

Main Rotor

a) Inflow Modelling - New theoretical approaches are available, but closely controlled test data for an articulated rotor is still limited.

b) Unsteady Aerodynamics - The trade-off for introducing this complexity needs evaluating for the band-widths of concern for Handling Qualities and Control System design.

c) Blade Flexibility - It is known that significant torsional wind-up occurs with the BLACK HAWK rotor blade. A flexible blade representation, at least torsionally, might increase confidence for expanded flight envelope simulation.

Empennage and Tail Rotor

a) Sideslip effects of main rotor wash at the tail are treated in a gross sense because of lack of experimental data other than the knowledge, from flight test, that a significant effect exists.

b) Tail rotor wash on the vertical tail has been ignored in the model based on the fact that this is consistent with the approximations inherent in the rotor downwash in the vicinity of the empennage. Data is available for improving the vertical tail blockage of the tail rotor without significantly increasing model complexity.

c) For some analysis tasks a more sophisticated tail rotor formulation may be necessary which includes torque and tip path plane tilt.

Aerodynamics of the Airframe at Low Speed

Analysis and validation in rearward and side flight are required to confirm the assumptions that have been made in the model that only the rotors are important.

Engine

The limitations of the linear engine model were identified and discussed in Section 3.6. As the BLACK HAWK simulation activity matures it may be appropriate to upgrade the engine representation.

Ground Effects

There is interest in the Handling Qualities effects of flying helicopters close to the ground for certain mission tasks. Recent experimental data may allow the formulation of an improved generalized model. This area is lacking especially for transient conditions.

Failure Modes Development

The BLACK HAWK model presented requires development to incorporate a full failure modes representation.

6.0 REFERENCES

1. Etkin, B; Dynamics of Flight, John Wiley and Sons Inc. 1959.

2. Kuczynski, W; Cooper, D; Twomey, W., Howlett, J: The Influence of Engine/Fuel Control Design on Helicopter Dynamics and Handling Qualities, AHS paper 79-37 Presented at the 35th Annual National Forum. May 1979.

3. Cooper, D; Howlett, J: Ground Based Helicopter Simulation, Symposium on the Status of Testing and Modelling Techniques for V/STOL Aircraft AHS 1972.

4. Gessow and Myers: Aerodynamics of the Helicopter, MacMillen Co. 1952.

5. Ormiston, R:; Peters, D; Hingeless Helicopter Rotor Response with Non-Uniform Inflow and Elastic Blade Bending, Journal of Aircraft Oct 1972.

6. Crews, S.; Hohenemser, K: An Unsteady Wake Model for a Hingeless Rotor, Journal of Aircraft Dec. 1973.

7. Harris, F.: Articulated Rotor Blade Flapping Motion at Low Advance Ratios, Journal of the American Helicopter Society, Jan 1972.

8. High Speed Aerodynamics and Jet Propulsion Volume VIII. Aerodynamic Components of Aircraft at High Speed. Princeton University Press.

9. Jepson, W.: Two Dimensional Test of four Airfoil Configurations with an Aspect Ratio of 7.5 and a 16 inch Chord up to a Mach Number of 1.1 SER-50977, April 1977.

10. Paglino, V.: Yawed Bladed Element Performance Method, SER-50620, Sept. 1969.

11. Klusman, S.; BLACK HAWK Lag Damper Force/Velocity Characteristics. Sikorsky Internal Memo. TEM-G2-0594 July 1978.

12. Houck, J.; Moore, F.; Howlett, J.; Pollock, K.; Browne, M.: Rotor Systems Research Aircraft Simulation Model NASA TM-78629, Nov. 1977.

13. Du Val, R.: Inertial Dynamics of a General Purpose Rotor Model, NASA TM-78557 March 1979.

14. Heyson, H.: Equations for the Induced Velocities Near a Lifting Rotor with Non-Uniform Azimuthwise Vorticity Distribution, NASA TN D-394, 1960.

15. Warner, J.; Flemming, R.: YUH-60A Quarter Scale Wind Tunnel Test Report. SER-70531 May 1973.

16. Rorke, J.: YUH-60A Quarter Scale Drag Reduction Wind Tunnel Test Report. SER-70097 July 1975.

17. Barnard, R.: YUH-60A/T700 Engine I.R. Suppressor Test Report. Appendix III Quarter Scale Infrared Suppressor Wind Tunnel Test. SER-70094 June 1976.

18. Ellison, D.; Mattham, L.: NSAF Stability and Control Datcom, McDonnell Douglass Corp., Project No. 8219, Flight Control Division, Air Force Flight Dynamics Laboratory, Wright-Patterson Air Force Base. Sept 1970.

19. Smith, H.; Schaefer, R.; Aerodynamics Characteristics at Reynolds Numbers of 3×10^6 and 6×10^6 of Three Airfoil Sections Formed by Cutting Off Various Amounts From the Rear Portion of the NACA 0012 Airfoil Section, NACA TN 2074, Feb 1950.

20. Bailey, F.: Simplified Theoretical Method of Determining the Characteristics of a Lifting Rotor in Forward Flight, NACA Report 716.

21. BLACK HAWK - Detailed Specification for the Stability Augmentation System and Flight Path Stabilization System Hardware Production Program. Prepared under Contract DAAJ01-73-C-0006, SES-701208.

22. BLACK HAWK - Detailed Specification for the Stability Augmentation System and Flight Path Stabilization System Hardware Production Program. Prepared under Contract DAAJ01-73-C-0006, SES-701209.

23. BLACK HAWK - MOS 35K Avionics Mechanics Course. Sikorsky Training Manual Publication.

24. UH-60A. Familiarization Training Course. Sikorsky Product Support Training Publication.

25. Curran, J.: T700 Fuel and Control System, AHS National Forum Paper, Preprint No. 771, May 1973.

26. General Electric: T700 Operation Manual.

27. Apalategeric and Adams. Aircraft Analytical Geometry.

28. Simley and Horne: Mechanical Properties of Pneumatic Tires With Special Reference to Modern Aircraft Tires. NACA TR-R-64.

29. Sheridan and Wiesman: Aerodynamics of Helicopter Flight Near the Ground. AHS Paper 77.33-04 May 1977.

30. Sikorsky Letter LTC AR Todd to R. Merrit. Free Hover Performance. 22 Oct. 1976.

1. Report No.	2. Government Accession No.	3. Recipient's Catalog No.
NASA CR-166310		

4. Title and Subtitle	5. Report Date
UH-60A Black Hawk Engineering Simulation Program: Volume II - Background Report	December 1981
	6. Performing Organization Code
7. Author(s)	8. Performing Organization Report No.
J.J. Howlett	SER 70602
	10. Work Unit No.
9. Performing Organization Name and Address United Technologies Sikorsky Aircraft Stratford, Connecticut 06602	11. Contract or Grant No. NAS2-10626
	13. Type of Report and Period Covered
12. Sponsoring Agency Name and Address National Aeronautics & Space Administration Washington, DC 20546 U.S. Army Aviation Research & Development Command	14. Sponsoring Agency Code

15. Supplementary Notes

Technical Monitor: Thomas S. Alderete, Mail Stop 243-5, NASA Ames Reseach Center, Moffett Field, CA 94035 (415) 965-6171, FTS 448-6171
Volume I - Mathematical Model is NASA CR-166309

16. Abstract

A non-linear mathematical model of the UH-60A BLACK HAWK helicopter has been developed under Contract NAS2-10626. This mathematical model, which is based on the Sikorsky General Helicopter (Gen Hel) Flight Dynamics Simulation, provides the NASA with an engineering simulation for Performance and Handling Qualities evaluations.

This mathematical model is a total systems definition of the BLACK HAWK helicopter represented at a uniform level of sophistication considered necessary for Handling Qualities evaluations. The model is a total force, large angle representation in six rigid body degrees of freedom. Rotor blade flapping, lagging and hub rotational degrees of freedom are also represented. In addition to the basic helicopter modules, supportive modules have been defined for the landing interface, power unit, ground effects and gust penetration.

Volume I of this report defines the mathematical model using a modular format. The documentation of each module is self-contained and includes a descriptive, mathematical definition and input for the BLACK HAWK. Volume II provides background and descriptive information supportive to an understanding of the mathematical model.

17. Key Words (Suggested by Author(s))	18. Distribution Statement
UH-60A BLACK HAWK Math Model Simulation Handling Qualities	U.S. Government Agencies Only Subject Category 08 Point of Contact: Thomas S. Alderete

19. Security Classif. (of this report)	20. Security Classif. (of this page)	21. No. of Pages	22. Price*
Unclassified	Unclassified	99	

Available: NASA Scientific & Technical Information Facility
B.W.I. Airport, MD 21240